COPY

Unclassified

SECURITY CLASSIFICATION OF THIS PAGE (*When Data Entered*)

REPORT DOCUMENTATION PAGE

READ INSTRUCTIONS BEFORE COMPLETING FORM

1. REPORT NUMBER	2. GOVT ACCESSION NO.	3. RECIPIENT'S CATALOG NUMBER
4. TITLE (*and Subtitle*) Advanced Cooling Technology Development Program (ACTD) Test Results From AEDC Track G Tests of Aerojet TCNTs Using Propylene Glycol		5. TYPE OF REPORT & PERIOD COVERED Analysis Report August 1981 - March 1983
		6. PERFORMING ORG. REPORT NUMBER ATC 3215:90
7. AUTHOR(s) Richard E. Walker Yuriko Taki		8. CONTRACT OR GRANT NUMBER(s) F04704-80-C-0022
9. PERFORMING ORGANIZATION NAME AND ADDRESS Aerojet TechSystems Company P. O. Box 13222 Sacramento, California 95813		10. PROGRAM ELEMENT, PROJECT, TASK AREA & WORK UNIT NUMBERS
11. CONTROLLING OFFICE NAME AND ADDRESS Department of Air Force Headquarters Ballistic Missile Office (AFSC) Norton Air Force Base, California 92409		12. REPORT DATE March 1983
		13. NUMBER OF PAGES 123
14. MONITORING AGENCY NAME & ADDRESS(*if different from Controlling Office*)		15. SECURITY CLASS. (*of this report*) Unclassified
		15a. DECLASSIFICATION/DOWNGRADING SCHEDULE

16. DISTRIBUTION STATEMENT (*of this Report*)

"~~Distribution Statement "A" of AFR 80-45 Applies~~

17. DISTRIBUTION STATEMENT (*of the abstract entered in Block 20, if different from Report*)

18. SUPPLEMENTARY NOTES

19. KEY WORDS (*Continue on reverse side if necessary and identify by block number*)

Re-Entry Vehicles
Transpiration Cooled Nosetip (TCNT)
Re-Entry Performance
Propylene Glycol as a Coolant

20. ABSTRACT (*Continue on reverse side if necessary and identify by block number*)

Two transpiration cooled nosetips using propylene glycol as the coolant were fabricated by Aerojet and tested in the Arnold Engineering Development Center (AEDC) Track G Facility. The nosetips, S/N G-10CT and G-11CT, used 347 stainless steel platelets and were hemispherical configurations, with nose radii of 0.65 inches and a 17° conical base half angle. Thermal and recession test results are presented and the temperature data are compared to computer code temperature predictions.

DD FORM 1 JAN 73 1473 EDITION OF 1 NOV 65 IS OBSOLETE

SECURITY CLASSIFICATION OF THIS PAGE (*When Data Entered*)

TABLE OF CONTENTS

Table of Contents (cont)

FIGURE LIST

Figure List (cont.)

Figure List (cont.)

TABLE LIST

1.0 INTRODUCTION

1.1 Background

Transpiration cooled nosetips (TCNT's) with hemispherical and OGIVE shapes have been designed, fabricated and tested by Aerojet over the last 10-15 years. These nosetips have all been built from 347 stainless steel and used the discrete injection platelet concept with water as the coolant. The most recent work involving these nosetips was conducted during the Advanced Ballistic Re-Entry Vehicle (ABRV) TCNT Development Program and is reported in Reference (1). The test results from this program showed the ability of the nosetip to survive in high aerodynamic heating and snow field density environments and also indicated that the basic nosetip analyses techniques were fairly accurate. Follow-on studies at Aerojet to the Reference (1) work have included investigations of alternate materials, shapes and coolants for TCNT applications. The alternate materials investigation resulted in the selection of molybdenum as a candidate nosetip material and a test plan to empirically evaluate the material using the AEDC Track G facility is contained in Reference 2. Alternate shapes to the hemispherical configuration used previously were evaluated both analytically and empirically and a flat face small corner radius design was found to yield significant coolant savings compared to the hemisphere. This work was reported in Reference (3).

The impetus for the work relating to alternate coolants, reported herein, were studies which indicated that other coolants have the potential for significantly reducing the amount of nosetip coolant required compared to water (References 4 and 5). ALRC has evaluated several different coolants for potential coolant weight savings compared to water (Reference 6). These studies led to a coolant screening test program (Reference 7) which was conducted in the Acurex/Aerotherm arc plasma generator (APG) test facility in Mountain View, California. The results of these tests (Reference 8) led to the selection of propylene glycol as the best potential coolant candidate for Track G evaluation among the 5 coolants tested.

Although the available data on coolant effectiveness for TCNT re-entry vehicle applications is very limited, the Reference

(4) and (5) studies identified, and to some extent verified, the performance improvement potential of ethylene glycol as compared to water. The bulk of the test data is contained in Reference (4) and was derived from plasma arc heater testing at very low pressures (.07 atm) but at the temperatures of interest (10,000 °R). The later test series of References (7) and (8) were also run at total gas temperatures in the range of 10,000 °R, which is adequate to induce coolant pyrolysis and thus produce some coolant kinetic decomposition and molecular dissociation effects. The test pressures were significantly higher than those of the previous tests (1 atm). Data from these tests indicated that both ethylene glycol and propylene glycol were superior to water as transpiration coolants in the high temperature regime (10,000 °R). The ratio of ethylene and propylene glycol flow rate to water flow rate for equivalent TCNT surface temperatures were approximately 50% and 20% respectively, and thus propylene glycol was selected for the AEDC Track G tests.

The Track G test series was conducted utilizing two 0.65 inch nose radius hemispherical nosetips. The internal hydraulics design for these nosetips was a modification of an existing design to allow for reduced coolant mass fluxes consistent with the anticipated reduction in required coolant flow rate. Three tests were conducted for this test series, with a cell pressure of 350 Torr and range entrance velocity of 17,000 ft/sec. The coolant mass flux was the independent parameter which was varied for the tests.

1.2 Test Objective and Goals

The objective of the test series was to define the magnitude of the coolant reduction possible with propylene glycol compared to water. Additionally, goals of the test series were:

1. To obtain photographic data relating to coolant atomization and vaporization compared to water.

2. To obtain test data to update the boundary layer blockage/downstream cooling/internal cooling computer model for propylene glycol.

The test objective and goals have been met, the coolant reduction possible with propylene glycol at these test conditions is approximately 50%.

1.3 Test Conditions and Configurations

Three tests were conducted with two propylene glycol cooled nosetips in the Track G facility at AEDC. The track conditions for these tests were as follows:

Cell Pressure	350 Torr
Cell Temperature	530°R
Launch Velocity	17000 ft/sec
Clear Air Conditions	

The two nosetips were made by Aerojet from 347 stainless steel platelets. The nosetips were hemispherical with nose radii of 0.65 inches, a 17° base half angle and 0.62 inch base radii. (A pre-test nosetip photograph is shown on Figure 3).

1.4 Test Data Results

Results from the propylene glycol cooled nosetip testing are summarized on table I.

The flowrates measured on tests 5749 and 5751 were significantly lower than the lowest water flowrates previously recorded for the hemispherical nosetip (W_{exit} = 0.10 lbm/sec). On these tests recession was a maximum of .050 inch. The thermal code predicted at or near melt temperatures over a substantial portion of the nosetip, although the code predicted a relatively cold stagnation region. Code improvements in the stagnation region are recommended and the possible form of these improvements have been identified. The code apparently does a very adequate job of predicting the downstream temperature, based on the observed recession. However, the thermal test data in this region was obscured by flare from the model holder.

On test 5768 the measured temperatures were equal to or slightly higher than on the two previous tests in the stagnation region. This may have been due to local flow blockage, a result of previous testing (Test 5749) with this nosetip. The data from station 29 on test 5768 are the best data from the test series, and indicates a hot region near the base of the nosetip. This hot region was predicted by the code and may have been present during the previous tests, but was obscured by flare.

Based on the observed relatively constant stagnation region temperature with Track station and some indications of a delay in coolant flow initiation, the nosetip may have been pre-heated to some unknown temperature at the early track stations. Additional and in particular lower sensing level thermal data are needed on future track tests to aid in data analysis and computer code correlation. Also, data on the high temperature characteristics of propylene glycol are needed in order to further improve the cooling code predictive capabilities.

2.0 TECHNICAL DISCUSSION

2.1 Coolant Selection

Propylene glycol was selected as the best candidate alternate coolant for water based on the test results reported in Reference (8). In addition to water and propylene glycol the coolants evaluated in the Reference (8) work were ethylene glycol, glycerol, and tertiary amyl alcohol. The cooling performance of these fluids relative to water is shown on Table 1. A comparison of propylene glycol and water physical properties at ambient temperature is provided on Table II. The data contained on Table II show some marked differences between the two coolants at ambient temperature. In addition to the room temperature property differences, coolant molecular dissociation differences between propylene glycol and water are expected to have a dominant influence on coolant effectiveness.

The difference in critical pressure between water and propylene glycol is significant because with water as the coolant, the Track testing yields nosetip boundary pressures (for the baseline 350 Torr cell pressure and 17,000 fps launch velocity) which are below the critical pressure; while with propylene glycol a significant portion of the cooling is done above the coolant critical pressure. The curves of Figure 1 show the Track G nosetip pressure distributions at Track entrance, the 2/3 point (40 ms) and track exit. These data show that the boundary pressure is above the critical pressure of propylene glycol for surface distances from the stagnation point of 0.40 to 0.52 inches, dependent on location in the Track.

TABLE I

COOLANT SCREENING CANDIDATES

Test Fluid	Performance Relative to Water*
Water	1.0
Propylene Glycol	~ 0.2
Ethylene Glycol	~ 0.5
Glycerol	> 1.0
Tert-amyl Alcohol	~ 0.3**

*$\frac{W_{Coolant}}{W_{Water}}$ for Equivalent Surface Temperatures

** Flowrate data questionable

TABLE II

PROPYLENE GLYCOL AND WATER PROPERTIES
COMPARISON AT AMBIENT TEMPERATURE (77°F)

	PROPYLENE GLYCOL	WATER
Molecular Weight	76.09	18.02
Critical Temperature, °F	665.6	705
Critical Pressure, psia	882	3206
Normal Boiling Point, °F	369.5	212
Heat of Vaporization (at NBP) Btu/lbm	306	970
Density, lbm/ft^3	64.8	62.4
Surface Tension, lbf/ft	.0025	.0049
Viscosity, lb/ft-sec	.030	.00055
Specific Heat, Btu/lb °R	.060	1.00

The viscosity ratio at room temperature between propylene glycol and water is 55:1. The relatively high viscosity of propylene glycol results in laminar Reynolds numbers throughout the flow metering region of the nosetip. The change in viscosity with temperature for this coolant is also considerable, which when coupled with change in laminar flow control results in significant changes in flow rate with temperature at a constant pressure drop. The influence of temperature on flowrate is shown by the curves of Figure 2. For both ground test and flight applications this increased sensitivity to temperature changes must be evaluated. Thus, although propylene glycol appears attractive from a coolant utilization standpoint, some significant operational differences between propylene glycol and water are expected (See References (8)and (9) for further discussions of coolant selection criteria and effectiveness characterization).

2.2 Nosetip Design

2.2.1 External Design

The external design of the nosetips used for the alternate coolant testing was the same as used on the nosetips of the Reference 1 study. The nosetips were made from 347 stainless steel platelets which had been diffusion bonded to form a nearly monolithic structure. The nosetip contour, a hemispherical nose radius of 0.65 inches with a half angle of 17° and 1.24 inch base diameter, was selected to provide a direct comparison with the previous data. Two nosetips, SN G-10CT and G-11CT, were fabricated for the test program. A pre-test photograph of nosetip S/N G-10CT is shown on Figure 3.

2.2.2 Internal Design

The two nosetips had identical internal designs. As with all ALRC nosetips, coolant flow control and distribution is achieved by through etched passages in the platelets. Flow control is accomplished in .0008 to .0019 inch thick metering platelets which generally use a branching network to meter and deliver the flow to the distribution passages and thus to the nosetip surface. On ALRC nosetips this metering occurs well below the surface, i.e., out of the

heat affected zone. A 0.200 inch setback from the surface is used on the current generation of 0.65 inch nose radius nosetips.

As with all previous ALRC nosetips, flow collection manifolds were included as an integral part of the design. These collection manifolds allowed the nosetips to be cold flow calibrated to define the relationship between pressure drop and flowrate in each of 15 independent hydraulic sections. The relationship between hydraulic section number, nosetip surface distance, and exit flow rate is shown on Table III. The collection manifolds are machined off the nosetip when the contour is machined.

2.3 Cold Flow Test Results

Both nosetips were cold flow tested at ALRC prior to being shipped to AEDC. The cold flow test results from nosetips S/N G-10CT and G-11CT are summarized on Figures 4 and 5, respectively. The nosetips were flow tested at nominal pressure drops of 100, 500, and 1000 psi with water and at a pressure drop of 1000 psi with propylene glycol and the flow from each of the 15 axial nosetip hydraulic sections was collected and measured. The data shown on the figures is presented in terms of the measured section flow rate over the design (predicted) section flow rate at a pressure drop of 1000 psi for both water and propylene glycol. For nosetip G-10CT the data show that most hydraulic sections flowed from approximately .65 to 1.35 times the predicted value. With the exception of Section 1 (which has a design coolant flow rate which produced overcooling compared to the ideal value by a factor of greater than 5), section 7 and section 14, the propylene glycol flow distribution is more uniform than the water flow distribution. The median flow factor was approximately 1.1 for water and 1.0 with propylene glycol. On a total flow basis the measured flow was 9% higher than that predicted for water and 12% higher than that predicted for propylene glycol.

The flow factors shown on Figure 5 for nosetip S/N G-11CT show similar results to those for nosetip S/N G-10CT, except that the flowrates with propylene glycol were less than the design values in the first four hydraulic sections. This lower than designed flow in the stagnation region on nosetip G-11CT may have contributed to

TABLE III

ALTERNATE COOLANT TIP HYDRAULIC
DESIGN MODIFICATION - PLATELET THICKNESS

SEC	ROWS	SURFACE DISTANCE, INCHES	PLATELET NO.	THICKNESS	$\dot{W}_{P.G.}$ (LBM/SEC) ΔP = 1000 psi	PLATELET ART WORK
1	0,1,2	0-.045	110, 119 102, 104 106 108	.0017 .0016 .0014 .0019	.00194	"Rev. A"
2	3,4,5	.045-.090	121 123	.0008 .0010	.00072	Track G Series 2 Platelet Design
3	6,7,8,9	.090-.148	125 127	.0012 .0012	.00236	
4	10,11,12, 13	.148-.206	129 131	.0014 .0013	.00303	
5	14,15,16, 17	.206-.262	133 135	.0014 .0014	.00361	
6	18,19	.262-.290	137	.0014	.00177	
7	20,21	.290-.317	139	.0014	.00181	
8	22,23	.317-.342	141	.0014	.00170	
9	24,25	.342-.368	144	.0013	.00142	
10	26,29	.368-.393	147	.0012	.00112	
11	28,29	.393-.418	150	.0012	.00115	
12	30,31	.418-.442	153	.0012	.00123	
13	32-39	.442-.534	155-163 166-178	.0012 .0011	.00354	
14	40-46	.534-.613	182-186 191-206	.0012 .0011	.00208	
15	47-60	.613-.818	210-236 240-262	.0009 .0008	.00205	

some increased stagnation point recession between Track stations X34 and X40 on test 5751 compared to test 5749 with nosetip C-10CT. The measured test stagnation region data indicated only slight temperature differences between the two tests.

2.4 Test Matrix and Test Conditions

The Track G test matrix for the two nosetips is shown on Table IV. The only operational difference between the three tests was the coolant flow rate. The flow rate on Test 5749 was significantly less than planned in the latter portion of the Track, as can be seen from Figure 6.

A flowrate increase was planned for the second test based on an evaluation of the data from the first test which indicated temperatures above the design values, as implied by some observed material loss. However, this increased flowrate was not realized. On the third test, test 5768, a substantial flowrate increase (somewhat greater than desired) was achieved. The test flowrates, as a function of time for all three tests, 5749, 5751 and 5768, are shown on Figure 6. Also shown on the figure is the minimum water flowrate from the previous test series. The pronounced difference in shape of the three curves is caused, in part, by the different propellant loading combinations used in the AEDC coolant pressurization subsystem. The lower coolant flow rate for these tests (particularly tests 5749 and 5751) compared to the test with the reference water cooled nosetip is evident from an inspection of the figure. For test 5749 the propylene glycol flow rate reduction relative to water was approximately 66%. (This compares to a flow rate reduction based on the coolant screening tests of 80%). On test 5768 the flow rate reduction compared to the minimum water flowrate test varied from 40% at 5 ms to 14% at 55 ms. Neither the water nor the propylene glycol nosetips had the optimum coolant distributions needed to make direct comparisons of actual coolant requirements. Based on the data from tests 5749 and 5751 a coolant reduction of over 50% appears possible with propylene glycol, as will be discussed in the following sections.

The logic path used during the testing compared to the pre-test logic diagram is shown on Figure 7. The first test (5749) was successful in that the flow rates were less than one half the

TABLE IV

TRACK G TEST MATRIX

TEST	TIP S/N	P_{CELL} (TORR)	INITIAL VELOCITY (KFPS)	WEATHER CONDITION	RANGE ENTRY COOLANT FLOWRATE	OBJECTIVE
5749	G-10 CT	350	17	Clear Air	.150 lbm/sec	Determine the amount of coolant reduction possible compared to water cooled nosetip
5751	G-11 CT	350	17	Clear Air	.134	Determine the amount of coolant reduction possible compared to water cooled nosetip
5768	G-10 CT	350	17	Clear Air	.230	Determine the amount of coolant reduction possible compared to water cooled nosetip

water flow rate and test data were obtained. The second test (5751) was planned to have increased flow rates compared to the first test, however the actual flow rate was within 10% of the test 5749 flow rate (Nosetip S/N G-11CT used on test 5751, was not recovered after the test). A review of the test data - laser photographs, x-ray photographs, and thermal plots - indicated that this test was essentially a repeat of test 5749, except at Station 41 (Track exit). At this station the photographs indicated substantially more material removal than was observed on Test 5749 (See Figures 12 and 13). This may have been due to a further 15% flow reduction at this station on test 5751 compared to test 5749. Because of the nearly identical flow rates on tests 5749 and 5751, additional information regarding temperature versus flow rate was not obtained from Test 5751. However, the ability to essentially repeat the thermal behavior on two nosetips tested at the same conditions did provide valuable verification of nosetip-to-nosetip thermal performance repeatability.

The free stream and nosetip stagnation conditions for these tests as predicted by ASCC-80, are shown on Figure 8. As can be seen the Mach number, stagnation enthalpy and stagnation pressure decay significantly during the test, and, consequently, cause a decrease in heating rate. However, the coolant flowrates also decay significantly during the test. These two influences, decreasing non blowing heating rate and decreasing coolant flow with time, tend to compensate one another. The combined effect is a predicted increase in peak heating (considering blowing and downstream cooling influences) from Track entrance to Track exit stations on tests 5749 and 5751 of approximately 9% and an increase in peak heating on test 5768 of 13%.

The non-blowing heat flux distribution predicted by ASCC-80 at range exit for the initial and final nosetip shapes are shown on Figure 9. The influence of the observed shape change which occurred during the test (5749) had a significant impact on the heating rate in the near stagnation point region (to a surface distance of .15 inches). The final shape from test 5749 was identical to the initial shape for test 5768.

2.5 Track Test Results

The results from the Track G tests include both nosetip thermal and recession data, in addition to the nosetip flowrate and test condition data presented previously. Thermal data was available from three stations, IC20, IC29, and IC41 on test 5749*, from stations IC11, IC20, IC29 and IC41 on test 5751 and stations IC20 and IC29 on test 5768[1]. The data from these three tests are summarized on the following table V[2].

TABLE V

NOSETIP TEST DATA SUMMARY

NOTE: ND = No Data
All Temperatures ± 200°R
* Sensing Level = 3000°R
** Sensing Level = 2430°R

Test No.	Nosetip S/N Configuration	Flow Rate, lbm/sec Ent.	Exit	IC4	IC11 (15 ms)	IC20 (25 ms)	IC29 (40 ms)	IC41 (55 ms)	Comments
				Station Temperature Data, °R					
5749	G10CT/Hemisphere Propylene Glycol	.15	.038	ND	ND	2400-2700 Stag Flare	2160-2520 Stag Flare	2350-2750 Stag	.045" Material Loss Over Most of Tip Much Flare
5751	G11CT/Hemisphere Propylene Glycol	.134	.036	ND	2380-2740 Stag 2430 Ring at 20-30°	2340-2700 Stag 2700 Spots at 10-20°	2300-2700 Entire Tip	2250-2650 Entire Tip	Nosetip Not Recovered Temperatures and Flow Rates Similar to Test 5749, Flare all Stations
5768	G10CT/Hemisphere Propylene Glycol	.23	.09	ND	All Below Sense Level*	2400-2800 Near Center**	2600-3000 Near Center 2340-2900 Base Region	ND	Second Test on Nosetip G10CT, Station 29 Data Best of Test Series, No Flare

As can be seen from the data contained on the above summary table, tests 5749 and 5751 yielded very similar results. During both tests there was a significant amount of flare. The station IC41 data on test 5749 and Station IC11 and IC41 data on test 5751 are probably the best data on those two tests and indicated

Note [1] See Tables V, VI, and VII for descriptions of station locations.
Note [2] A comprehensive data compilation may be found in Reference 10.

2400-2700°R temperatures. Data from test 5768 show Station IC20 peak thermal data are similar to that observed in the previous tests, even though the coolant flow rates were significantly higher. Station IC29 data from this test indicates higher temperatures then evidenced in the previous tests. However, these higher temperatures are localized at the stagnation point and in the base region. A cold surface (below the 2160°R sensing level) was indicated between the stagnation region and base region. The IC station 29 data from test 5768 at is probably the best thermal data of tne test series. However, Test 5768 was conducted with a previously tested nosetip (nosetip G-10CT was also used on test 5749). The x-ray photographs show a substantial local material loss occurred on test 5768 at an angle of from 5 to 25° off the stagnation point, extending over a circumferential distance of approximately 30°. This mass loss was probably caused by local flow starvation due to internal or external flow blockage, a consequence of the carbon deposited on the tip during cool down on the previous test. Thus the higher measured temperatures on test 5768 may have been a result of local coolant flow reductions, even though the total flow rate was higher than on previous tests. The use of a previously tested nosetip posed two problems which should be avoided in the future: (1) the flow distribution was altered from the as-built condition and; (2) the material loss on the second test was difficult to define because of a lack of a valid reference point. The first of these two problems could be partially overcome by a thorough cleaning and dehydration immediately following the test. (Currently the AEDC test facility is not setup to do this). The second problem may be overcome by defining a nosetip contour reference point on the nosetip stem. This reference point should be at the origin of the nosetip hemispherical arc radius and all recession measurements should be referenced to this arc. For substantial nosetip coolant slot blockage or non-hemispherical shapes resulting from previous tests, light machining and electro polishing would both remove the blockage and provide a better defined nosetip contour, i.e., allow improved subsequent recession measurements and produce more nearly designed heat flux profiles.

2.5.1 Tests 5749 and 5751

Data from tests 5749 and 5751 are contained in Appendix A. These data include laser and x-ray photographs, and image converter camera thermal plots. As was mentioned previously the thermal test data is somewhat distorted due to model flare, a probable consequence of the low flow rates on these tests. These two tests were essentially identical in terms of coolant flow rates and the resulting thermal response. The nosetip used on test 5749, S/N G-10CT, was recovered and thus post test inspection was possible. The nosetip used on test 5751, S/N G-11CT, was not recovered and thus no post test inspections could be performed. For this reason the analysis concentrated on a discussion of test 5749 however, the data was treated as a composite from tests 5749 and 5751. A post test 5749 photograph is shown on Figure 10 and pre and post contour comparisons are shown on Figure 11. The post test photographs shows some local axial depressions on the nosetip surface in the downstream region. The pre and post test contours shown on Figure 11 indicate up to about .050 of material was removed. Material removal appeared to be greatest near the stagnation point (S = .075 to .150 in.) and near the 45° (sonic) point. In flight nosetip contours for Test 5749, shown on Figure 12, indicate that some very minor shape change may have occurred as early as Station X7 but that most of the shape change occurred between Stations X18 and X28. Inflight nosetip contour data for test 5751 is shown on Figure 13. These data indicate similar shape changes occurred on test 5751, except at Station X40. The Station X40 contour shows more material removal on Test 5751 than on Test 5749. This may be the result of lower flow rates at X40 on Test 5751 and lower than design stagnation region hydraulic admittances. The composite thermal data from all available stations is shown on Figure 14 along with the predictions from the downstream cooling (DSC) code at Stations IC11 (15 ms) and IC41 (55 ms). These data indicate the predicted temperatures are lower than the measured temperatures in the stagnation region. However, the model predicts temperatures in the melt region over

much of the nosetip, which appears consistent with the observed recession data.

Temperature data downstream of approximately S = .3 in. is not available. The observed model flare, the temperature sensitivity range of the IC units, and the melting point of the 347 stainless steel nosetip combine to obscure the real nosetip surface temperature. Therefore, the data analysis and computer code calibrations were limited to ascertaining if the observed test results, including measured recession, post test nosetip inspection (Test 5749) and thermal trends were in general agreement.

The stagnation point thermal data shown on Table V indicates nearly constant temperatures between Stations IC11 and IC41. The expected trend would be increasing temperature with increasing Track station number due to the nosetip thermal transient response. However, Station IC4 data (5 ms) is needed for a better assessment of early time heating to accurately define nosetip thermal response. Also, determinations should be made of the actual flow rate initiation at the surface of the nosetip to define the length of time, if any, that the nosetip remains uncooled.

The measured nosetip recession and post test inspection indicated the nosetip surface was at or near the melt temperature over most of the surface at some time during the tests. Temperature predictions made using the downstream cooling code were shown on Figure 14 and indicated that the nosetip was at or near melt at 55 ms over most of the surface ($S > .35$ in). At 15 ms (Station 11) the prediction indicated melt conditions from S = .63 to S = .75 inches. This should be a conservative prediction since it is based on a steady state analysis. For both times the code predicted a relatively cold stagnation region. The stagnation region has historically yielded higher test temperatures than the various codes predicted. The current nosetip thermal performance code (DSCC), is amenable to calibration based on mechanistic relationships. The code could thereby be correlated with the stagnation region thermal test data, thus enhancing the applicability of the code. Two possible techniques could be used for this calibration. One technique would be to reduce the amount of cooling effectiveness in the stagnation

region based on considerations of the amount of coolant flow which is predicted to remain in the boundary layer. This assessment could be based on coolant to boundary layer momentum ratio considerations. A second technique, which could be used in conjunction with the first technique, is to use a stagnation point roughness augmentation factor which decreases with distance as the influence of uniform blowing mitigates the surface roughness influence.

Stagnation point surface roughness heat flux augmentation factors of 2 to 3 are predicted by the ASCC-80 code for the nosetip. When the downstream cooling code was used to correlate results from the ABRV Series II tests (Reference 1) a smooth wall assumption with local blockage based on vaporized coolant flow provided the best correlation in the downstream regions, but underpredicted the stagnation point. Data exists (Reference 11), and was cited in Reference (1), which suggests that blowing mitigates roughness influences. However, the reduction in roughness augmentation is probably a cumulative effect and may require 3 to 10 injection points and subsequent boundary layer buildup to reduce the augmentation to zero. Thus, calibration of the code at the stagnation point in a mechanistic manner appears to be an achievable goal for future consideration.

The downstream cooling code has been modified to include propylene glycol properties in addition to water properties. However, high temperature characteristics, such as energy absorption due to chemical dissociation, were not available. Therefore, to characterize the cooling capability of propylene glycol estimates of the effective energy absorption relative to water were made based on molecular bond energy estimates. For high temperature boundary layers an effectiveness of 1.5 to 2 times water was estimated. The downstream cooling model thus used propylene glycol properties for the analysis but used an effective heat capacity for the high temperature region of 1.5 that of water. In addition, since the track tests were conducted at pressures above the critical pressure of propylene glycol over a substantial portion of the nosetip, the coolant vaporization calculations were suppressed. These modifications to the code resulted in the predictions previously shown on Figure 14.

These predictions, when modified to include the updated stagnation region model discussed previously, should yield results which provide adequate correlation to the existing test data. Further model improvements to better characterize high temperature propylene glycol cooling effectiveness and operation above critical pressure are, of course, recommended. However, test data for a wider range of conditions and of better quality than is currently available is needed to justify much additional modeling effort.

2.5.2 Test 5768

Test 5768 was the second test using nosetip S/N G-10CT. The flowrates for this test were substantially higher than on tests 5749 or 5751. Higher flow rates were used in an attempt to reduce a suspected nosetip early heating problem due to flow initiation delay or blast tank effects. Thermal data was available from only two Track stations, IC29 and IC41, on this test and the data indicated the same or slightly higher temperatures in some local regions near the stagnation point and at the base than were measured on Tests 5749 or 5751. However, the use of a previously tested nosetip and the reduction of model flare possibly contributed to the observed higher nosetip temperatures. The altered shape caused by recession on Test 5749 changed the heat flux distribution as was shown on Figure 9 and the coolant flow distribution was also altered. (Cold flow results indicated a 10% decrease in hydraulic admittance (flow rate) as a consequence of test 5749).

The thermal data from test 5768 is shown on Figure 15 together with the downstream cooling code predictions for Stations IC20 (25 ms) and IC29 (40 ms). The data show the hot stagnation region and, for Station 29, a hot region near S = .6 inches. The model predicts a hot region near S = .6 but, as on Tests 5749 and 5751, does not predict the hot stagnation region.

The inflight and post test nosetip recession data for test 5768 are shown on Figures 16 and 17, respectively. A post flight photograph is shown on Figure 18. The data on Figure 16 show negligible shape change (.010 in.) during the test. However, comparison of the post test nosetip profiles from test 5768 (Figure 17) with the post test profiles from test 5749 (Figure 11) indicate some

material loss in a local circumferential region 5 to 25° from the stagnation point. Based on the inflight laser photographs (Appendix B) this material loss had started prior to Station IC11 and was probably the result of local flow starvation. As mentioned previously, the determination of recession on a previously used nosetip with prior recession is difficult. A reference arc based on the original nosetip radius with the reference origin located at the original center point of the un-recessed hemisphere will greatly enhance the recession data usefulness. The apparent lack of any further recession on Test 5768, except for the local region near the stagnation point, tends to support the temperature prediction of reduced heating on this test compared to tests 5749 and 5751. The measured higher temperatures near the stagnation region on this test are probably caused by local flow starvation in the observed area of additional nosetip recession. The high temperatures near the base region may also have been present on tests 5749 and 5751, but were masked by flare on those tests.

3.0 CONCLUSIONS AND RECOMMENDATIONS

The following conclusions and recommendations resulted from the testing and data analysis of the propylene glycol cooled nosetips.

3.1 Conclusions

- Propylene glycol appears to offer a significant (~50%) increase in cooling efficiency compared to water.

- The cooling code provides a fair correlation with the test data, however, a larger and more precise empirical data base is needed to further improve the code.

- Additional code updates for stagnation region heating are needed and basic analytical or empirical studies of high temperature propylene glycol properties (including super critical pressure operation) are required to allow increased confidence in code extrapolations to flight conditions.

- o The Track G data acquisition systems don't currently provide sufficient temperature measurement stations and a sufficiently low threshold temperature to allow the resolution desirable for data correlations.

- o Repeat tests of nosetips that have had significant shape change and/or whose flow distribution has been altered significantly from the as built condition may produce unreliable data.
- o The properties differences between propylene glycol and water, particularly the viscosity, need to be evaluated from a systems standpoint.

3.2 Recommendations

- o The nosetip test data base should be expanded to provide more detailed information on the cooling effectiveness of propylene glycol. The tests should include both Track G (with increased thermal data resolution)and also more basic tests (or analytical efforts) to quantify the decomposition kinetics of propylene glycol.

- o Various cooling code updates and calibrations to an improved data base should take place as data become available (some basic code improvements could begin without further data generation).

- o A study which includes long term storage and flight systems applications should be initiated for nosetips using propylene glycol.

- o Re-test of nosetips for detailed data trend definition should be limited only to those whose surface contours and hydraulic behavior are well defined.

REFERENCES

1. Lee, T. G., et. al., Advanced Ballistic Re-Entry Vehicle (ABRV) TCNT Development Program, ReportNo. 290770-004-001, April 1980

2. Taki, Y., "Test Plan for ACTD Testing of a Molybdenum Nosetip in the AEDC Track G Facility", ALRC TAR 9751:0940, 16 February 1983

3. Walker, R. E., and Taki, Y., "Active Cooling Technology Development Program (ACTD) Transpiration Cooled Nosetip Shape Optimization Study Final Report", ALRC TAR 9751:0956, 21 March 1983

4. Lee, T. G., Ward, T. E., and Chester, R. W., Transpiration Erosion Nosetip Development, Final Report, Contract No. DNA 001-74-C-0126, 30 November 1976

5. Rothwell, W. S., Brandt, W.E., and Nakashiji, N. Alternate Coolants for Transpiration Cooled Nosetips, Final Report AFRPL-TR-76-27, Contract FO 4611-72-C-0091, 27 April 1976

6. Ito, J. I., Alternate Coolant Study for ACTD Program, ALRC Thermodynamic Analysis Report 9751:0774, 14 January 1982

7. Hidahl, J. W., Coolant Screening Test(s) Plan, ALRC Inter-Office Memo 9776:NT-014, 5 January 1982

8. Hidahl, J. W., "Coolant Screening Test Technical Report", ALRC Inter-Office Memo 9770:NT-057, 19 January 1983

References (cont.)

9. Walker, R. E., Ito, J. I., "Active Cooling Technology Development (ACTD) Program Transpiration Coolant Nosetip Alternate Coolant Study Final Report", ALRC TAR 9751:0966, 29 March 1983

10. "BMO/SDL Impactor Technology Program Range Test (TCNT Phase) (U) Transmittal Notice Data 2-9-83 (U)", Operating Contractor Calspan Field Services, Inc., Arnold AF Station, Tennessee 37389

11. Jaffe, N. A., et al., "Final Technical Report Nosetip Cooling Technology(NCT) Program Investigation of Discrete Injection Cooling", Aerotherm Division/Acurex Corporation Technical Report, SAMCO TR 73-380, October 1973

TABLE VI TEST 5749 TRACK PARAMETERS

SHOT 5749

MODEL WEIGHT = 6.43000D 02GRAMS   MODEL BETA = 8.96100D 01LBS/SQ F   RANGE TEMP. = 5.30170D 02DEG.R
UP RANGE PRESS. = 3.51150D 02TORR   DOWN RANGE PRESS. = 3.51150D 02TORR

RANGE 3 TRACK INSTRUMENTATION	DISTANCE FT.	TIME SEC.	VELOCITY FT./SEC.	PSTAG ATM.	HSTAG BTU/LB.
RANGE ENTRANCE	0.0	0.0	1.69500D 04	1.41404D 02	5.86134D 03
X1	2.55000D 00	1.50442D-04	1.69418D 04	1.41275D 02	5.85578D 03
IC1	2.97300D 01	1.75642D-03	1.68541D 04	1.39898D 02	5.79666D 03
SL1	3.88600D 01	2.29777D-03	1.68248D 04	1.39438D 02	5.77695D 03
L2	5.28600D 01	3.12950D-03	1.67799D 04	1.38732D 02	5.74883D 03
X2	5.41700D 01	3.20754D-03	1.67757D 04	1.38666D 02	5.74402D 03
IC4	9.46300D 01	5.62496D-03	1.66467D 04	1.36638D 02	5.65796D 03
X7	1.50920D 02	9.01089D-03	1.64688D 04	1.33839D 02	5.54033D 03
X10	2.20980D 02	1.32915D-02	1.62503D 04	1.30399D 02	5.39769D 03
IC11	2.32980D 02	1.40331D-02	1.62129D 04	1.29810D 02	5.37347D 03
L11	2.41230D 02	1.45419D-02	1.61874D 04	1.29409D 02	5.35699D 03
DOV3	3.05150D 02	1.85087D-02	1.59911D 04	1.26320D 02	5.23095D 03
X15	3.12670D 02	1.89782D-02	1.59682D 04	1.25958D 02	5.21630D 03
X16	3.77800D 02	2.30763D-02	1.57710D 04	1.22857D 02	5.09136D 03
IC19	3.93110D 02	2.40470D-02	1.57249D 04	1.22134D 02	5.06243D 03
L19	3.98110D 02	2.43649D-02	1.57100D 04	1.21899D 02	5.05304D 03
X23	4.72670D 02	2.91376D-02	1.54880D 04	1.18420D 02	4.91483D 03
L24	4.92980D 02	3.04497D-02	1.54281D 04	1.17483D 02	4.87787D 03
5 FRAME LASER	5.22160D 02	3.23422D-02	1.53425D 04	1.16145D 02	4.82529D 03
X28	5.77800D 02	3.59837D-02	1.51804D 04	1.13620D 02	4.72652D 03
IC29	5.91480D 02	3.68849D-02	1.51408D 04	1.13005D 02	4.70257D 03
L29	5.98130D 02	3.73226D-02	1.51216D 04	1.12708D 02	4.69102D 03
X34	6.97800D 02	4.39685D-02	1.48367D 04	1.08304D 02	4.52062D 03
L35	7.21300D 02	4.55581D-02	1.47701D 04	1.07282D 02	4.48131D 03
X40	8.17800D 02	5.21385D-02	1.45008D 04	1.03175D 02	4.32394D 03
IC41	8.31480D 02	5.30818D-02	1.44630D 04	1.02602D 02	4.30209D 03
L41	8.41360D 02	5.37648D-02	1.44357D 04	1.02190D 02	4.28638D 03
SL42	8.53730D 02	5.46215D-02	1.44017D 04	1.01677D 02	4.26679D 03
RECOVERY TUBE	8.75240D 02	5.61163D-02	1.43427D 04	1.00788D 02	4.23294D 03

TABLE VII TEST 5751 TRACK PARAMETERS

SHOT 5751

MODEL WEIGHT = 6.45000D 02GRAMS MODEL BETA = 9.21960 01LBS/SQ F RANGE TEMP. = 5.34040 02DEG.R
UP RANGE PRESS. = 3.49050 02TORR DOWN RANGE PRESS. = 3.49050 02TORR

RANGE 3 TRACK INSTRUMENTATION	DISTANCE FT.	TIME SEC.	VELOCITY FT./SEC.	PSTAG ATM.	HSTAG BTU/LB.
RANGE ENTRANCE	0.0	0.0	1.697000 04	1.408700 02	5.875810 03
X1	2.550000 00	1.502660-04	1.696210 04	1.407470 02	5.870450 03
IC1	2.973000 01	1.754260-03	1.687780 04	1.394310 02	5.813530 03
SL1	3.886000 01	2.294850-03	1.684960 04	1.389910 02	5.794540 03
L2	5.286900 01	3.125320-03	1.680640 04	1.383170 02	5.765520 03
X2	5.417000 01	3.203280-03	1.680240 04	1.382540 02	5.762820 03
IC4	9.463000 01	5.616630-03	1.667820 04	1.363140 02	5.679880 03
X7	1.509200 02	9.003640-03	1.650700 04	1.336370 02	5.566470 03
X10	2.209200 02	1.326540-02	1.629660 04	1.303440 02	5.428720 03
IC11	2.329800 02	1.400490-02	1.626060 04	1.297810 02	5.405320 03
L11	2.412900 02	1.451230-02	1.623610 04	1.293970 02	5.389410 03
GOV3	3.051500 02	1.846650-02	1.604700 04	1.264370 02	5.267570 03
X15	3.126700 02	1.893440-02	1.602480 04	1.260910 02	5.253400 03
X16	3.778000 02	2.301710-02	1.583470 04	1.231180 02	5.132490 03
IC19	3.931100 02	2.396390-02	1.579030 04	1.224250 02	5.104480 03
L19	3.981100 02	2.430050-02	1.577590 04	1.221990 02	5.095380 03
X22	4.726700 02	2.905210-02	1.556170 04	1.188590 02	4.961450 03
L24	4.929800 02	3.035800-02	1.550390 04	1.179590 02	4.925610 03
5 FRAME LASERS	5.221400 02	3.224110-02	1.542130 04	1.166740 02	4.874600 03
X28	5.778800 02	3.586370-02	1.526480 04	1.142460 02	4.778740 03
IC29	5.914800 02	3.675990-02	1.522650 04	1.136540 02	4.755480 03
L29	5.981100 02	3.719490-02	1.520800 04	1.133680 02	4.744240 03
X34	6.978000 02	4.380110-02	1.493270 04	1.091270 02	4.578500 03
L35	7.213800 02	4.538020-02	1.486830 04	1.081410 02	4.540340 03
X40	8.178900 02	5.119150-02	1.460780 04	1.041750 02	4.387070 03
IC41	8.314800 02	5.285150-02	1.457130 04	1.036210 02	4.365770 03
L41	8.413600 02	5.352950-02	1.454490 04	1.032230 02	4.350460 03
SL42	8.537300 02	5.437980-02	1.451200 04	1.027260 02	4.331360 03
RECOVERY TUBE	8.752400 02	5.586280-02	1.445490 04	1.018670 02	4.298340 03

TABLE VIII TEST 5768 TRACK PARAMETERS

SHOT 5768

MODEL WEIGHT = 6.28000 02GRAMS   MODEL BETA = 9.5884D 01LBS/SQ F   RANGE TEMP. = 5.3184D 02DEG.R
UP RANGE PRESS. = 3.5005D 02TORR   DOWN RANGE PRESS. = 3.5005D 02TORR

RANGE G TRACK INSTRUMENTATION	DISTANCE FT.	TIME SEC.	VELOCITY FT./SEC.	PSTAG ATM.	HSTAG BTU/LB.
RANGE ENTRANCE	0.0	0.0	1.66800D 04	1.367320 02	5.680520 03
X1	2.550000 00	1.52878D-04	1.66724D 04	1.366140 02	5.67550 03
IC1	2.973000 01	1.78470D-03	1.65921D 04	1.353540 02	5.622 [illegible]
SL1	3.886000 01	2.33467D-03	1.65652D 04	1.349320 02	[illegible]
L2	5.286000 01	3.17952D-03	1.65240D 04	1.342860 02	[illegible]
X2	5.417000 01	3.25875D-03	1.65201D 04	1.342250 02	[illegible]
IC4	9.463000 01	5.71313D-03	1.64017D 04	1.323680 02	[illegible]
X7	1.509200 02	9.15721D-03	1.62384D 04	1.298 [illegible] 02	[illegible]
X10	2.209200 02	1.34809D-02	1.60376D 04	1.26652 [illegible] 02	[illegible]
IC11	2.329500 02	1.42405D-02	1.60032D 04	1.261 [illegible] 02	[illegible]
L11	2.412300 02	1.47556D-02	1.59797D 04	1.257450 02	[illegible]
IC13	3.051500 02	1.87728D-02	1.57972D 04	1.2291 [illegible] 02	[illegible]
X15	3.126700 02	1.92485D-02	1.57781D 04	1.2258 [illegible] 02	[illegible]
X16	3.778000 02	2.33946D-02	1.55964D 04	1.1974 [illegible] 02	[illegible]
IC19	3.931100 02	2.43762D-02	1.55540D 04	1.1907 [illegible] 02	[illegible]
L19	3.981100 02	2.46973D-02	1.55402D 04	1.188 [illegible] 02	[illegible]
X23	4.726700 02	2.95206D-02	1.53356D 04	1.1567 [illegible] 02	[illegible]
L24	4.929800 02	3.08454D-02	1.52803D 04	1.14 [illegible] 02	[illegible]
5 FRAME LASER	5.221400 02	3.27562D-02	1.52013D 04	1.13 [illegible] 02	[illegible]
X28	5.778000 02	3.64310D-02	1.50516D 04	1.112 [illegible] 02	[illegible]
IC29	5.914800 02	3.73397D-02	1.50150D 04	1.1 [illegible] 02	[illegible]
L29	5.981100 02	3.77809D-02	1.49973D 04	1.104350 02	[illegible]
X34	6.978000 02	4.44786D-02	1.47338D 04	1.063 [illegible] 02	[illegible]
L35	7.213600 02	4.60786D-02	1.46723D 04	1.054530 02	[illegible]
X40	8.178000 02	5.26999D-02	1.44228D 04	1.016 [illegible] 02	[illegible]
IC41	8.314800 02	5.36483D-02	1.43878D 04	1.011490 02	[illegible]
L41	8.413600 02	5.43347D-02	1.43625D 04	1.007700 02	[illegible]
SL42	8.537300 02	5.51958D-02	1.43310D 04	1.002970 02	[illegible]
RECOVERY TUBE	8.752400 02	5.66977D-02	1.42793D 04	9.947950 01	4.195420 03

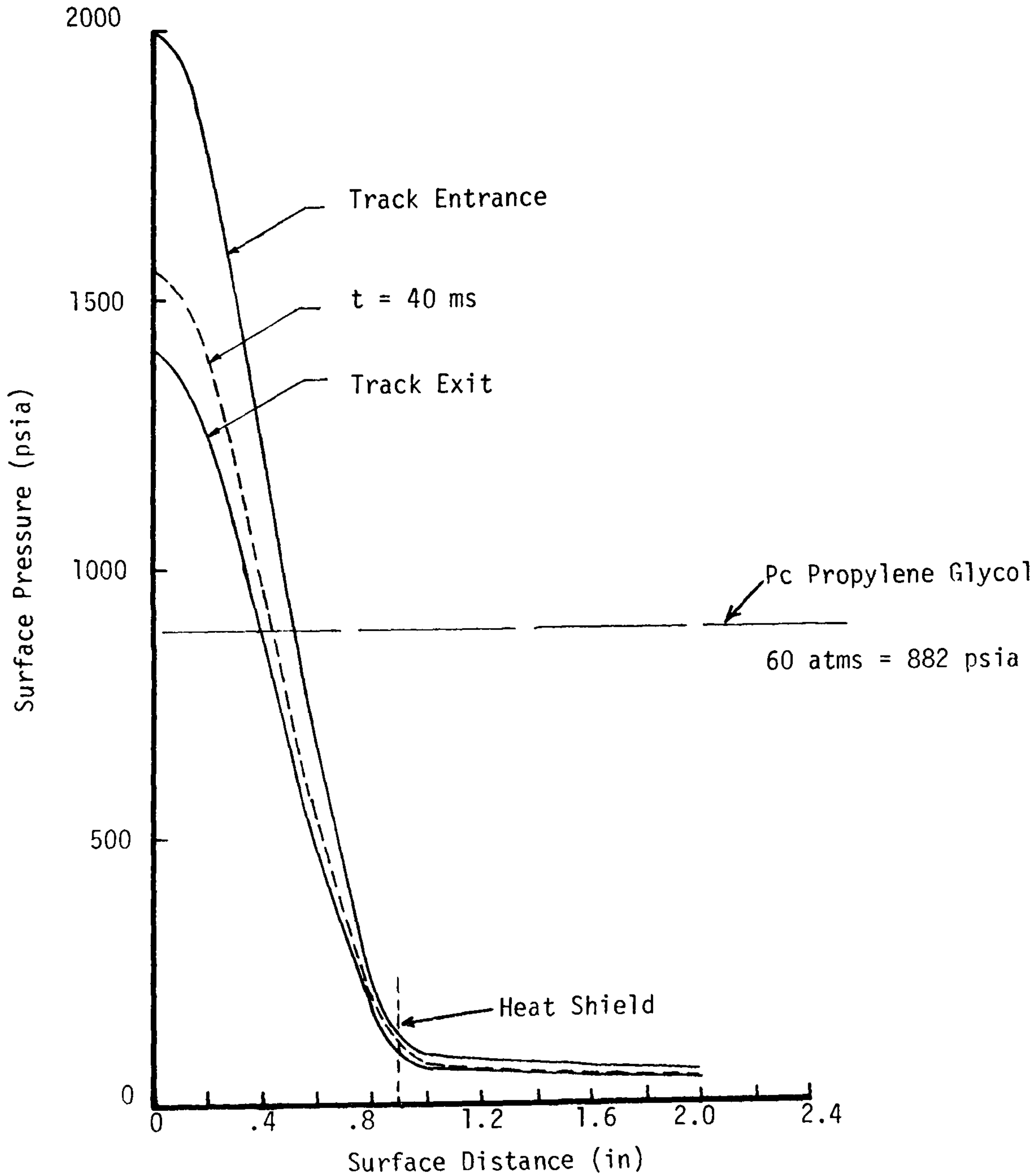

Figure 1. Nosetip Surface Pressure Distributions

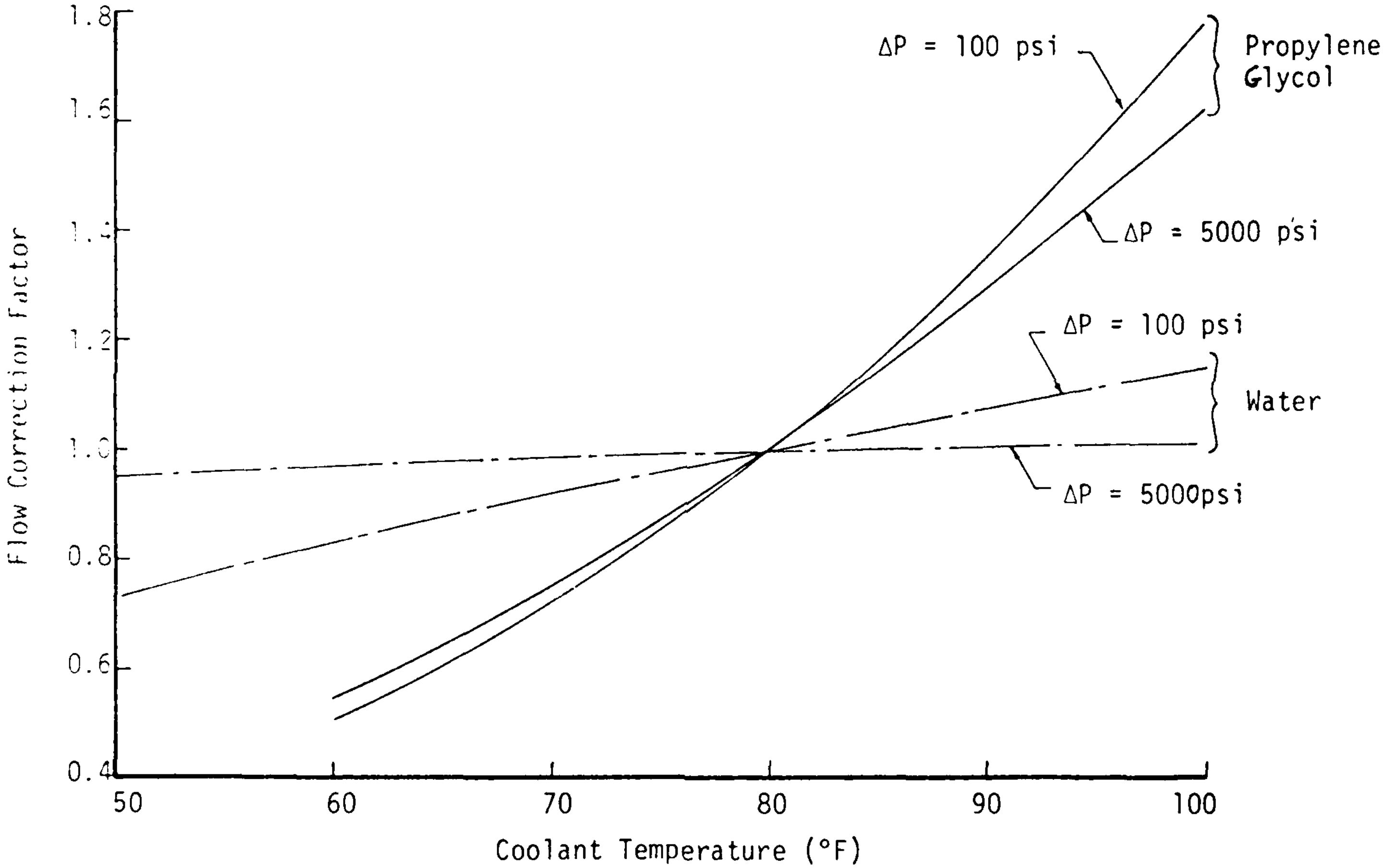

Figure 2. Influence of Coolant Temperature (Viscosity) on Flow Rate for Propylene Glycol and Water

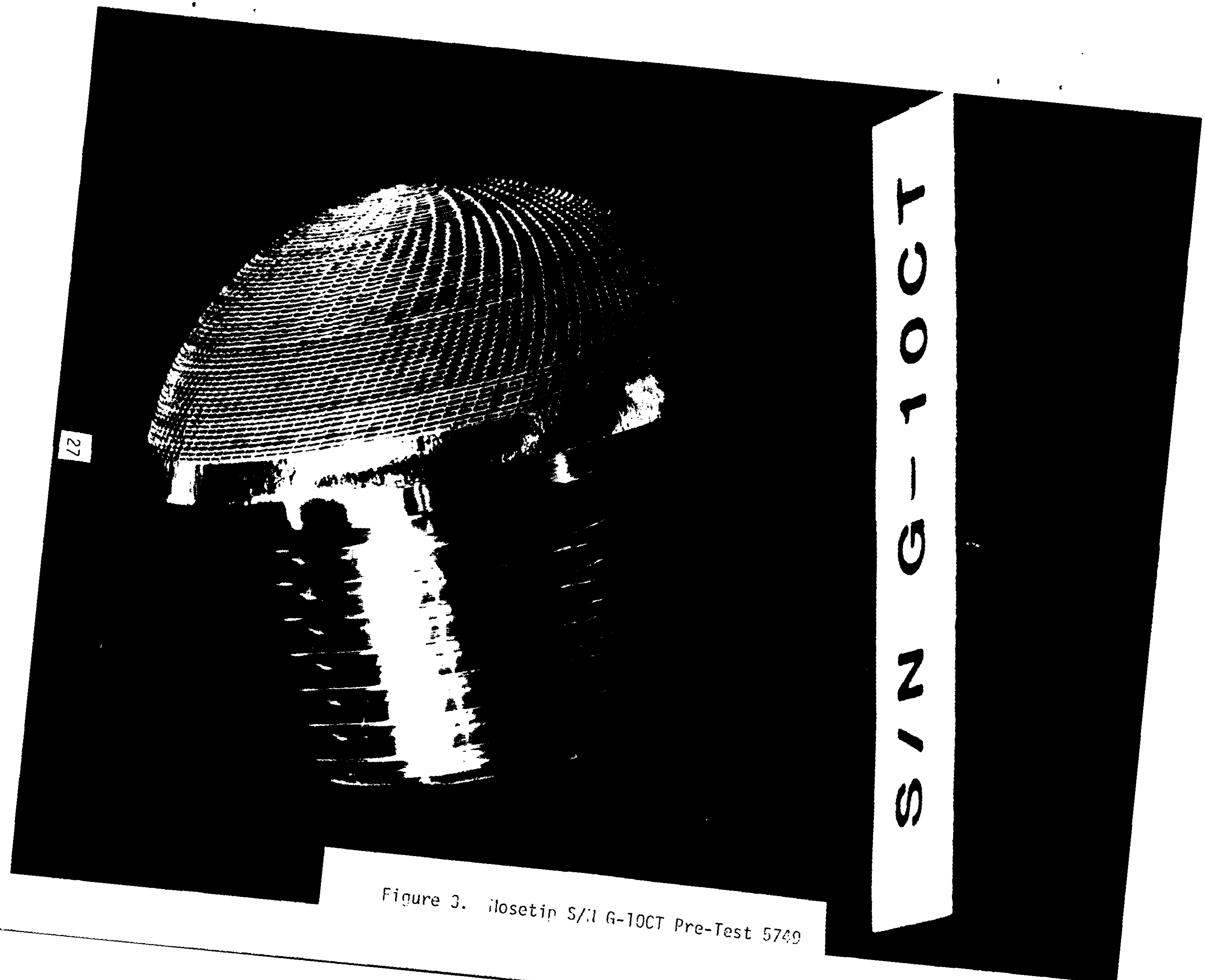

Figure 3. Nosetip S/N G-10CT Pre-Test 5749

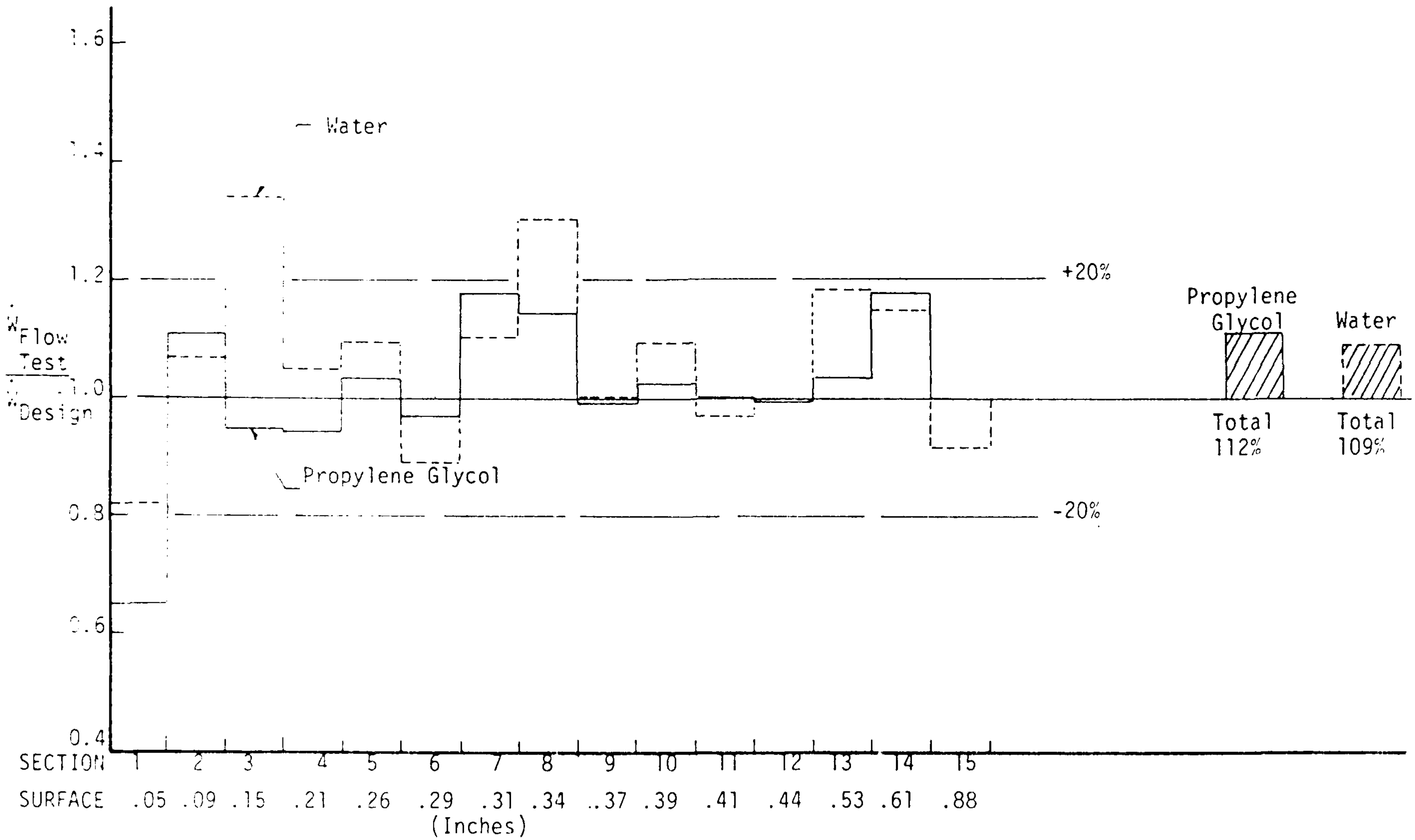

Figure 4. Cold Flow Calibration of Nosetip S/N G-10CT

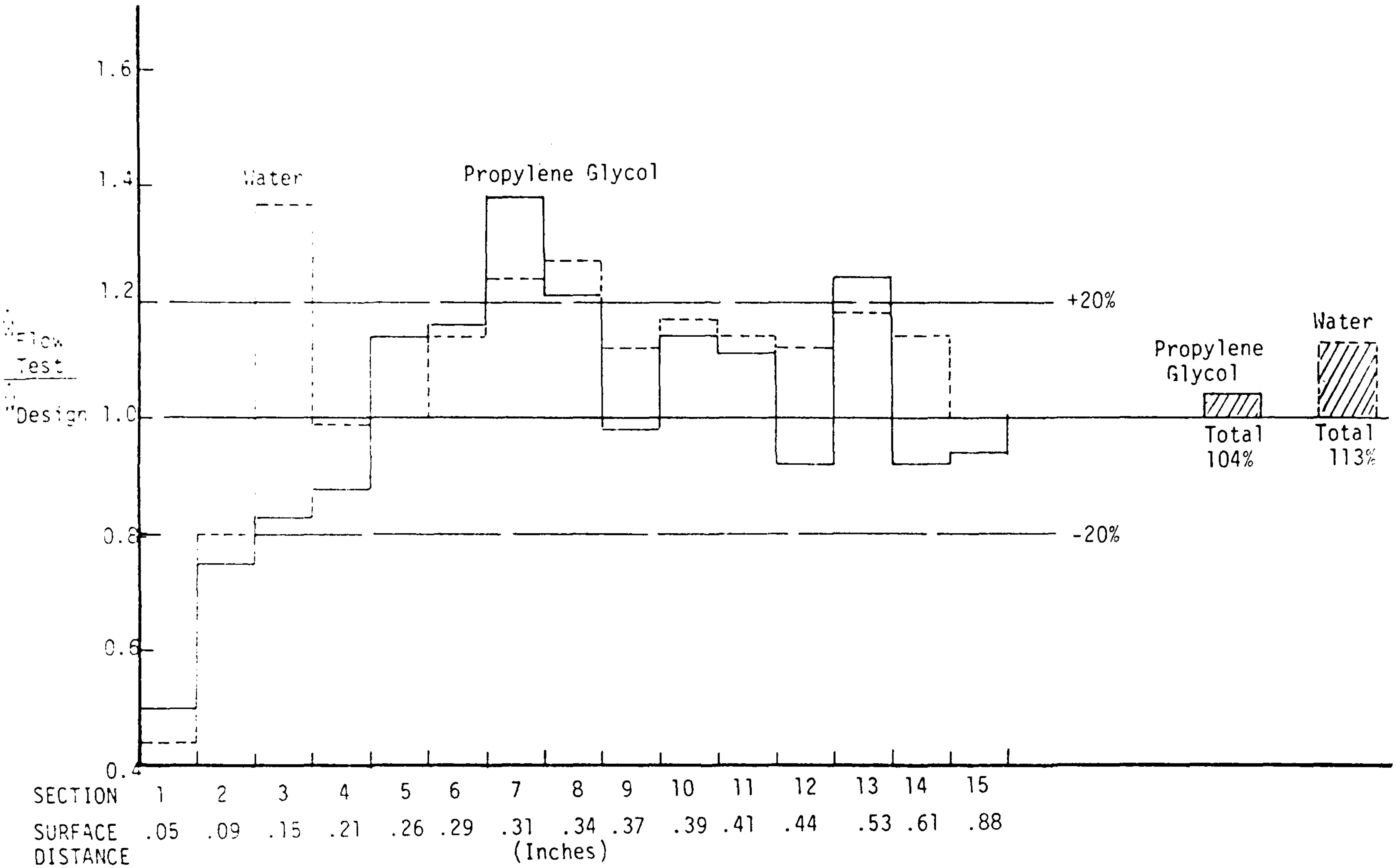

Figure 5. Cold Flow Calibration of Nosetip S/N G-11CT

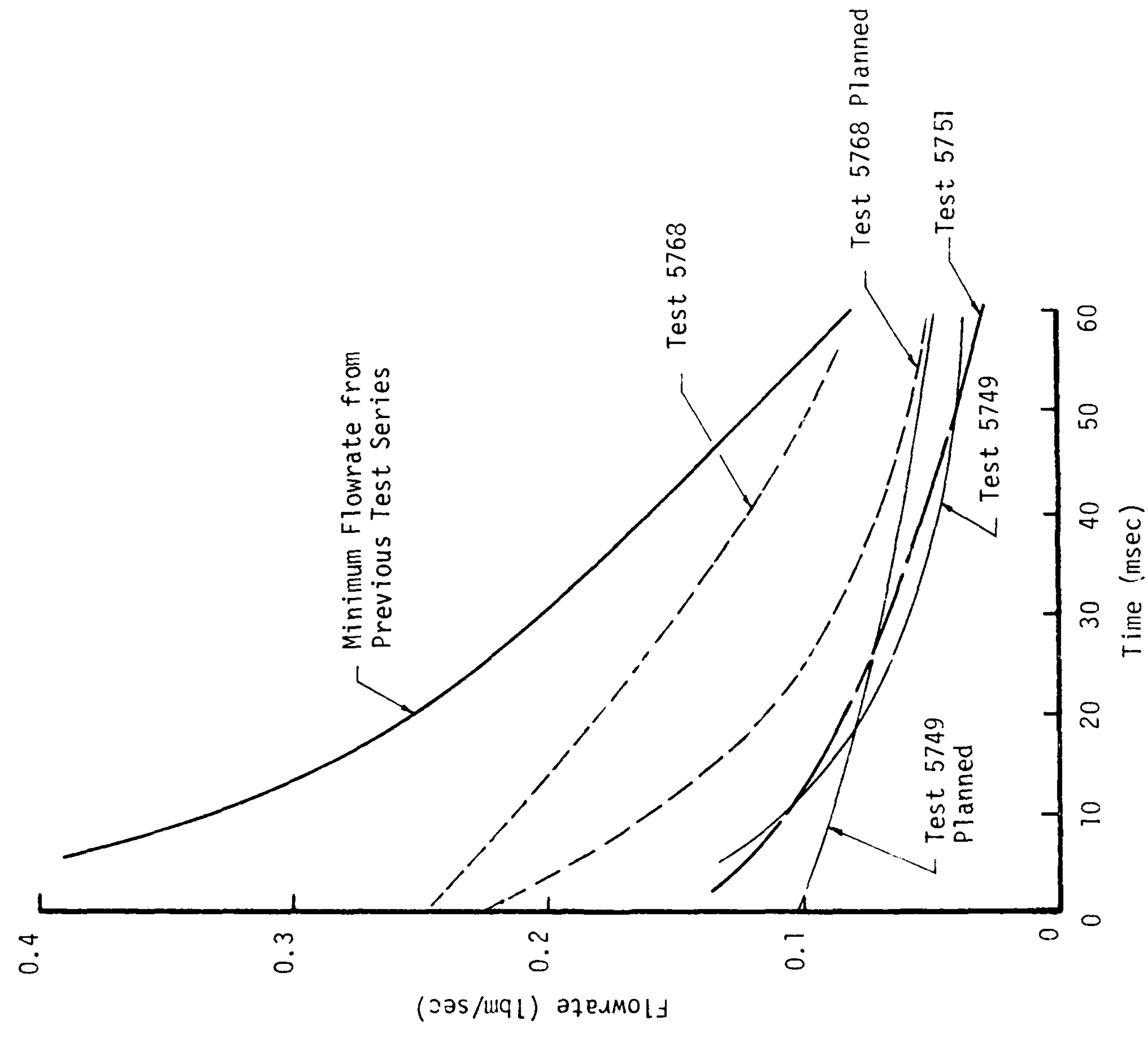

Figure 6. Nosetip Flow Rate Histories

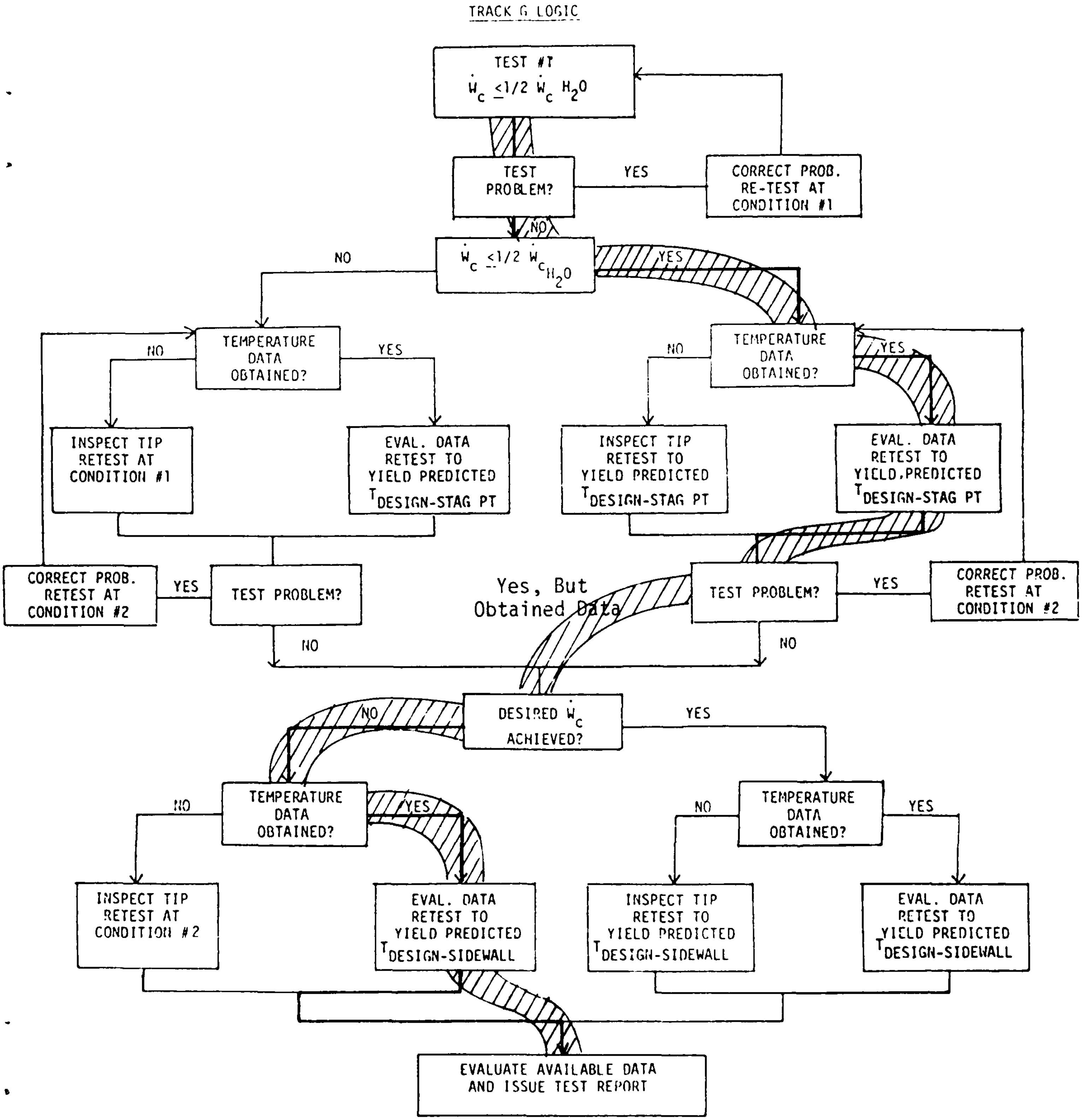

Figure 7. Track G Test Logic

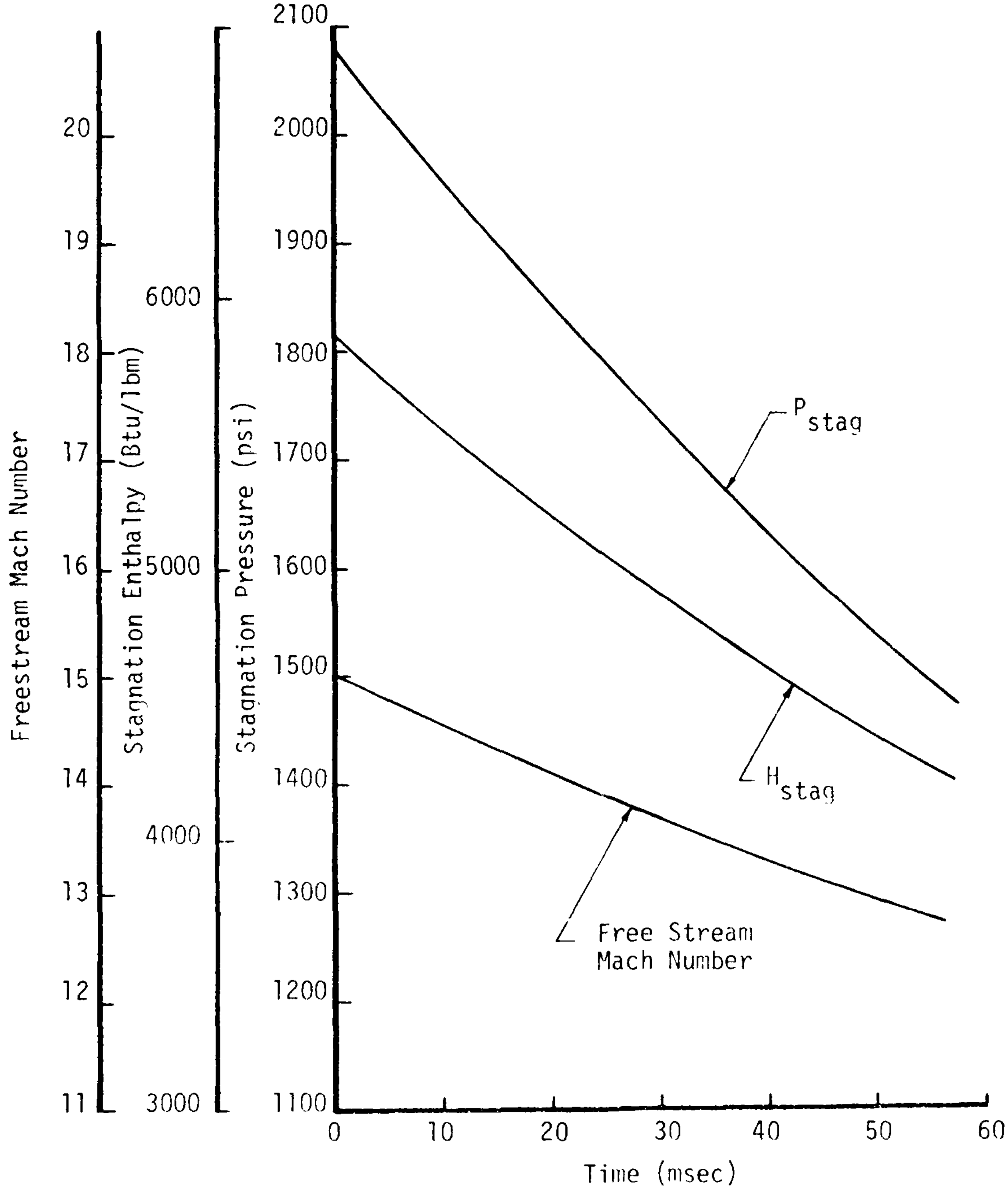

Figure 8. Track G Freestream and Stagnation Conditions

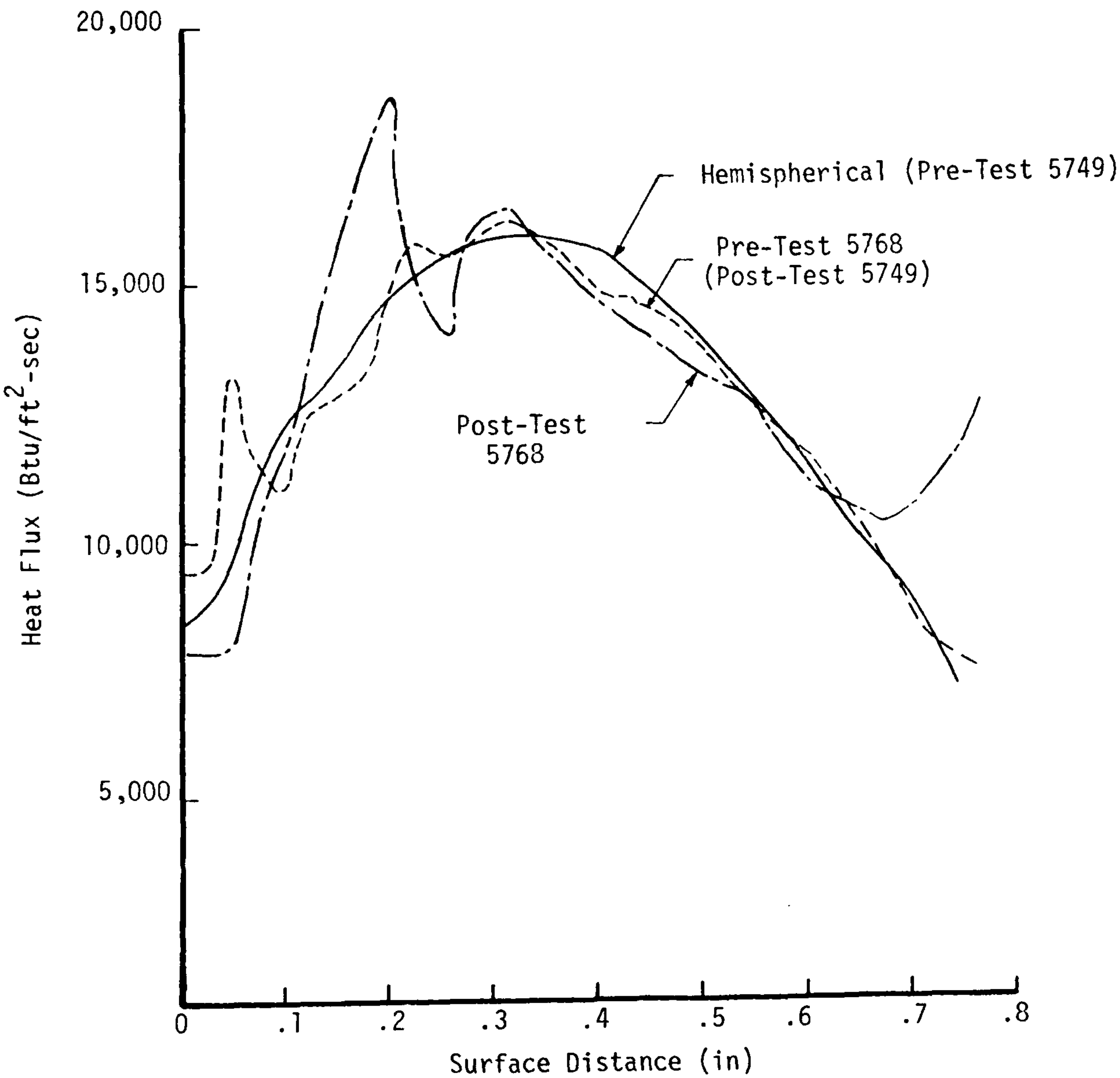

Figure 9. Non-Blowing Heat Flux Profile Comparisons, Track Exit

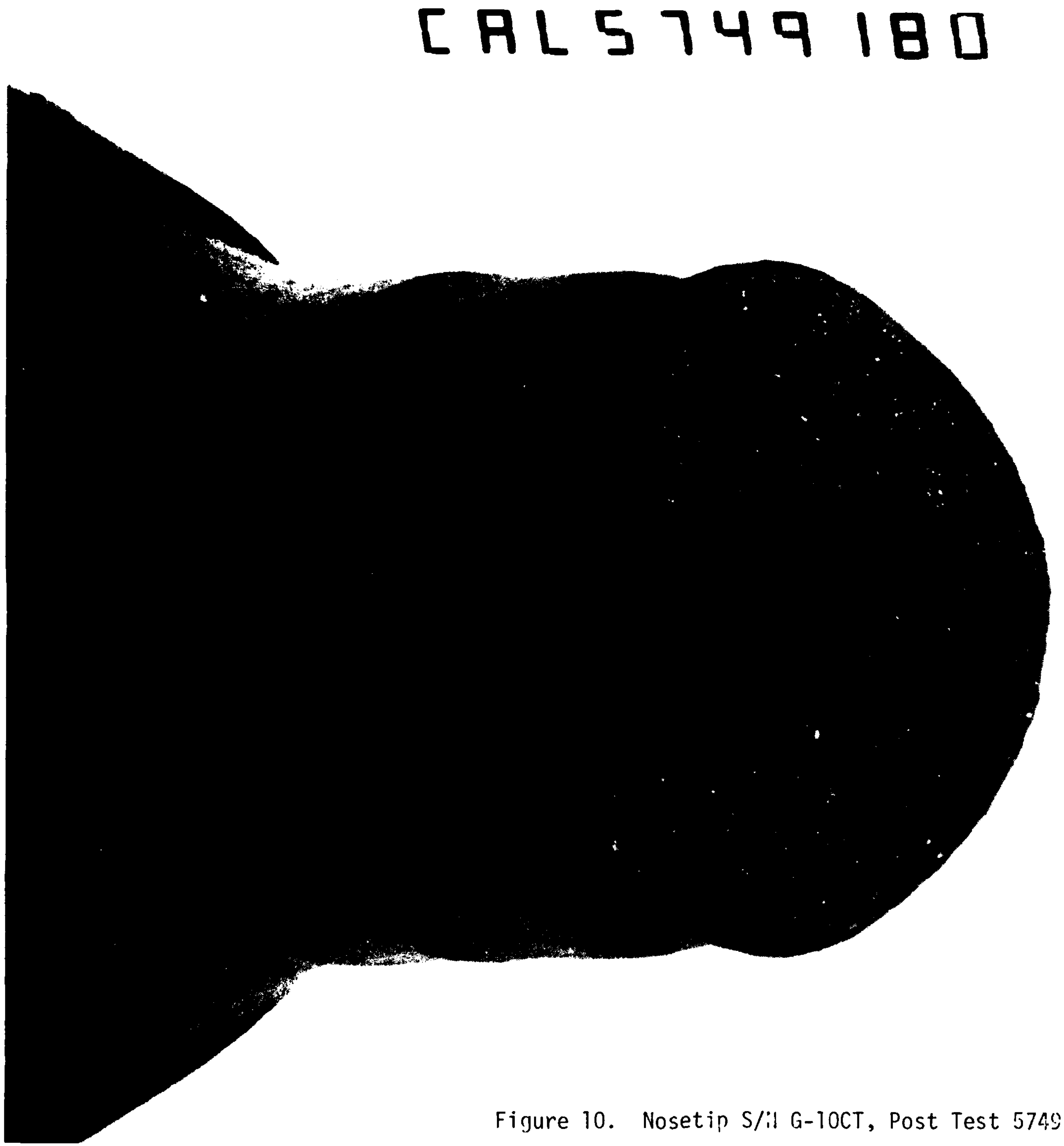

Figure 10. Nosetip S/N G-10CT, Post Test 5749

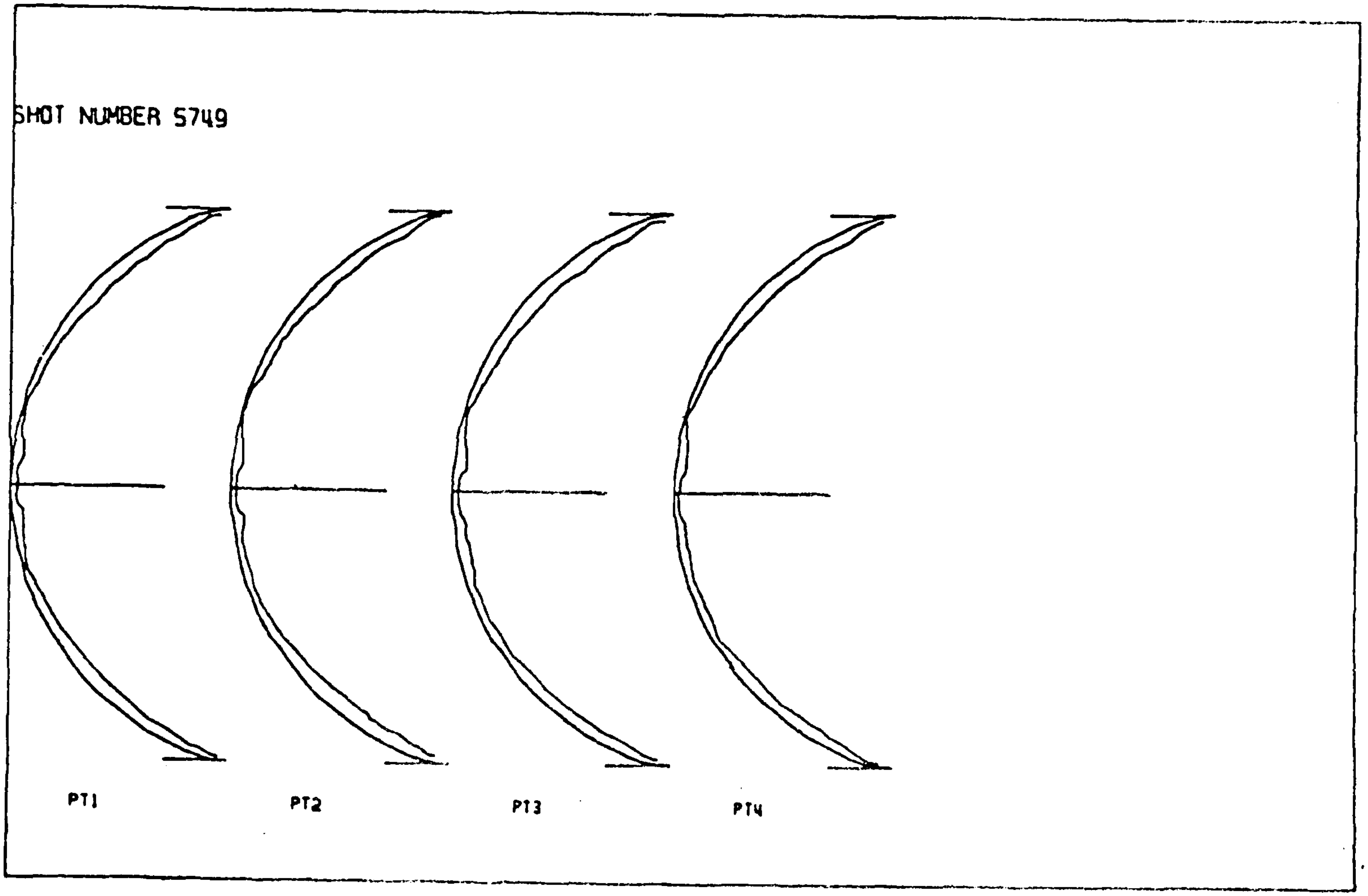

Figure 11. Post-Test 5749 Nosetip Contour Comparison

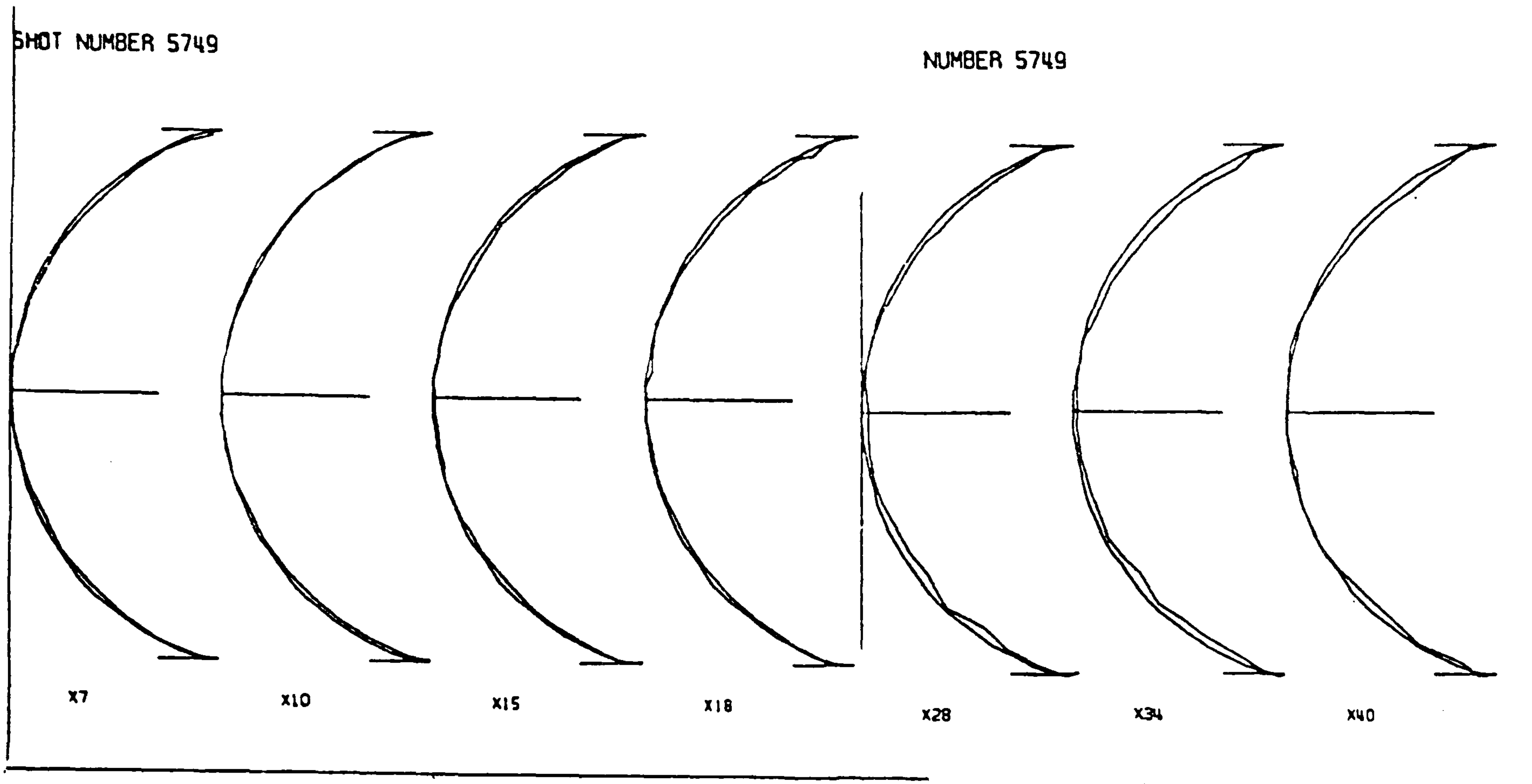

Figure 12. Inflight Nosetip Contour Changes, Test 5749

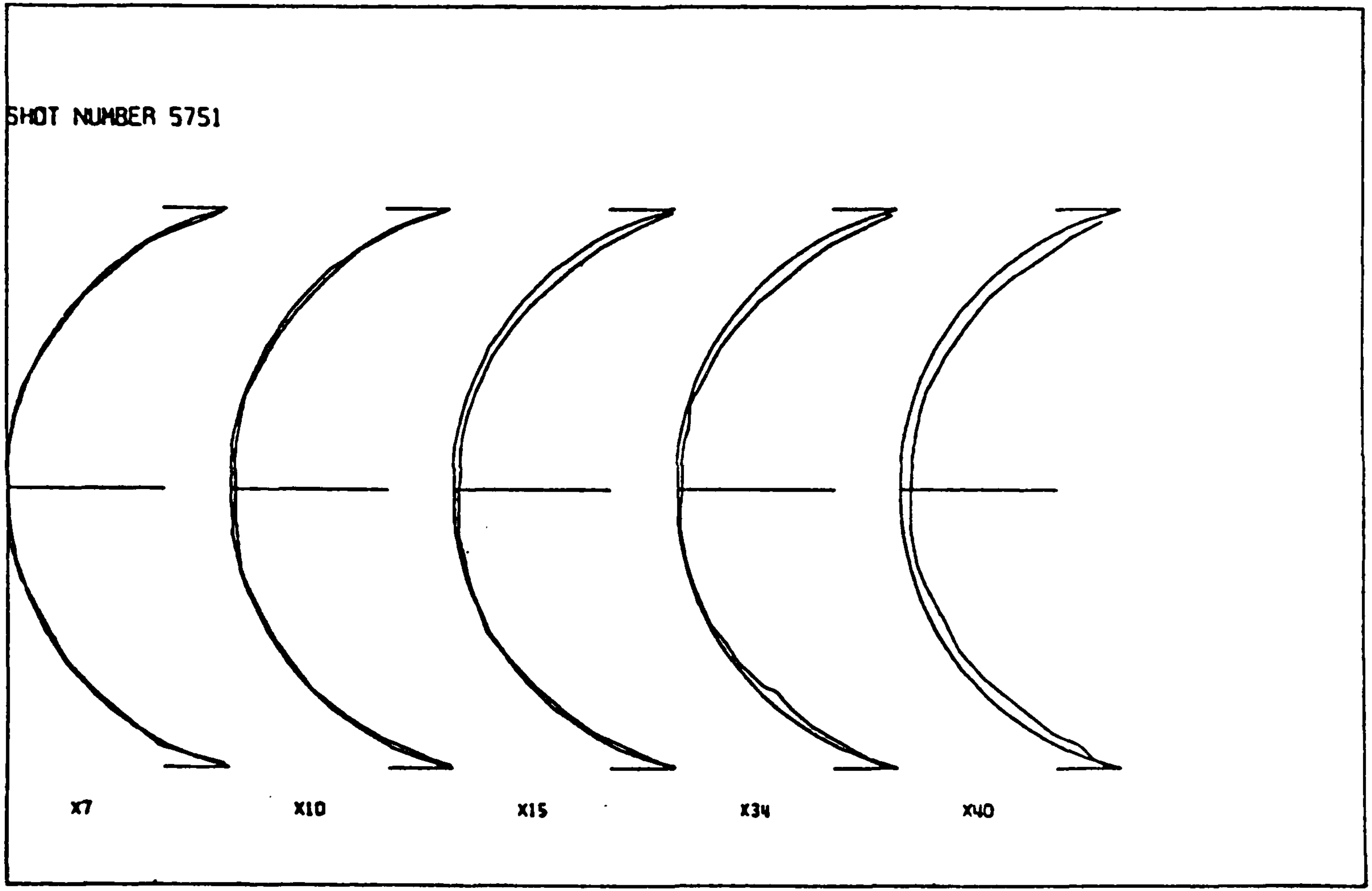

Figure 13. Inflight Nosetip Contour Changes, Test 5751

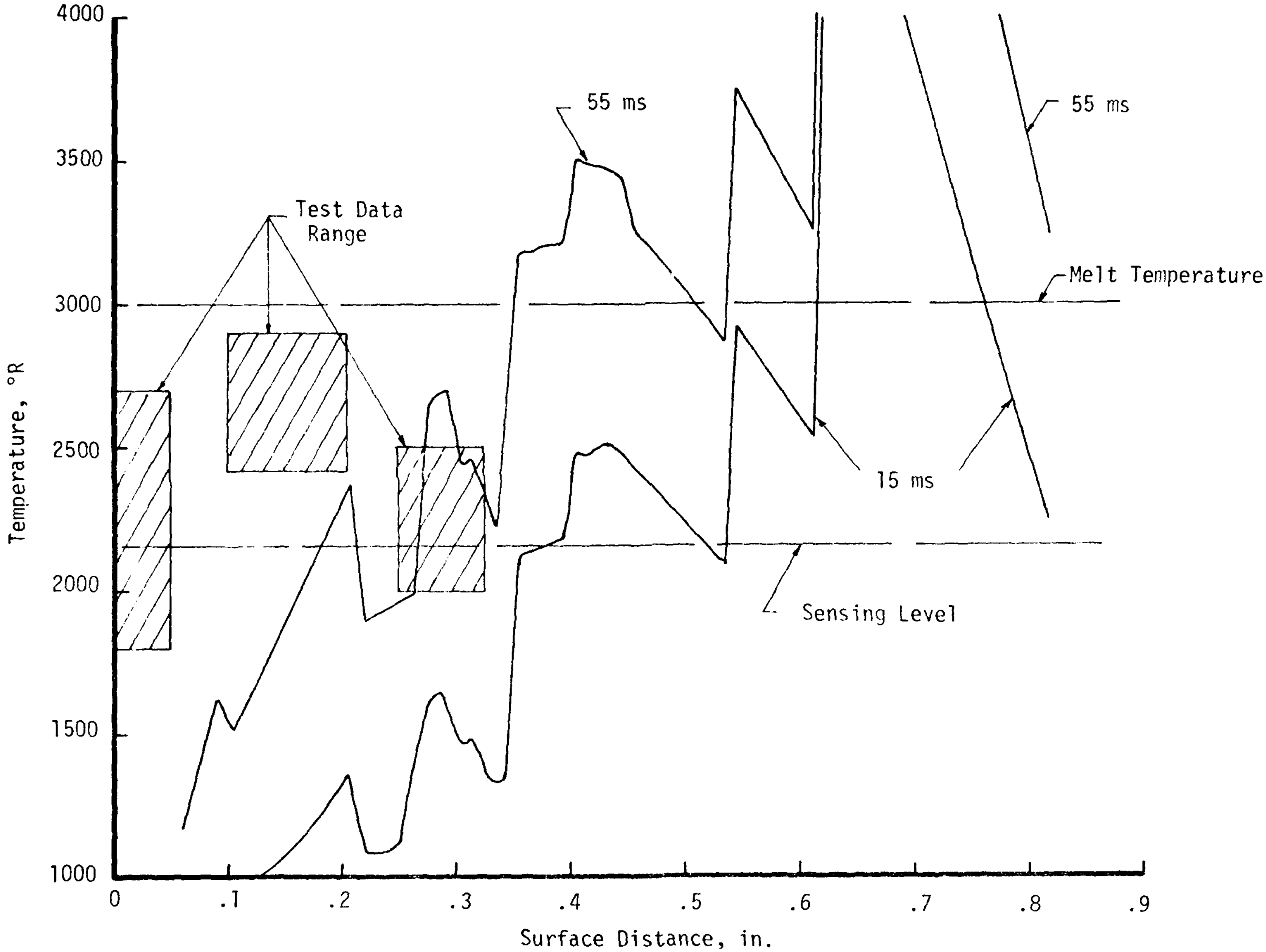

Figure 14. Test 5749 and 5751 Thermal Test Data Comparison with Code Predictions

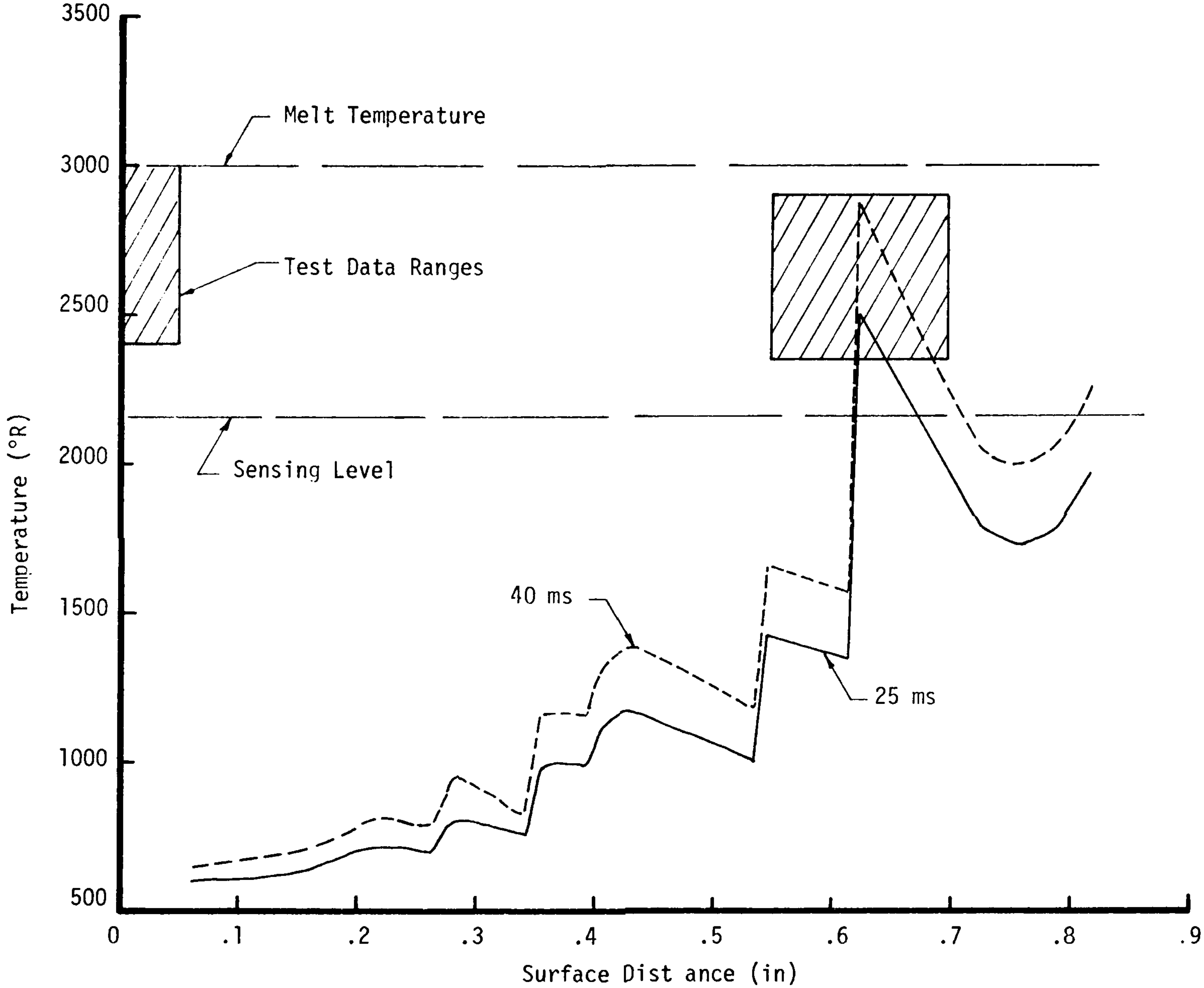

Figure 15. Test 5768 Thermal Test Data Comparison with Code Predictions

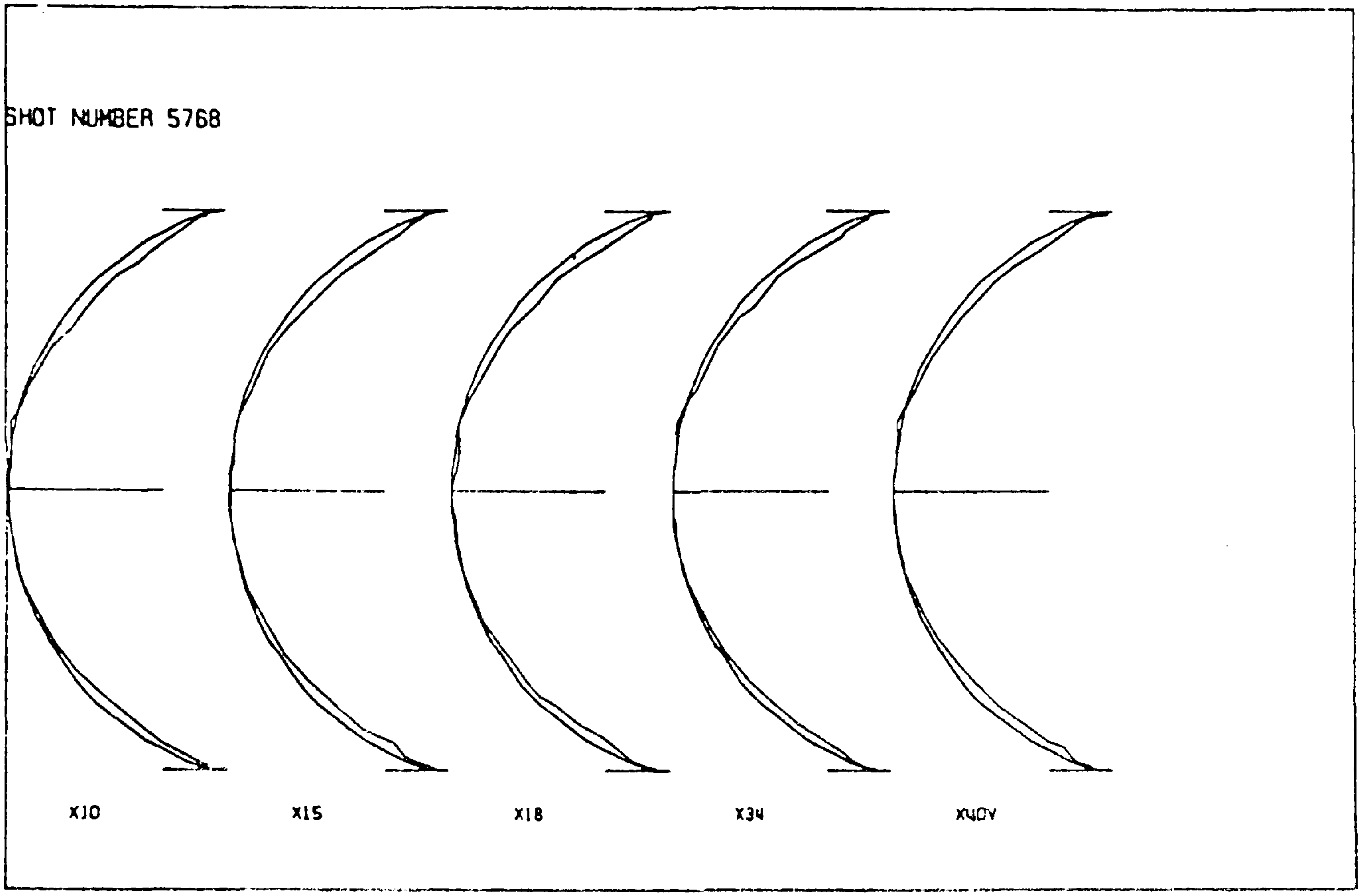

Figure 16. Inflight Nosetip Contour Changes, Test 5768

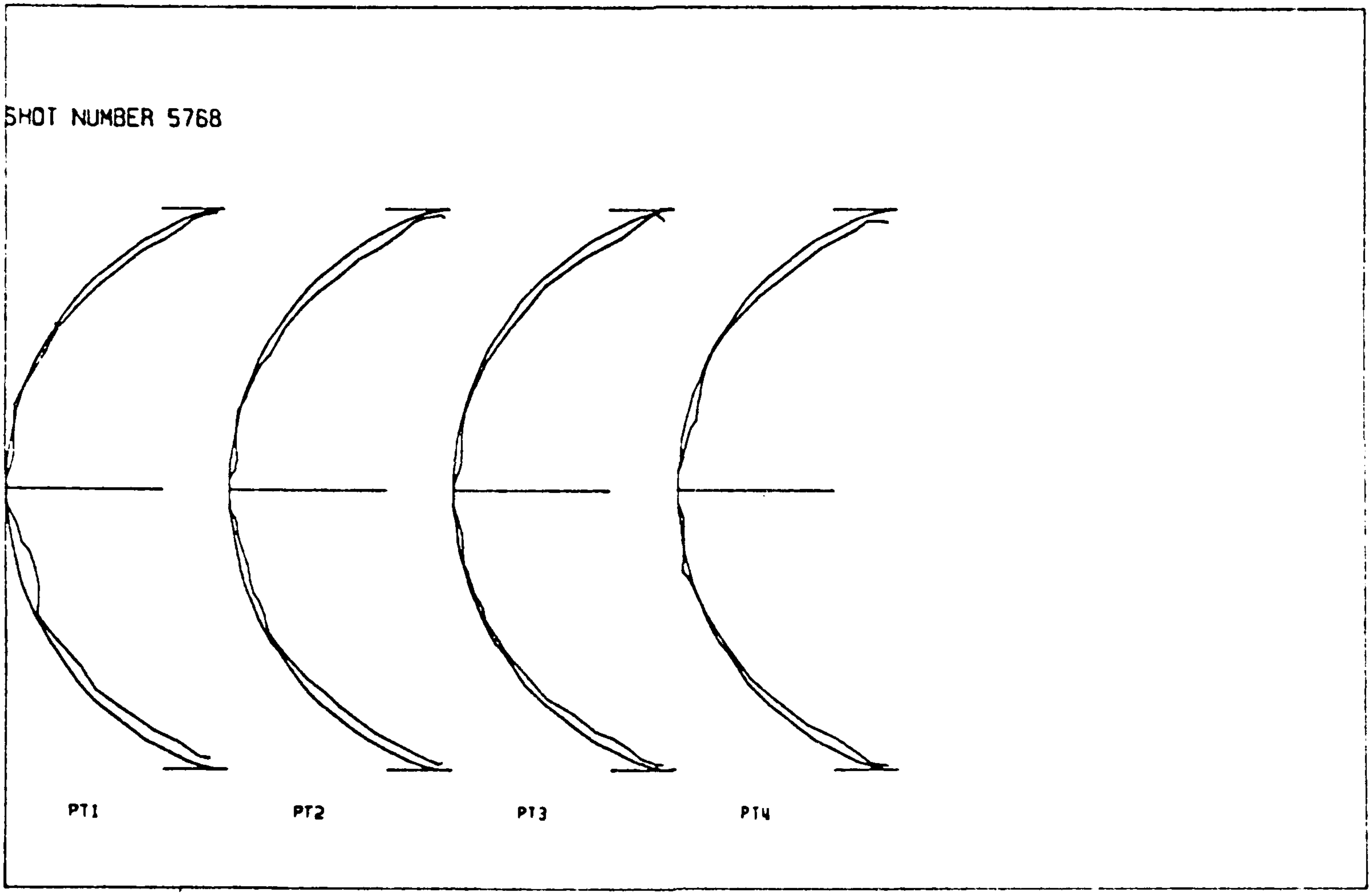

Figure 17. Post-Test 5768 Nosetip Contour Comparison

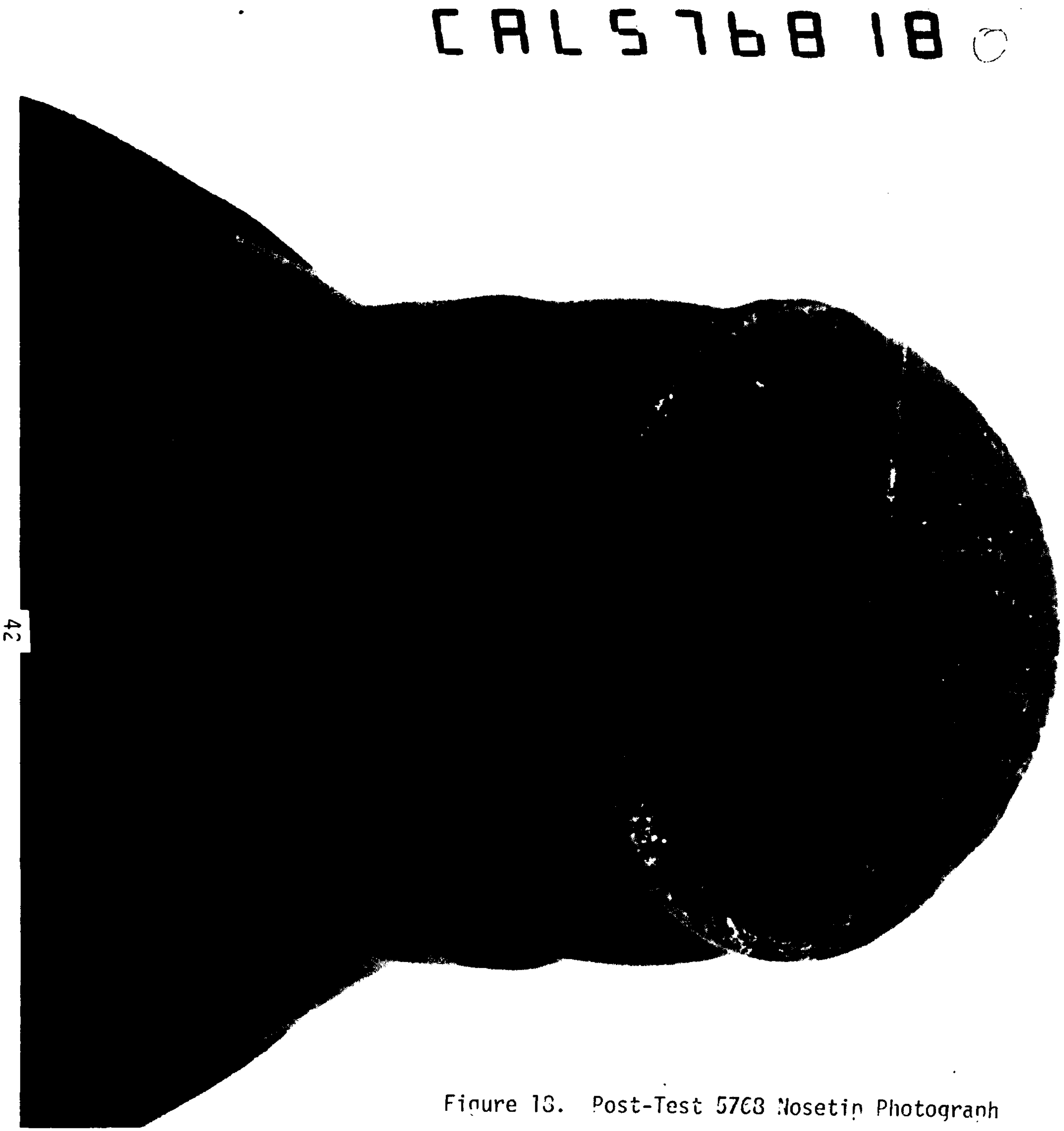

Figure 18. Post-Test 5768 Nosetip Photograph

APPENDIX A

TEST 5749 AND 5751

LASER PHOTOGRAPHS

X-RAY PHOTOGRAPHS

THERMAL PLOTS

SEE TABLES V AND VI FOR DESCRIPTION
OF TRACK STATION NUMBERS

TEST 5749

LASER PHOTOGRAPHS

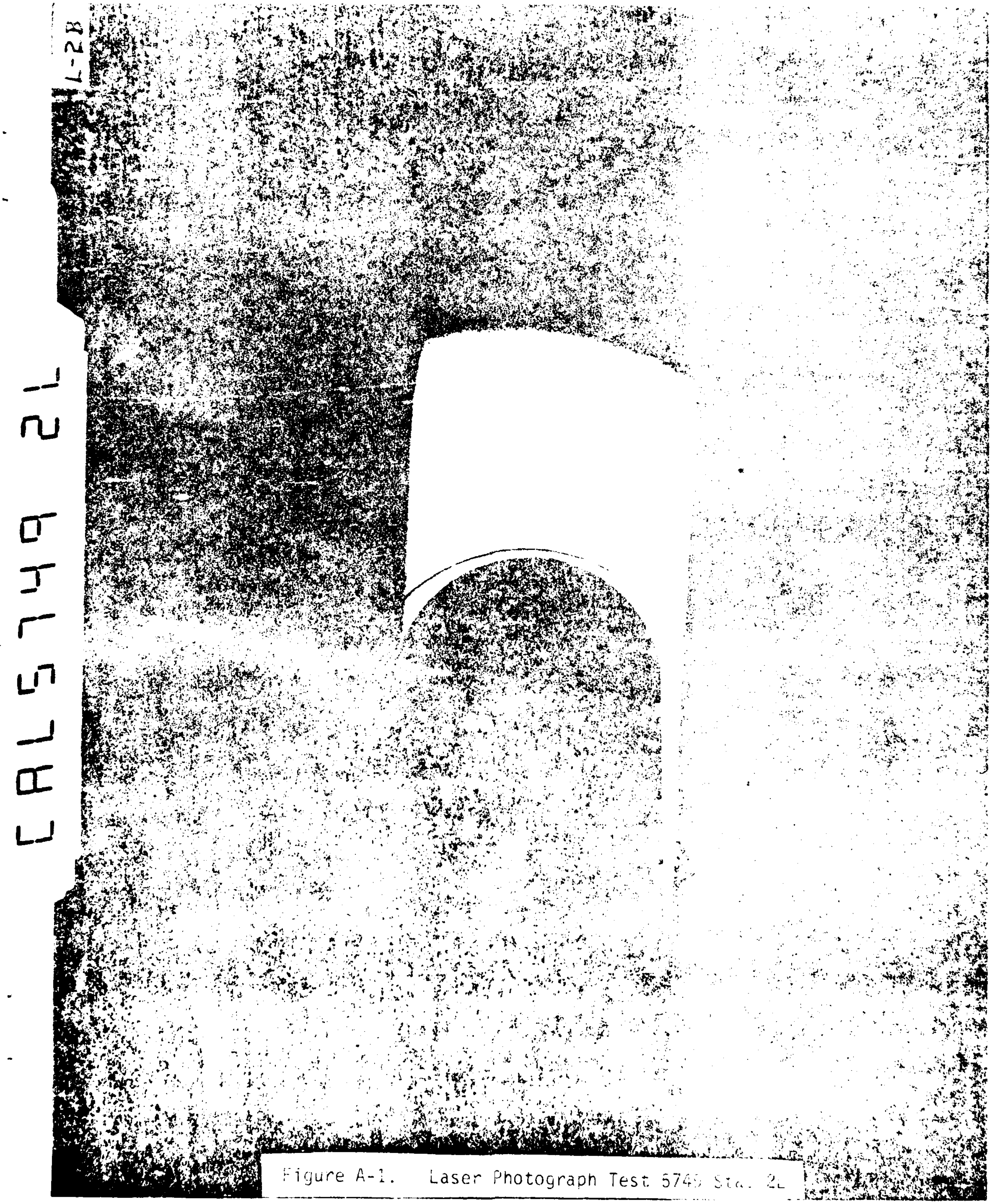

Figure A-1. Laser Photograph Test 5749 Sta. 2L

Figure A-2. Laser Photograph Test 5749 Sta. 8

Figure A-3. Laser Photograph Test 5749 Sta. 1

Figure A-4. Laser Photograph Test 5749 Sta. 19U

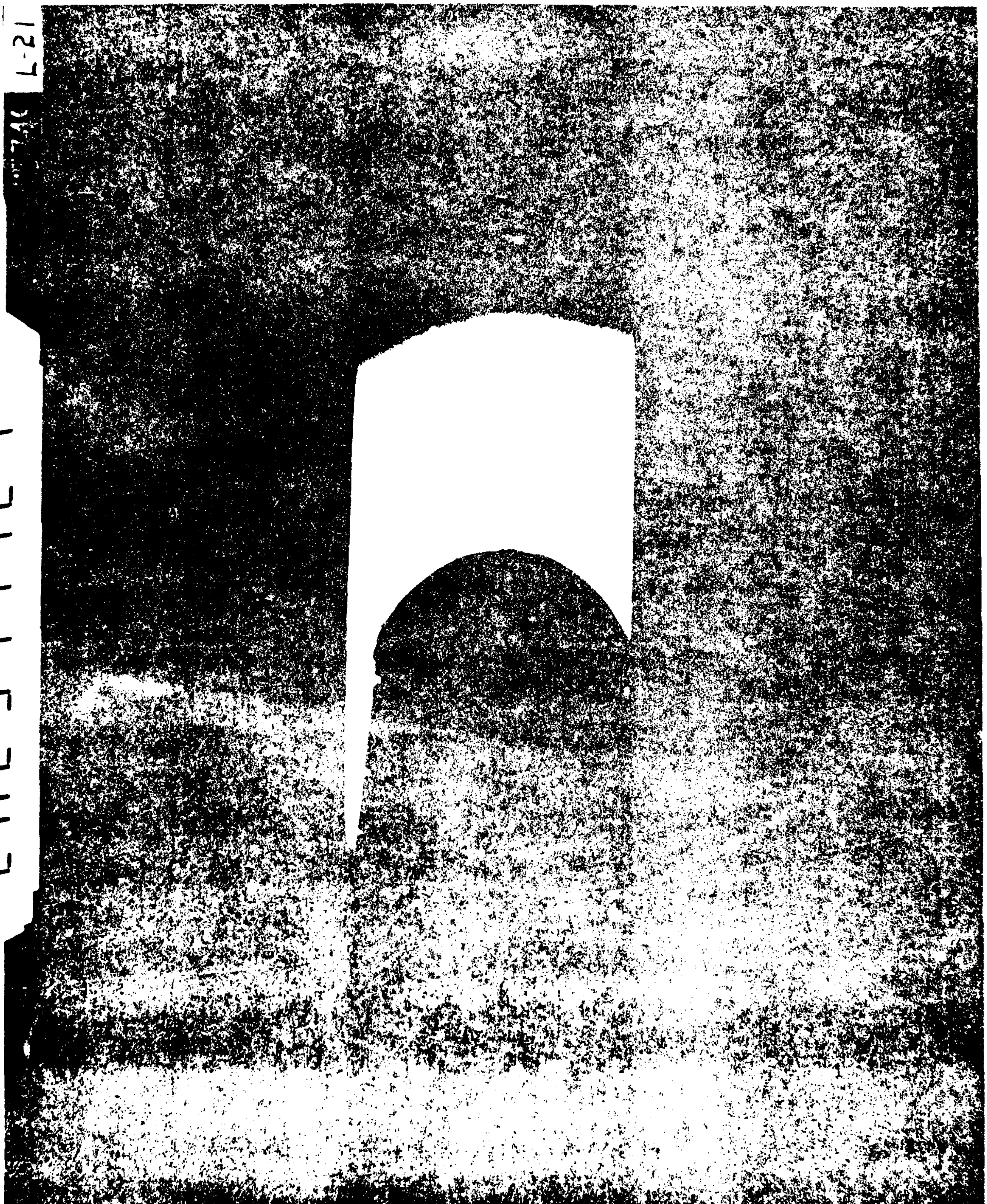

Figure A-5. Laser Photograph Test 5749 Sta. 21

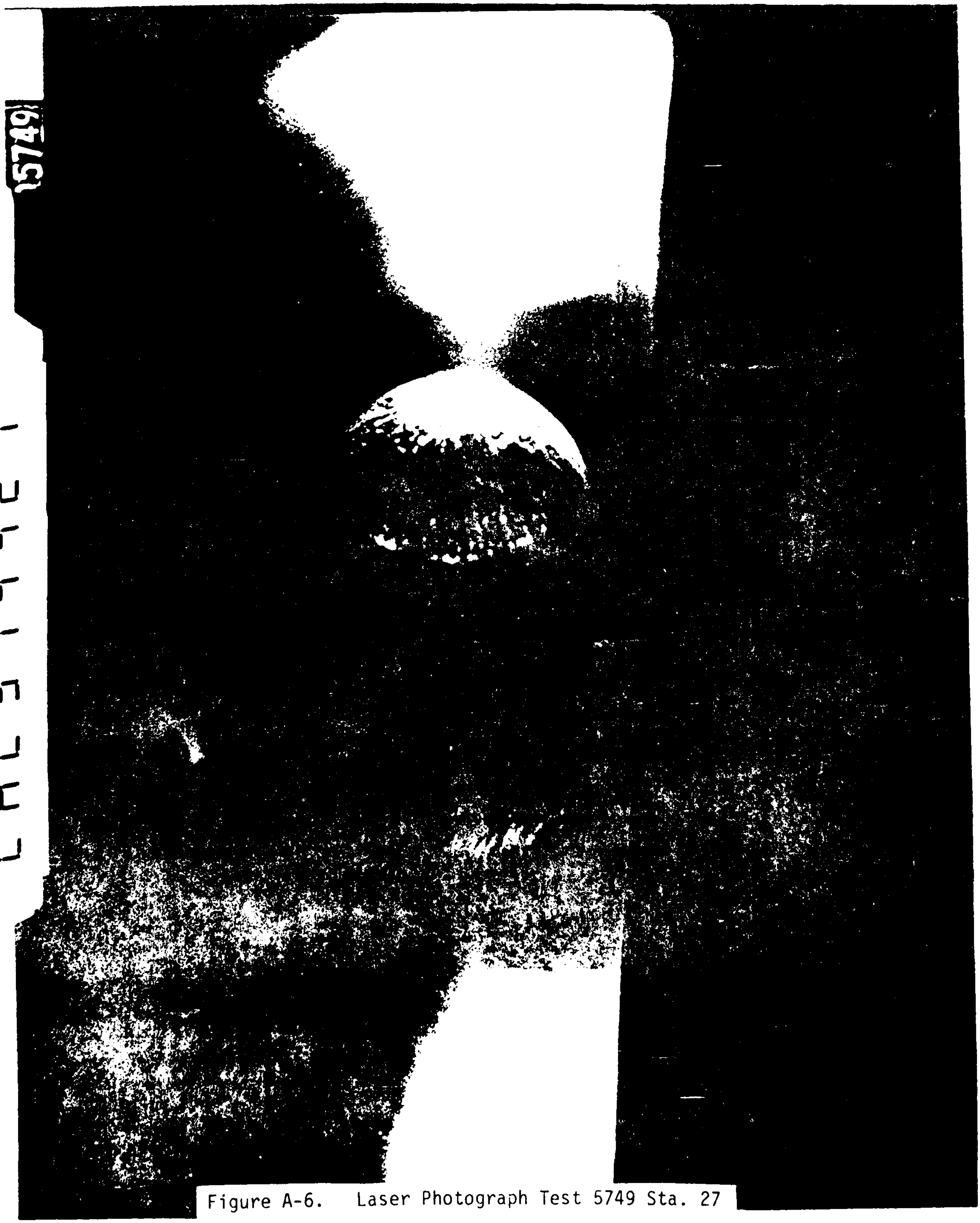

Figure A-6. Laser Photograph Test 5749 Sta. 27

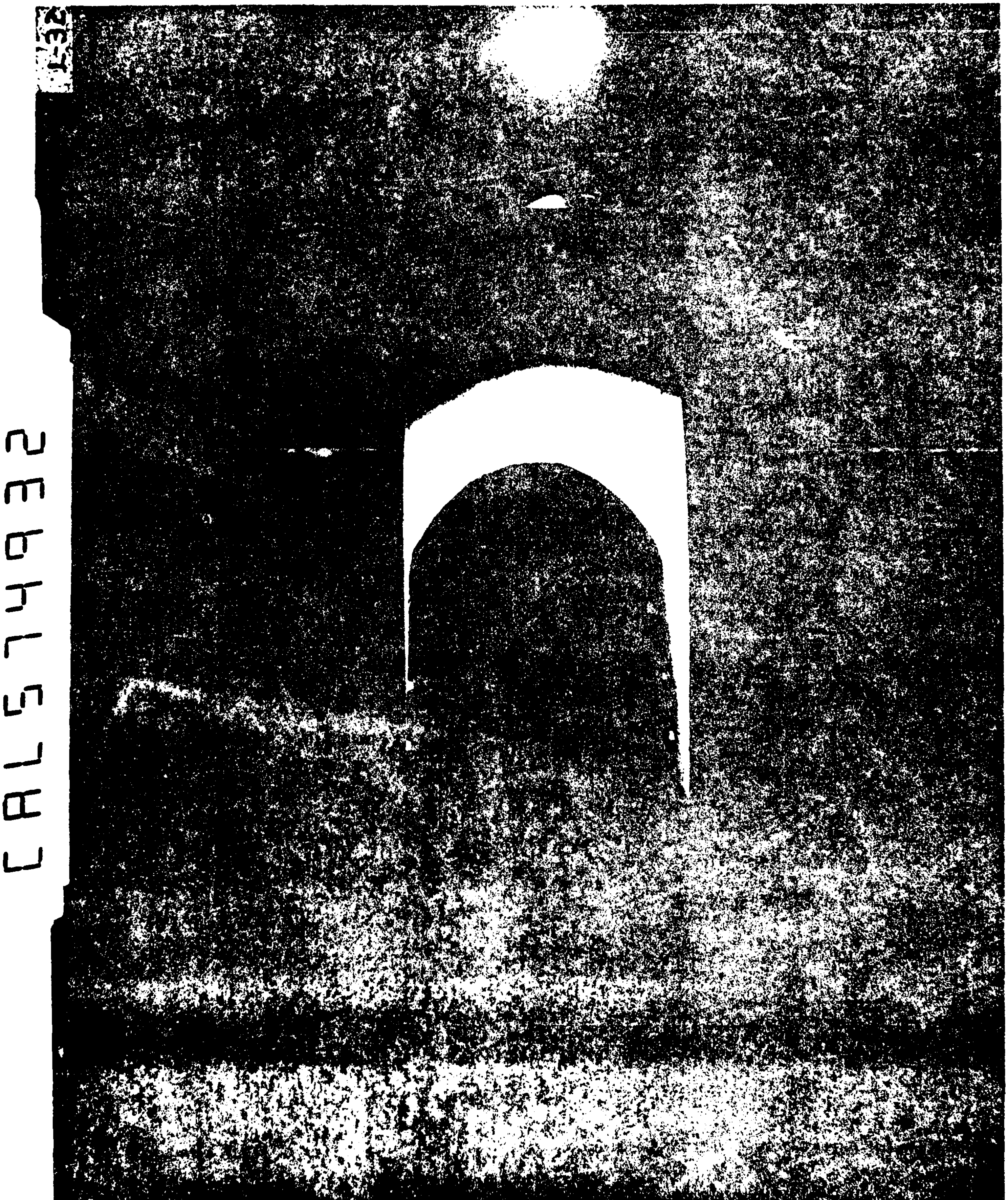

Figure A-7. Laser Photograph Test 5749 Sta. 32

Figure A-8. Laser Photograph Test 5749 Sta. 35

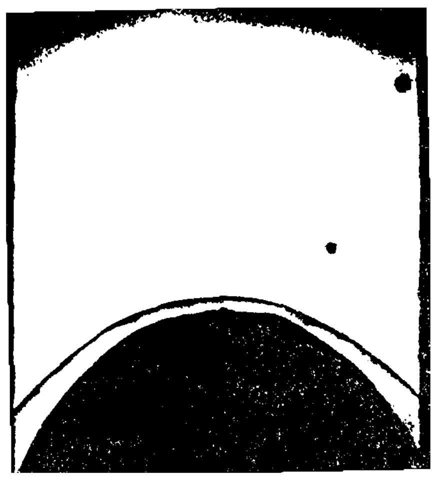

TEST 5751

LASER PHOTOGRAPHS

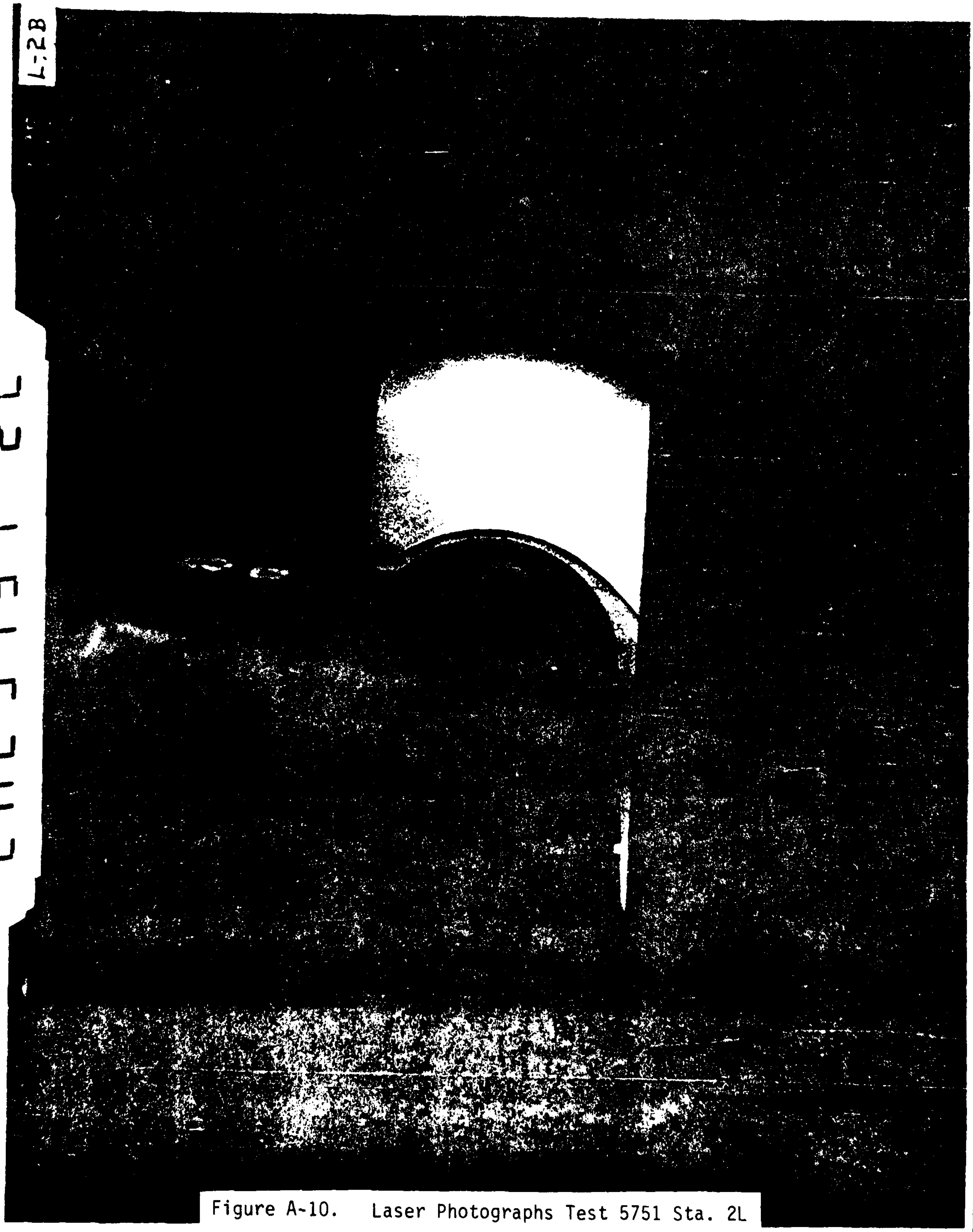

Figure A-10. Laser Photographs Test 5751 Sta. 2L

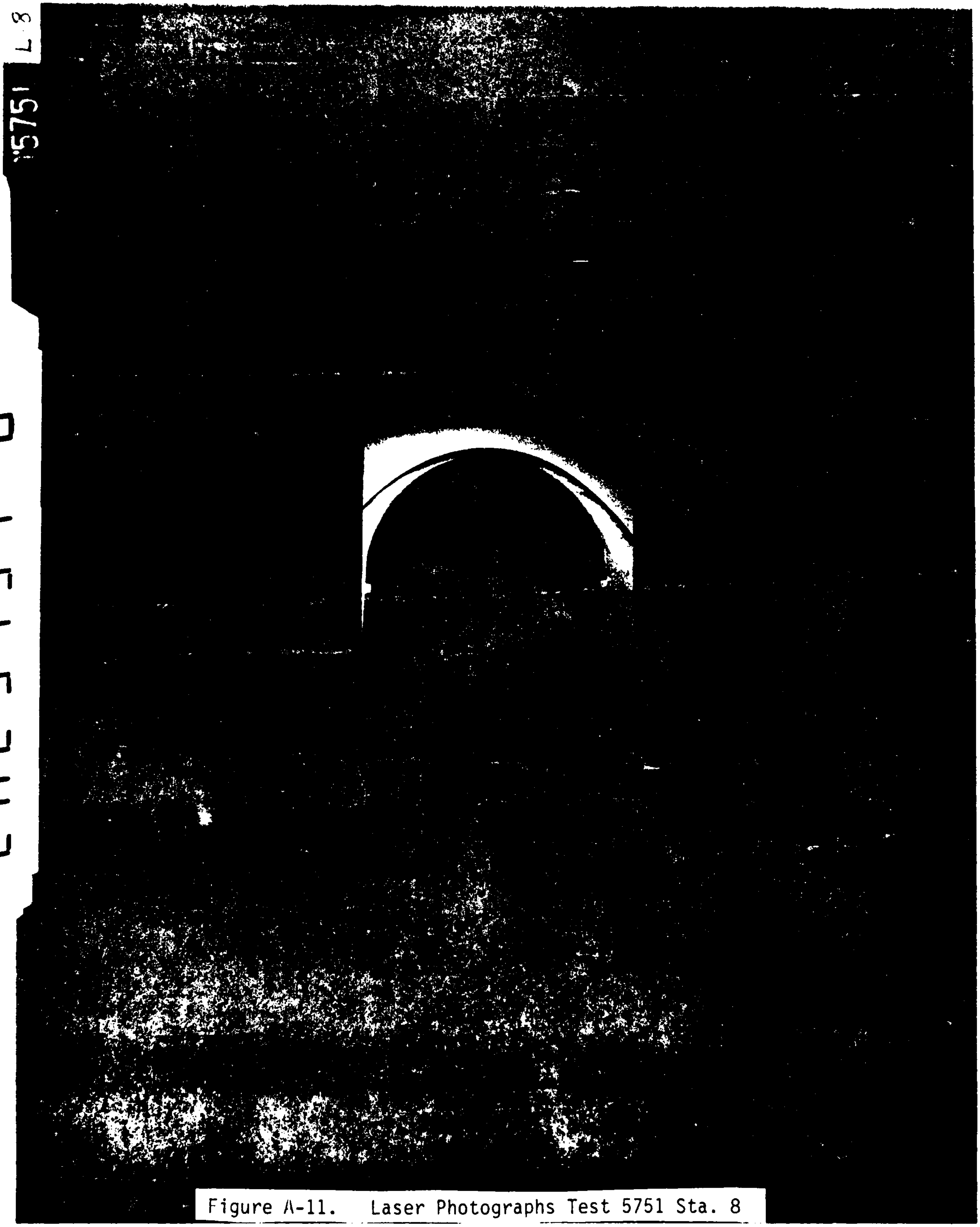

Figure A-11. Laser Photographs Test 5751 Sta. 8

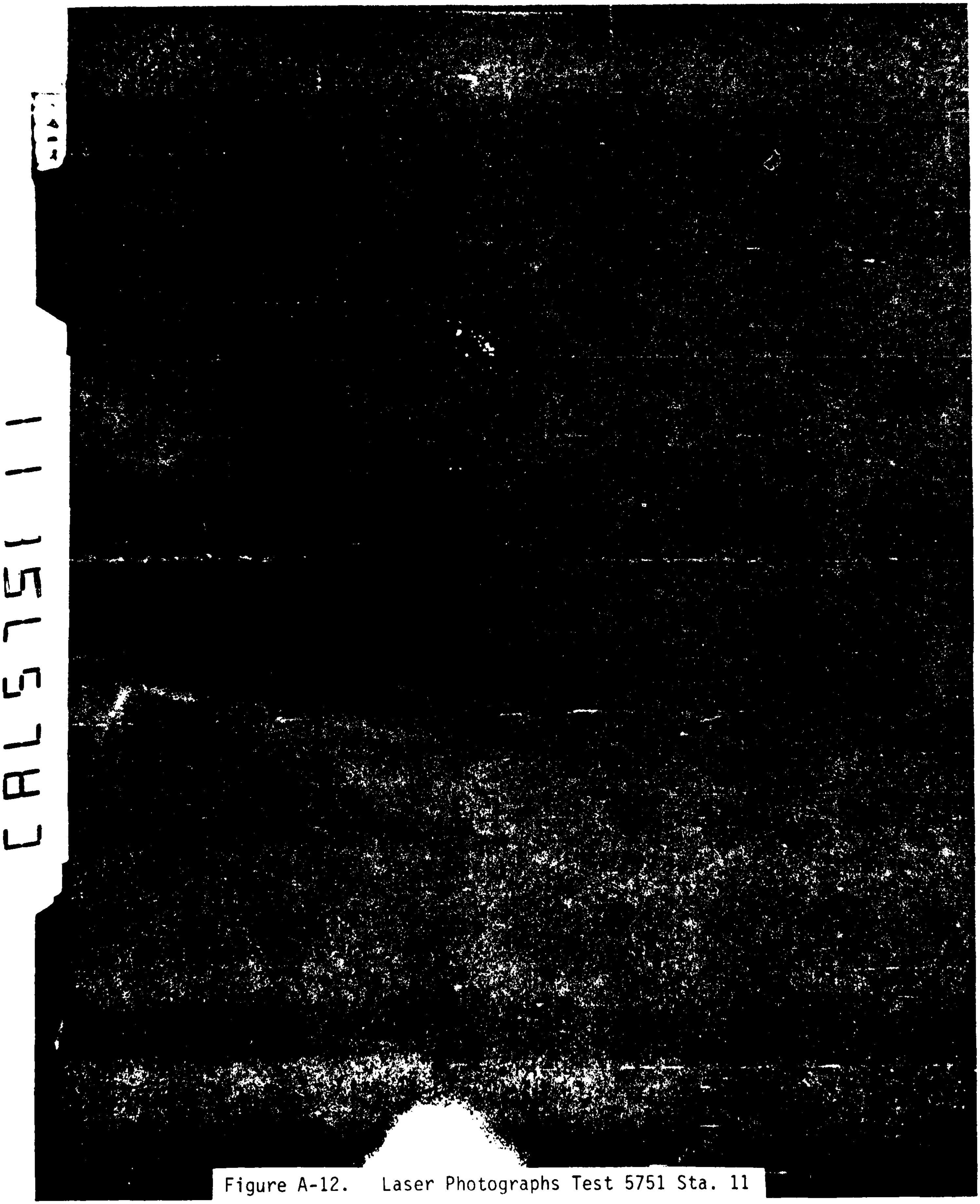

Figure A-12. Laser Photographs Test 5751 Sta. 11

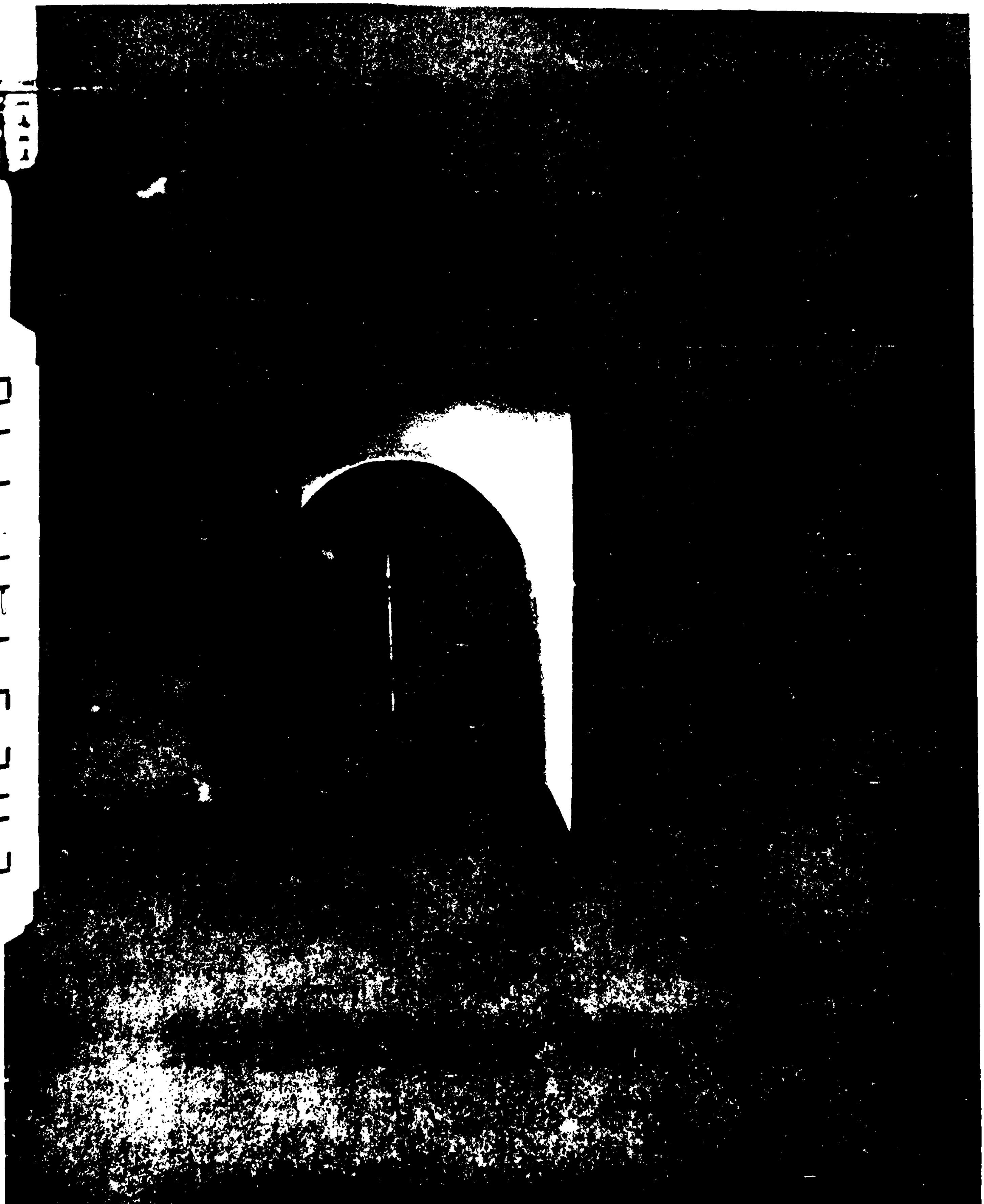

Figure A-13. Laser Photographs Test 5751 Sta. 19U

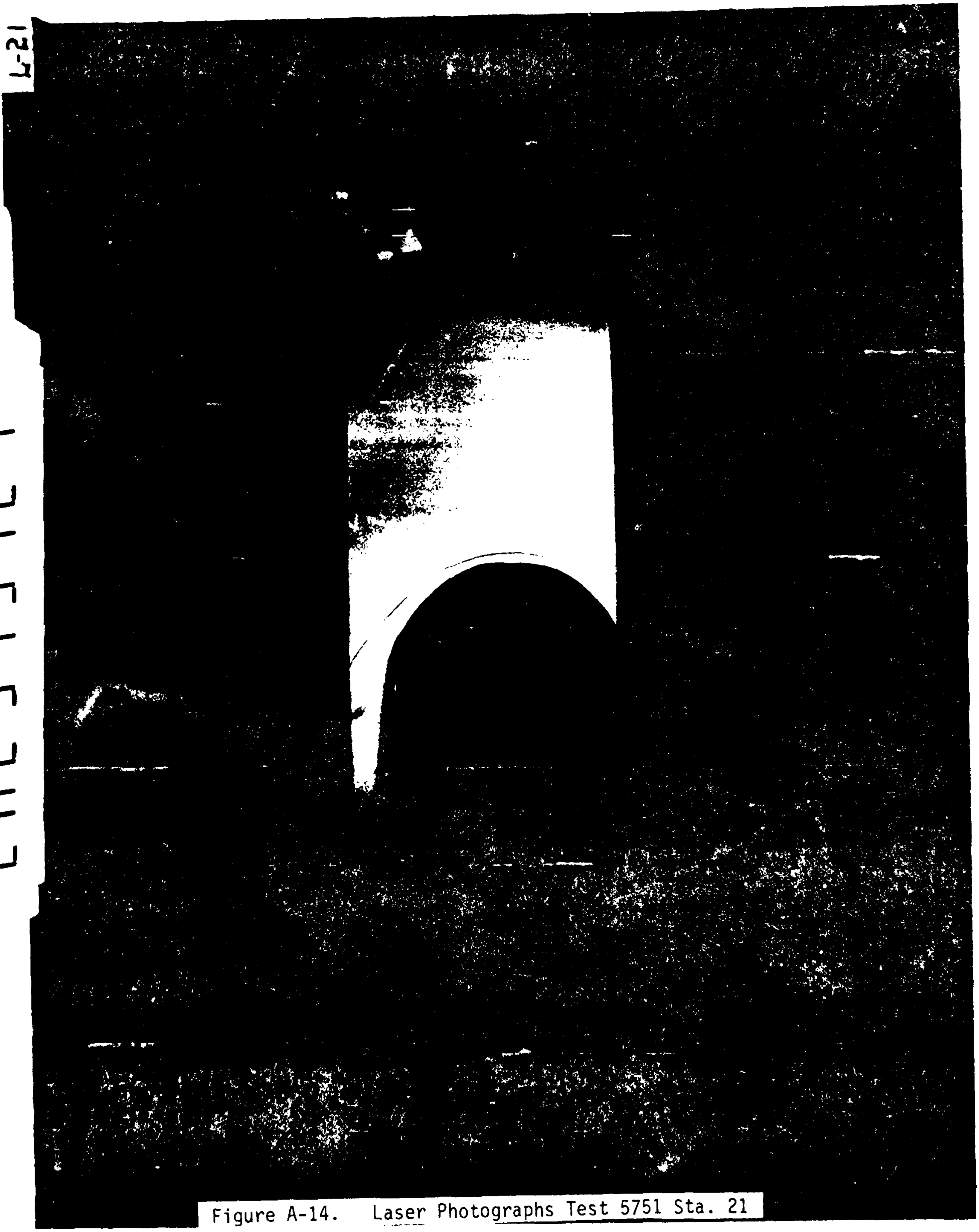

Figure A-14. Laser Photographs Test 5751 Sta. 21

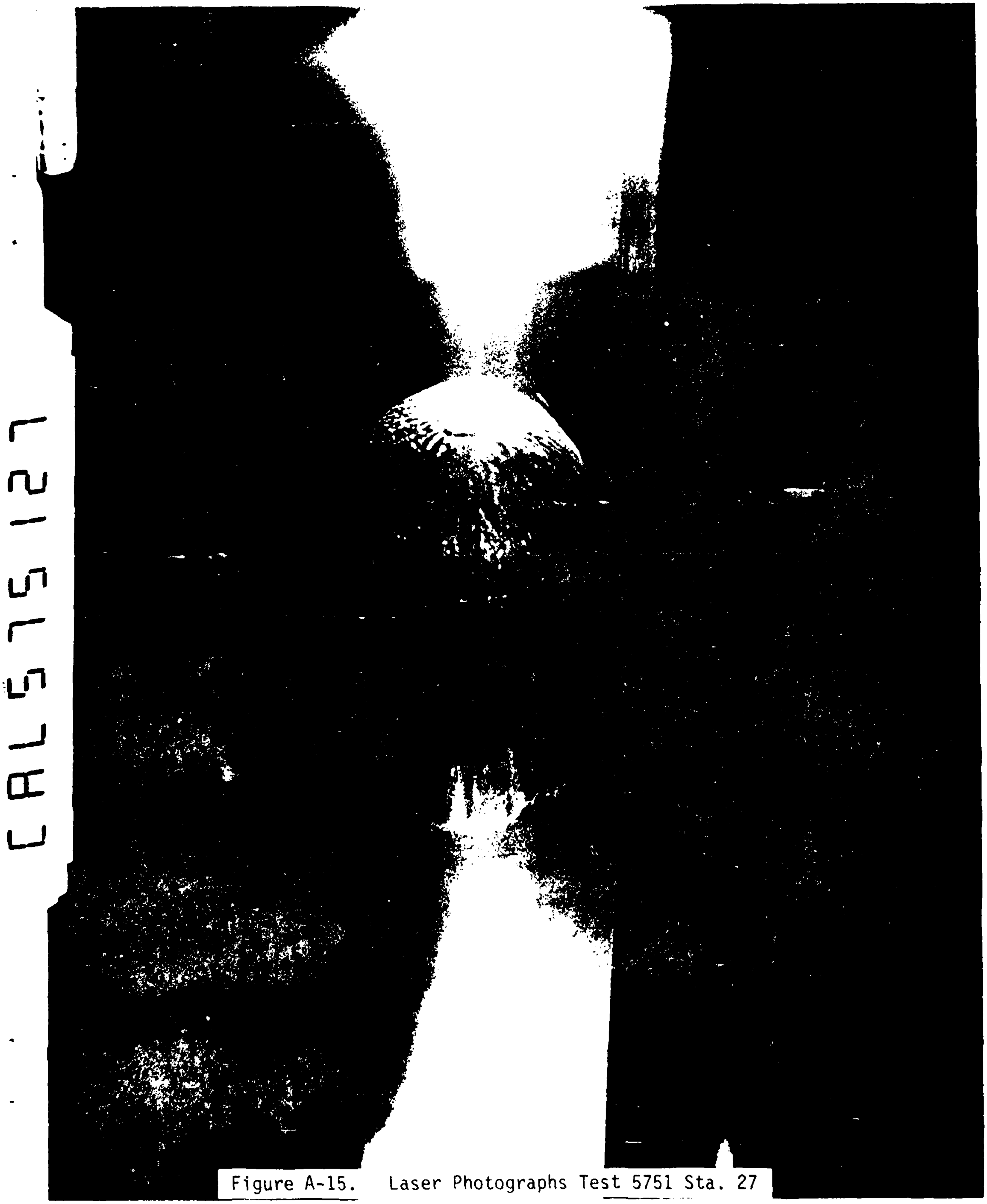

Figure A-15. Laser Photographs Test 5751 Sta. 27

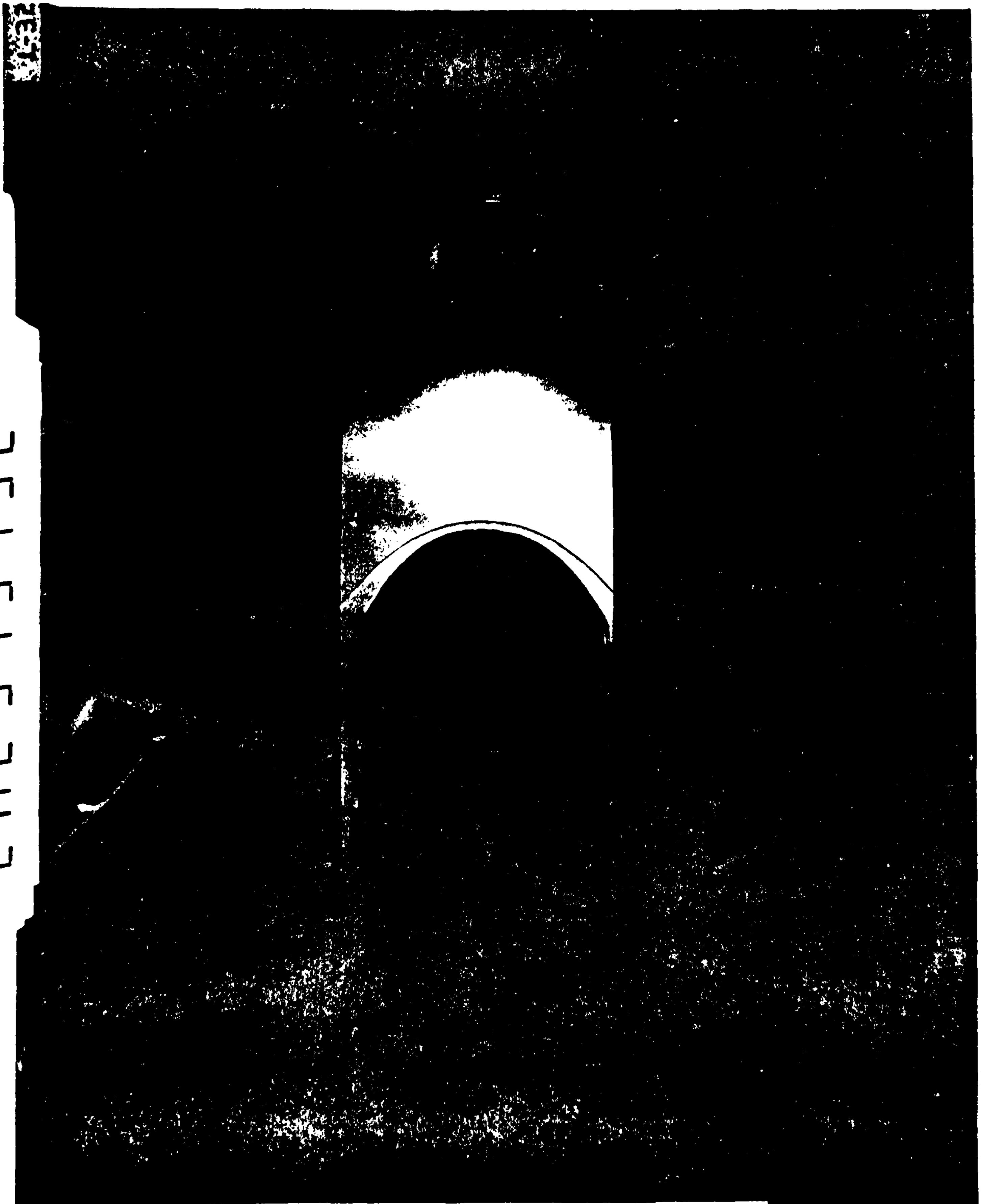

Figure A-16. Laser Photographs Test 5751 Sta. 32

Figure A-17. Laser Photographs Test 5751 Sta. 35

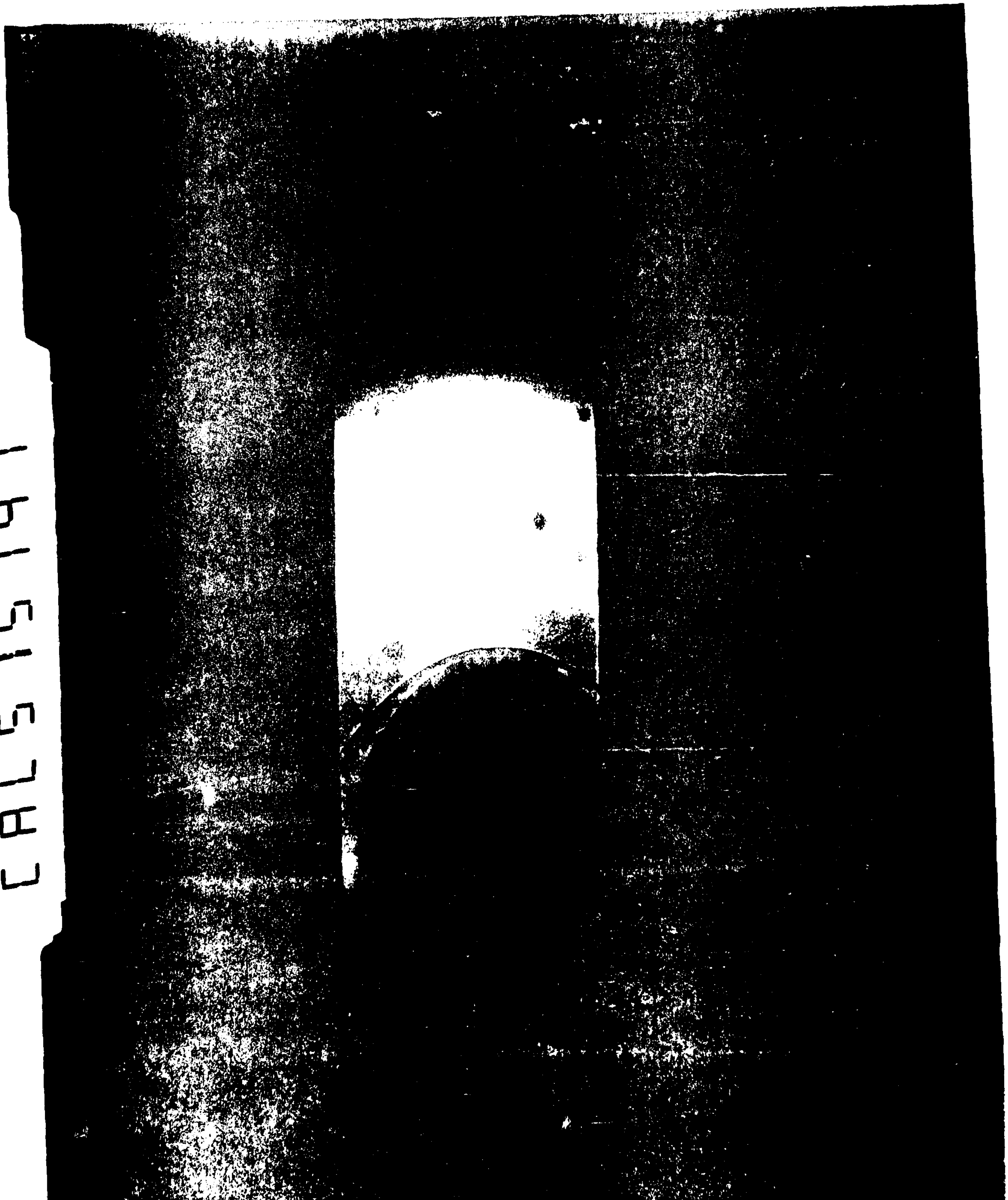

Figure A-18. Laser Photographs Test 5751 Sta. 41

TEST 5749

X-RAY PHOTOGRAPHS

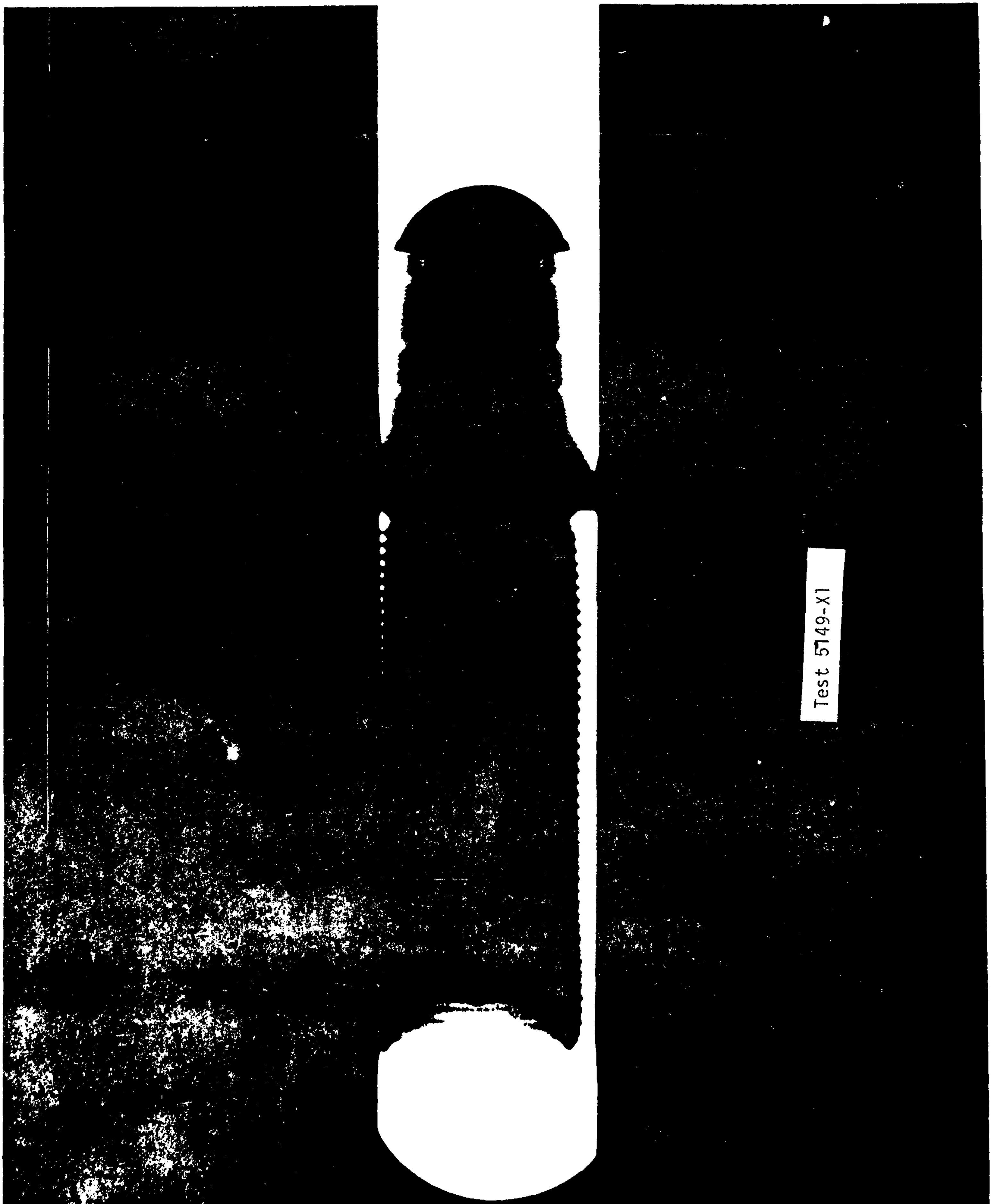

Figure A-19. X-Ray Photographs Test 5749 Sta. X-1

Figure A-20. X-Ray Photographs Test 5749 Sta. X-7

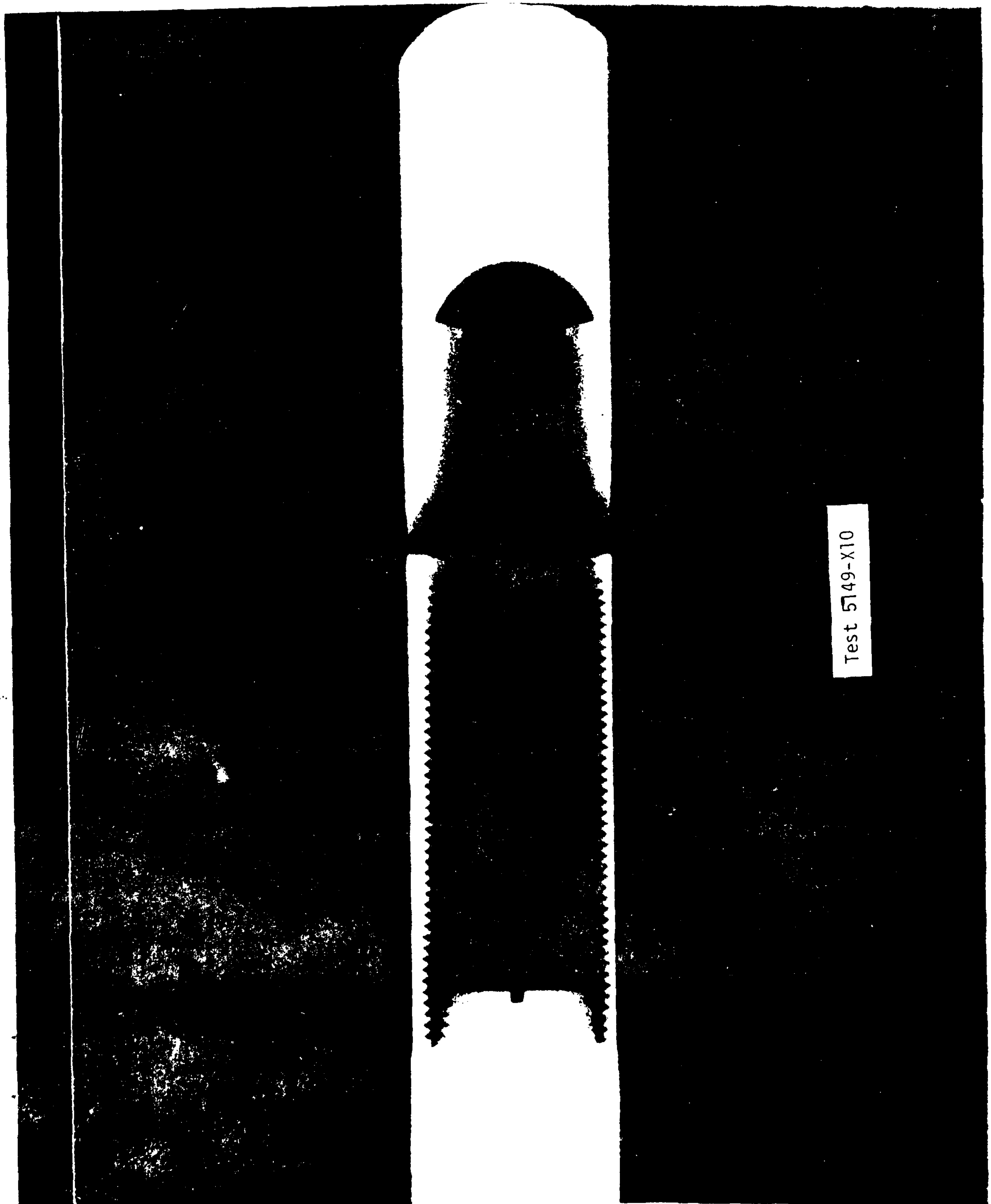

Figure A-21. X-Ray Photographs Test 5749 Sta. X-10

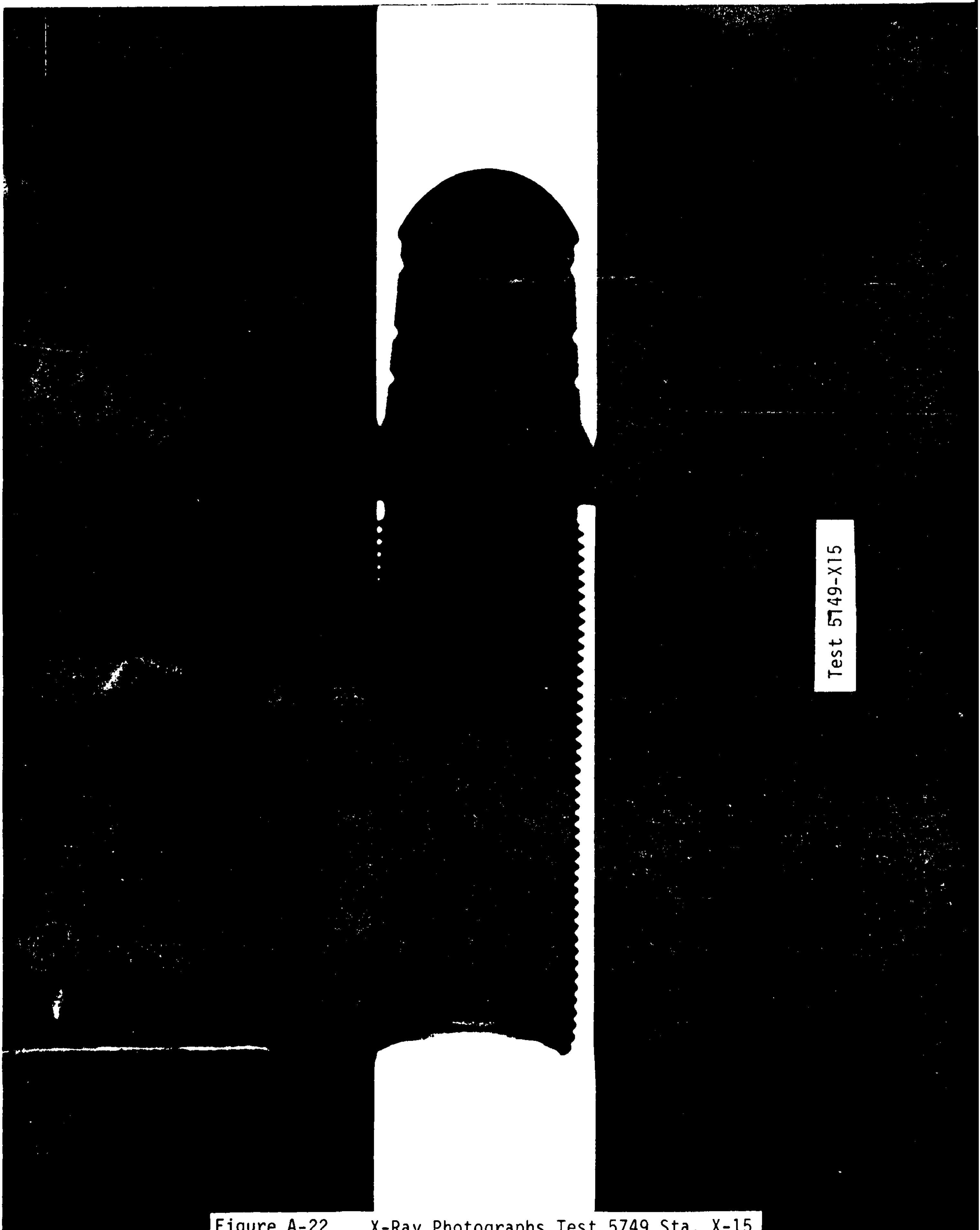

Figure A-22. X-Ray Photographs Test 5749 Sta. X-15

Figure A-10. Laser Photographs Test 5751 Sta. 2L

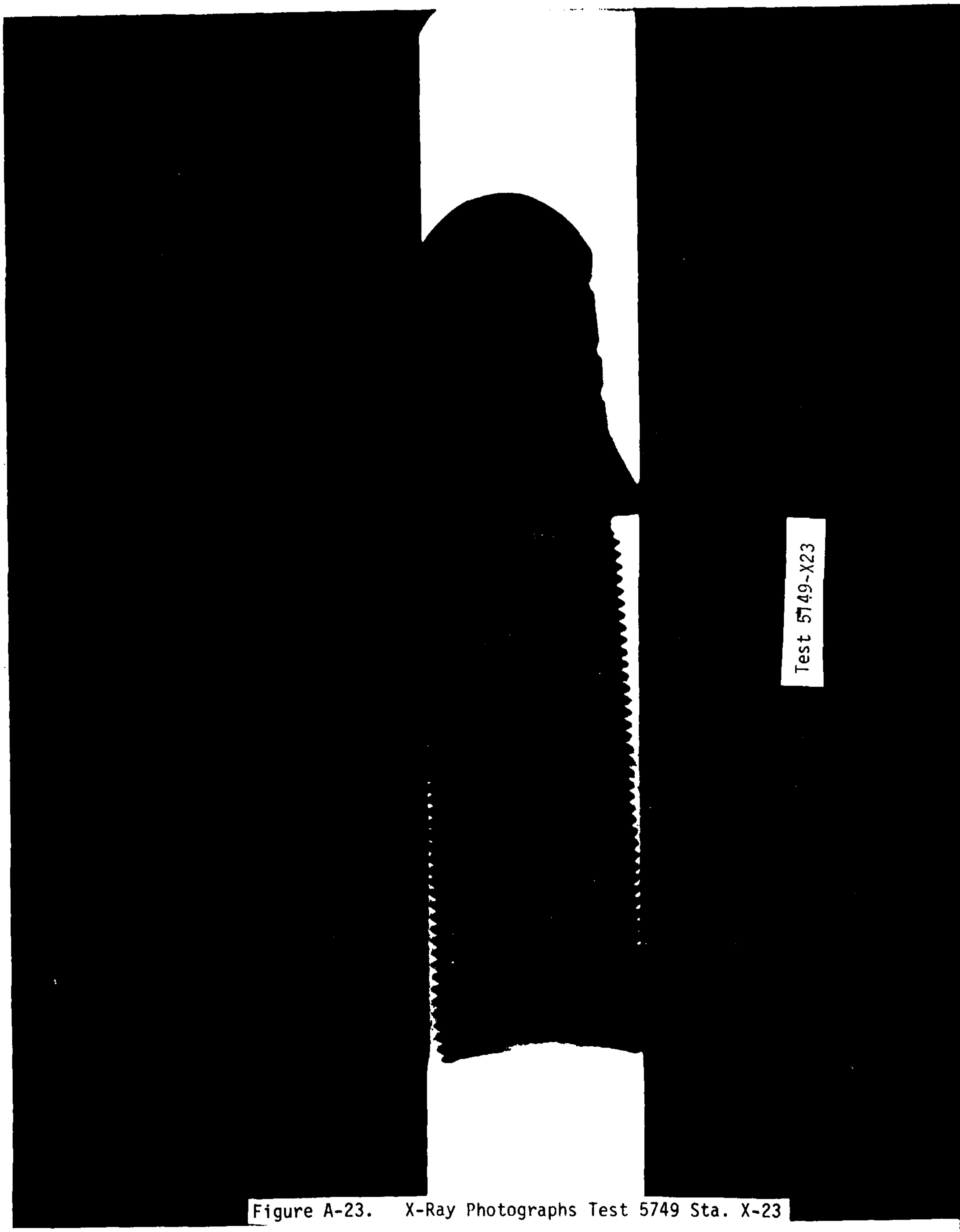

Figure A-23. X-Ray Photographs Test 5749 Sta. X-23

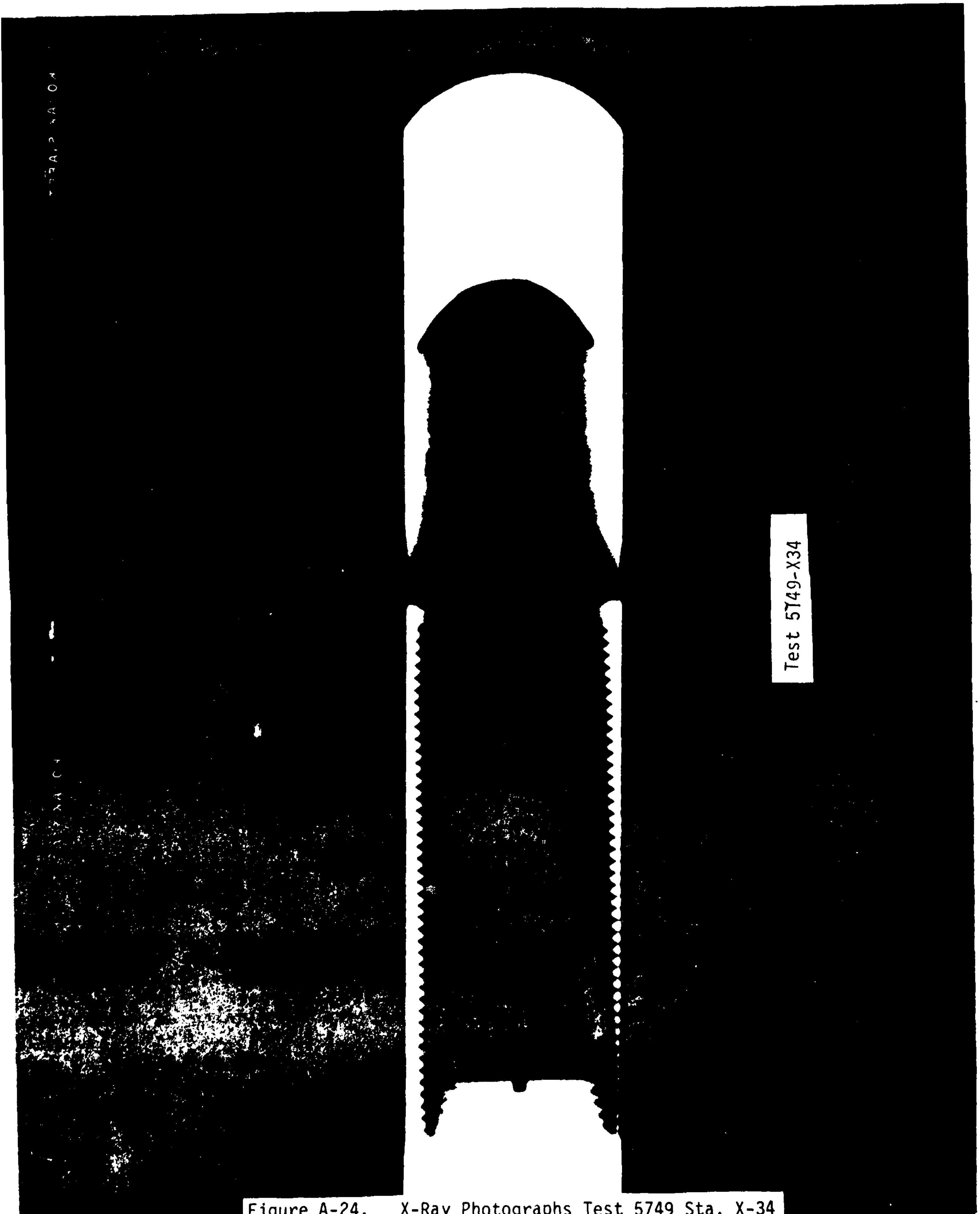

Figure A-24. X-Ray Photographs Test 5749 Sta. X-34

Figure A-25. X-Ray Photographs Test 5749 Sta. X-40

TEST 5751

X-RAY PHOTOGRAPHS

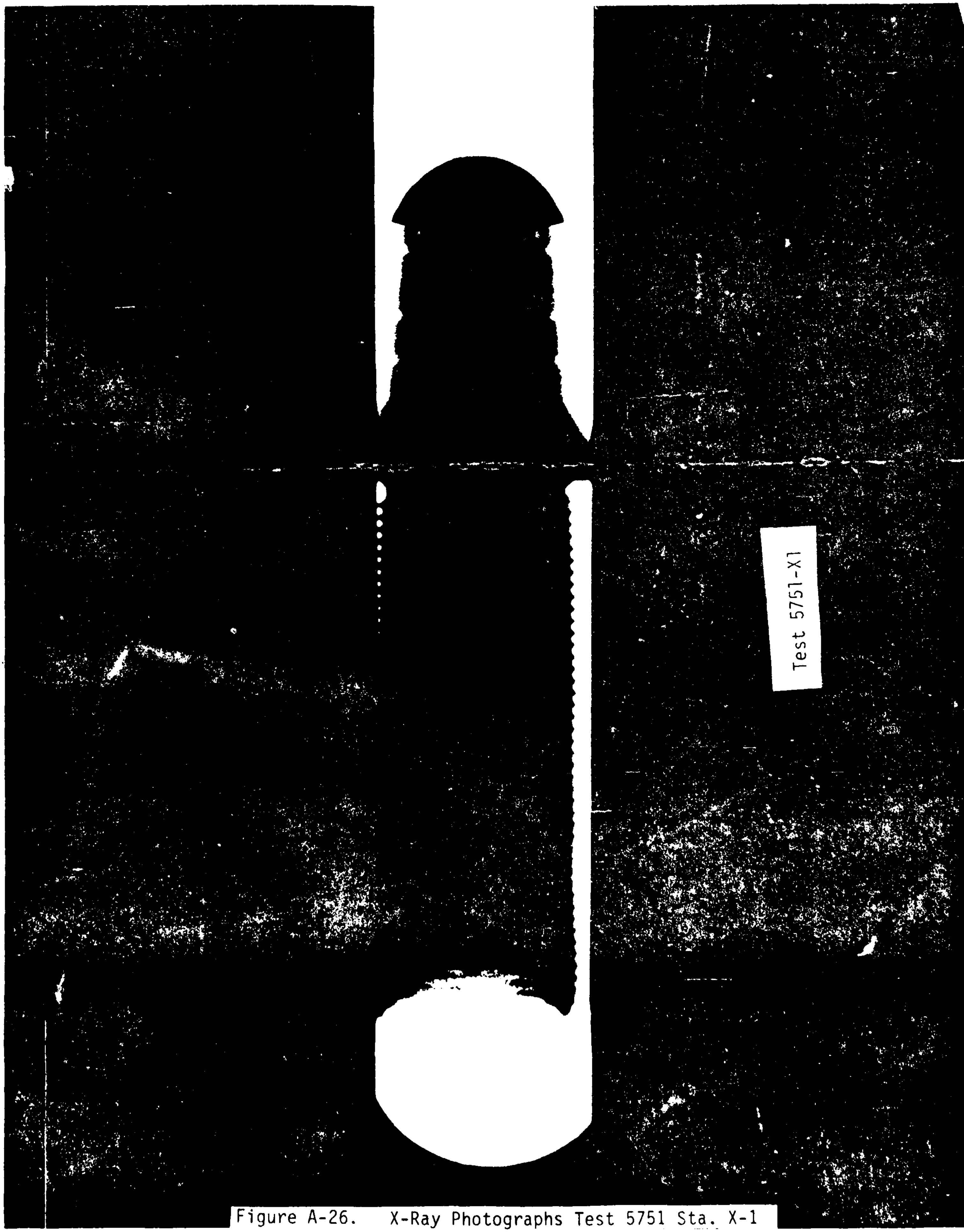

Figure A-26. X-Ray Photographs Test 5751 Sta. X-1

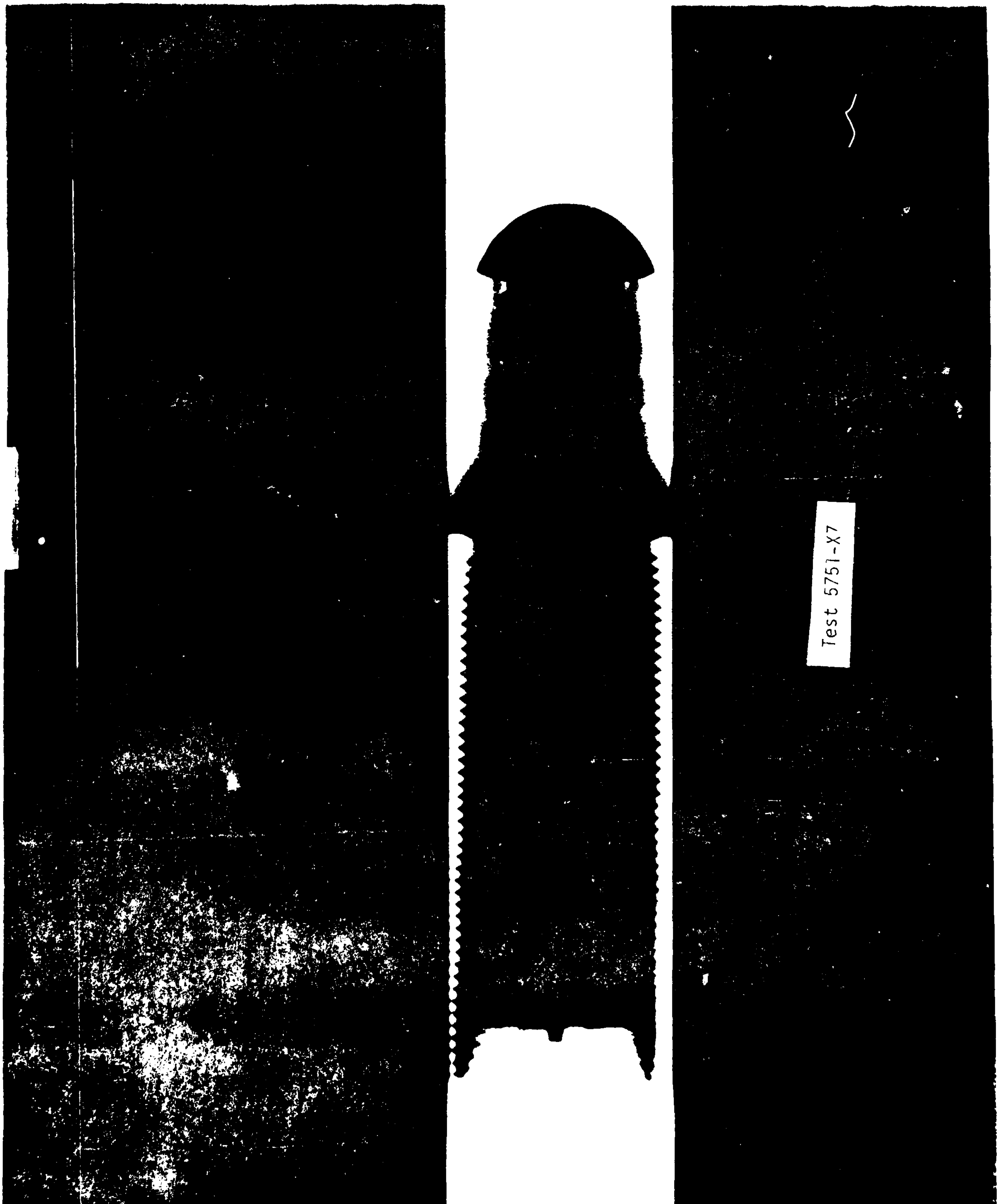

Figure A-27. X-Ray Photographs Test 5751 Sta. X-7

Figure A-28. X-Ray Photographs Test 5751 Sta. X-10

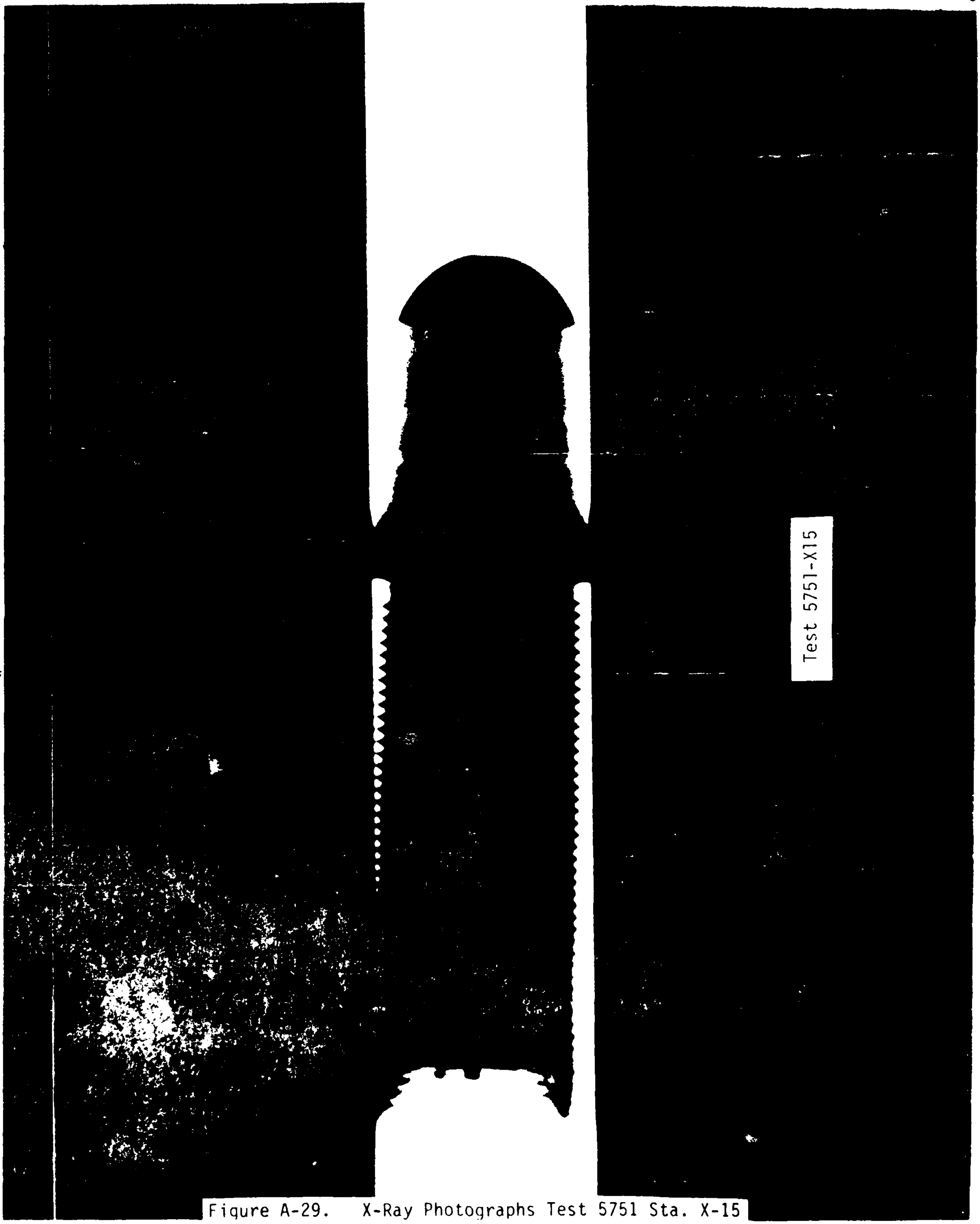

Figure A-29. X-Ray Photographs Test 5751 Sta. X-15

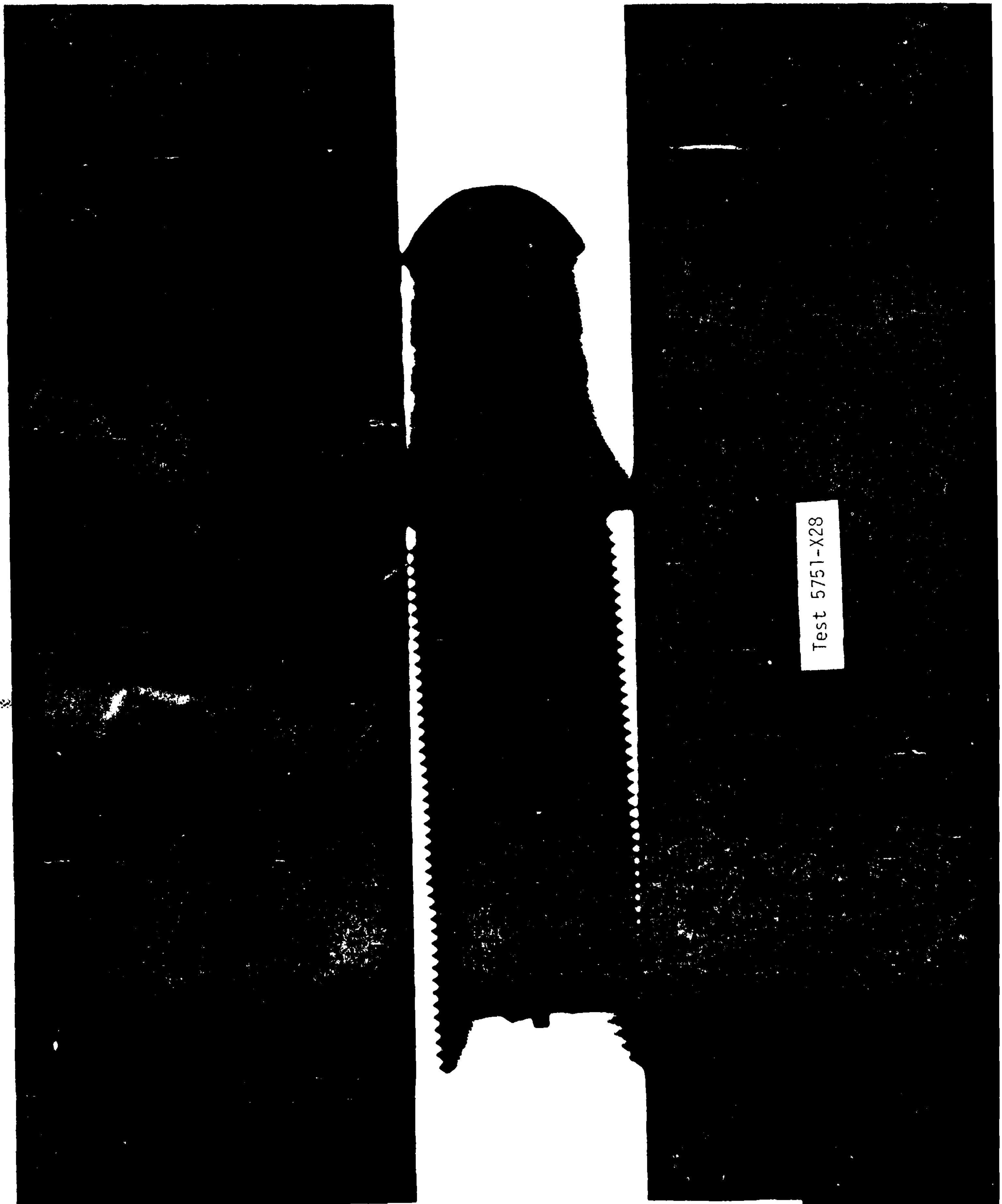

Figure A-30. X-Ray Photographs Test 5751 Sta. X-28

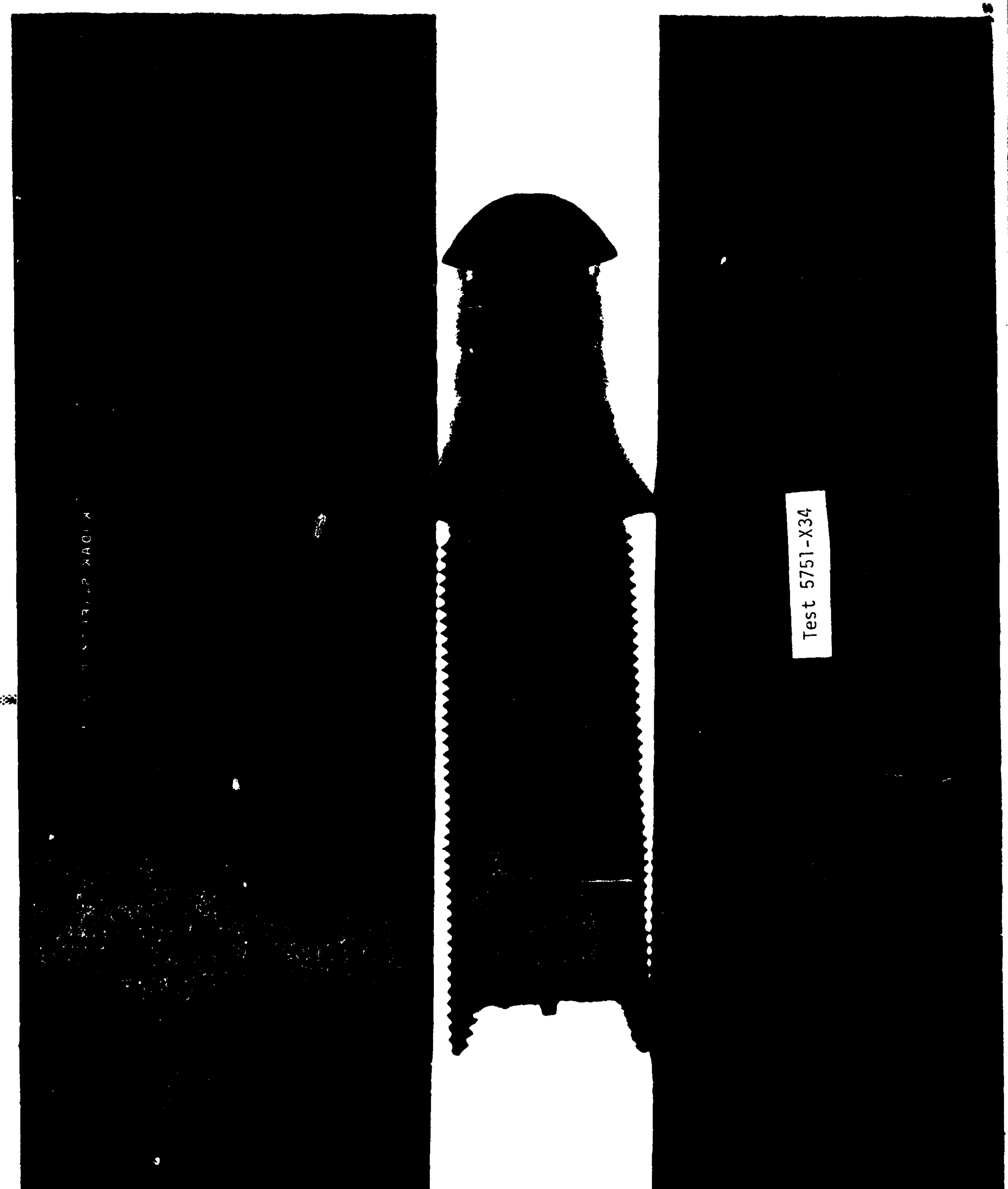

Figure A-31. X-Ray Photographs Test 5751 Sta. X-34

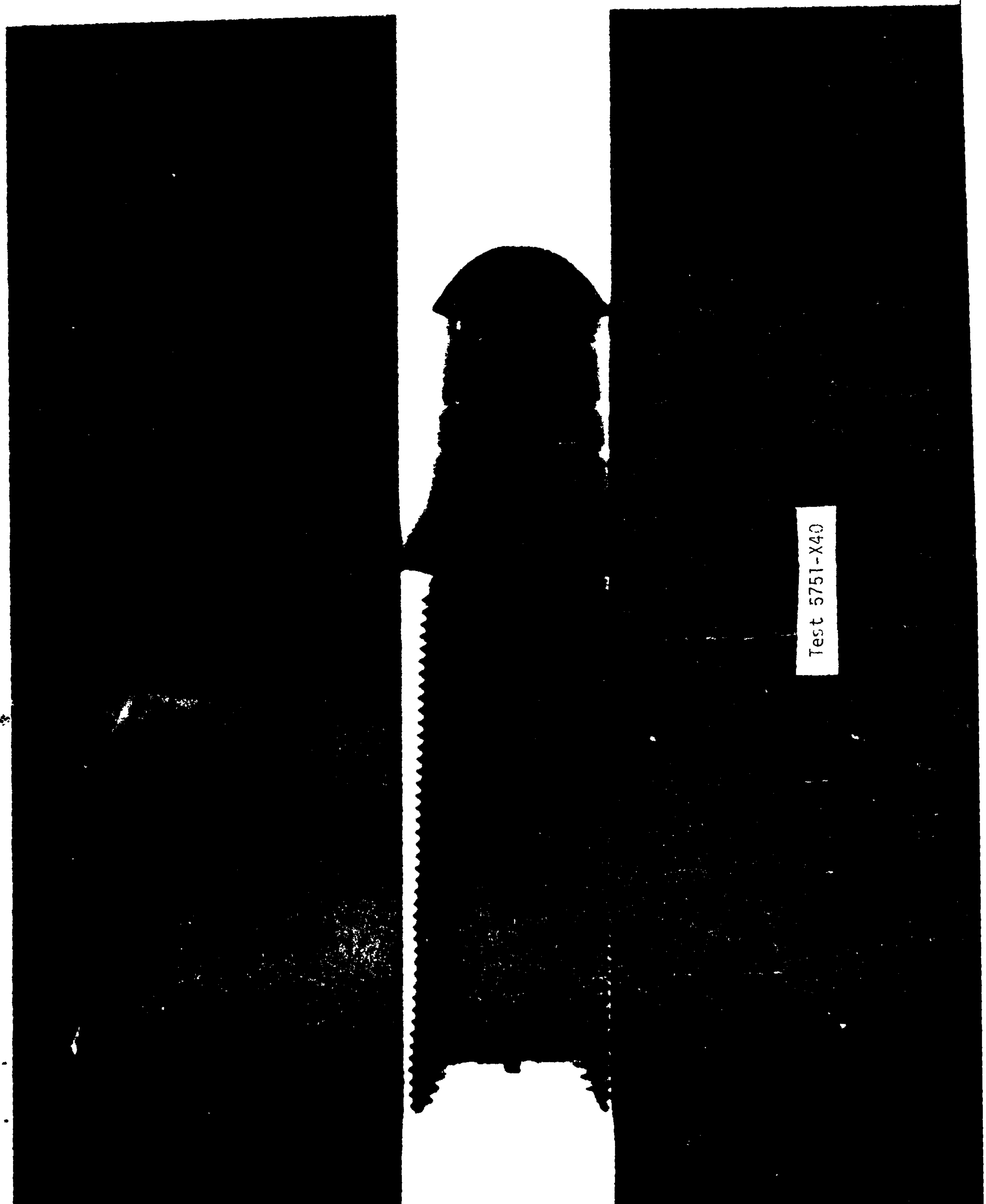

Figure A-32. X-Ray Photographs Test 5751 Sta. X-40

TEST 5749

THERMAL PLOTS

TEST 5749
G-10CT

G-10CT

ID NO. 3091542
PV080376
S1UL140217

DASHED CURVES ON ROW AND SCAN DATA REPRESENT THE ESTIMATED TEMPERATURE RANGE W/O FLARE.

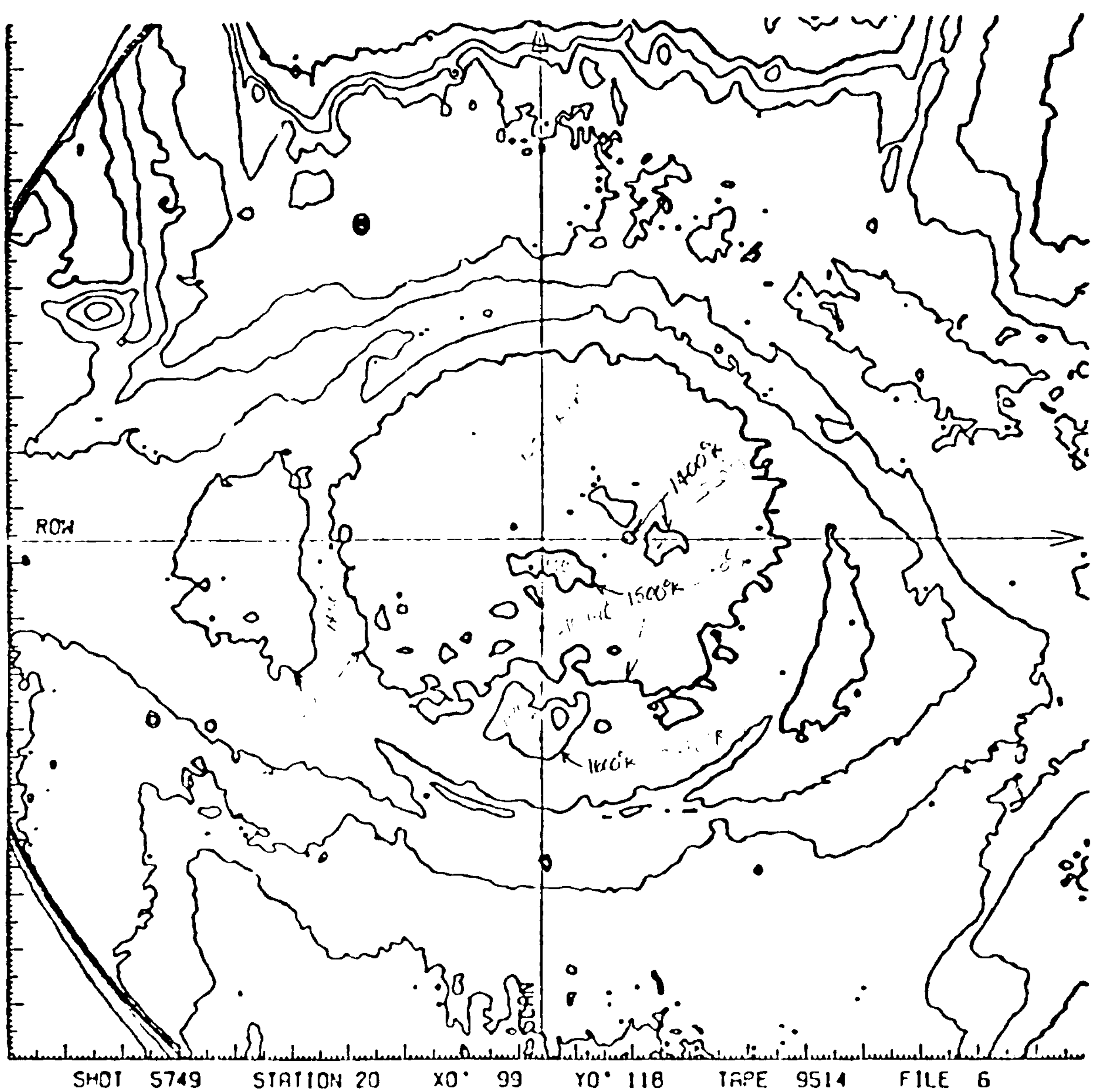

FLIGHT
FLIGHT
UP

PRELIMINARY
UNCHECKED DATA

Figure A-33. Thermo Plots Test 5749 Sta. 20

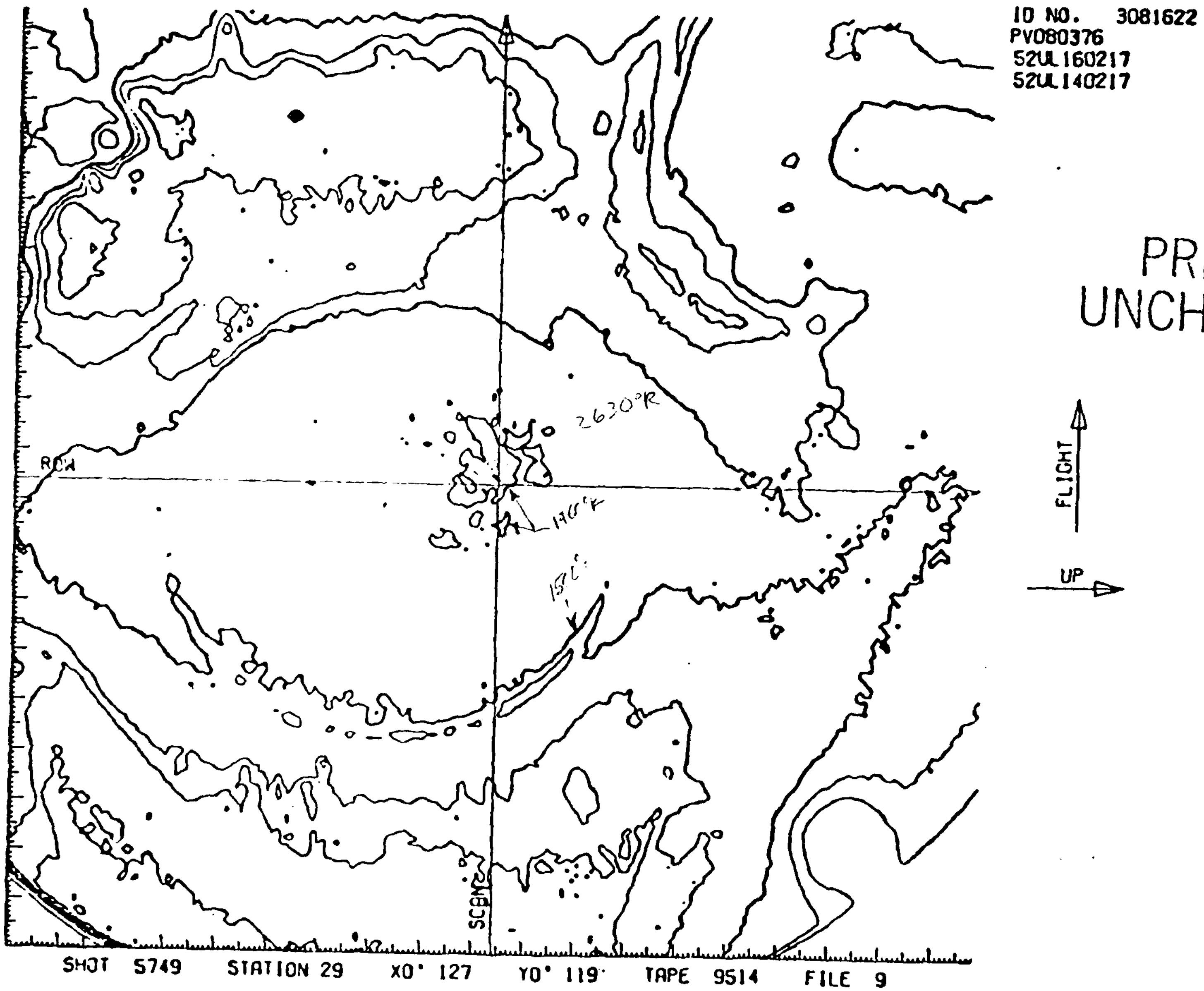

PRELIMINARY
UNCHECKED DATA

Figure A-34. Thermo Plots Test 5749 Sta. 29

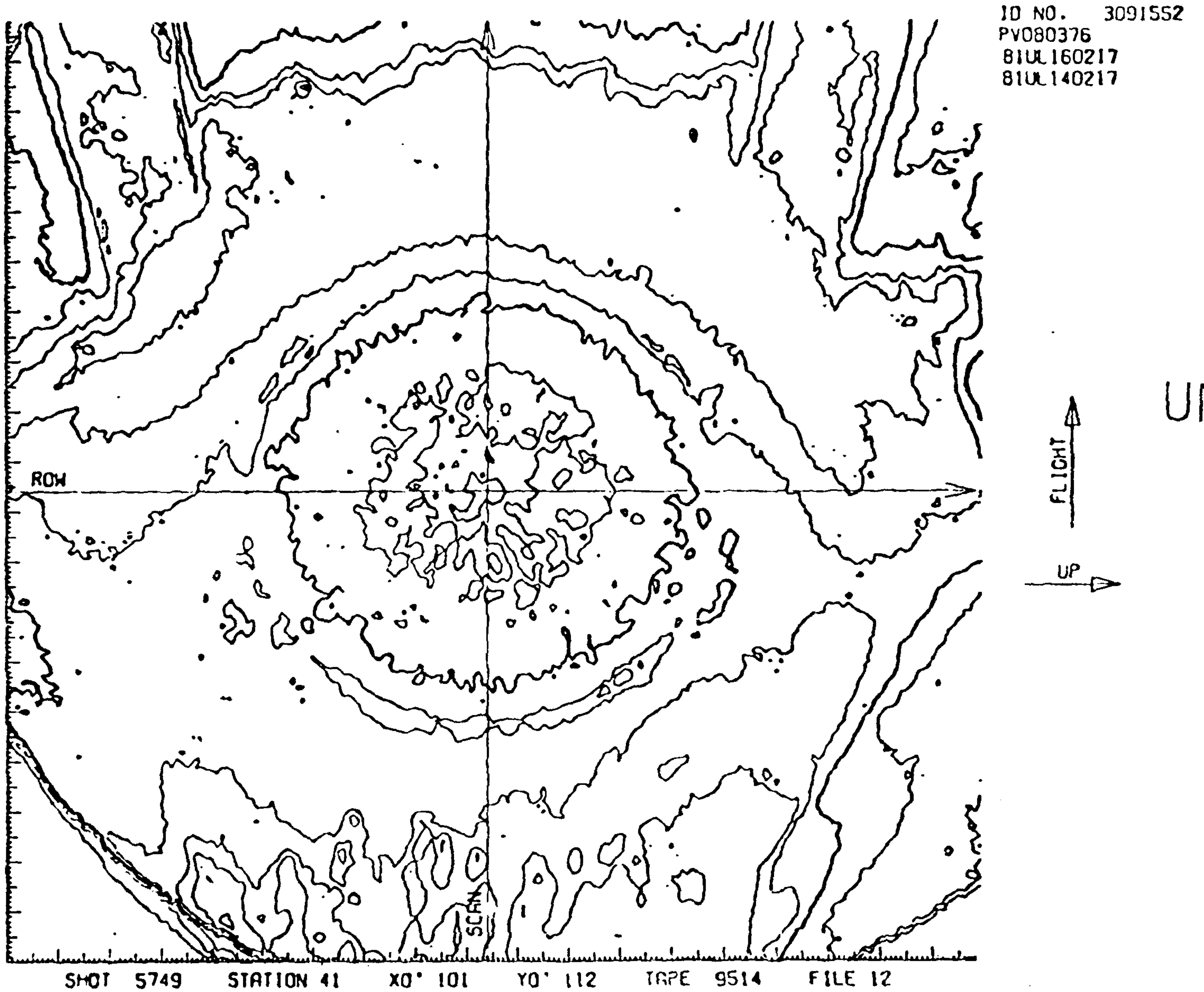

PRELIMINARY
UNCHECKED DATA

Figure A-35. Thermo Plots Test 5749 Sta. 41

TEST 5751

THERMAL PLOTS

TEST 5751 G-11CT

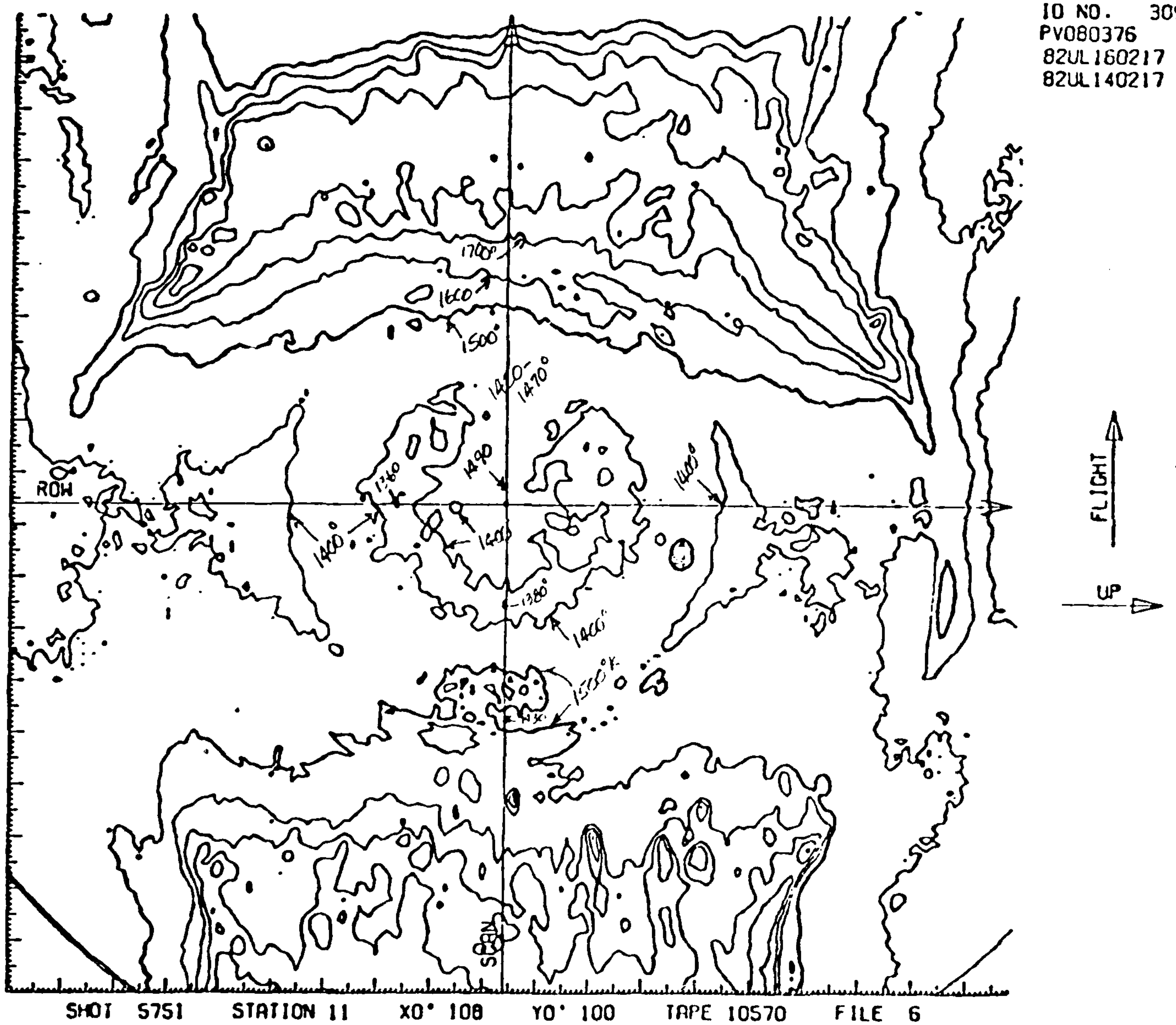

PRELIMINARY
UNCHECKED DATA

DASHED CURVES ON
ROW AND SCAN DATA
REPRESENT THE
ESTIMATED TEMP-
ERATURE RANGE
W/O FLARE

Figure A-36. Thermo Plots Test 5751 Sta. 11

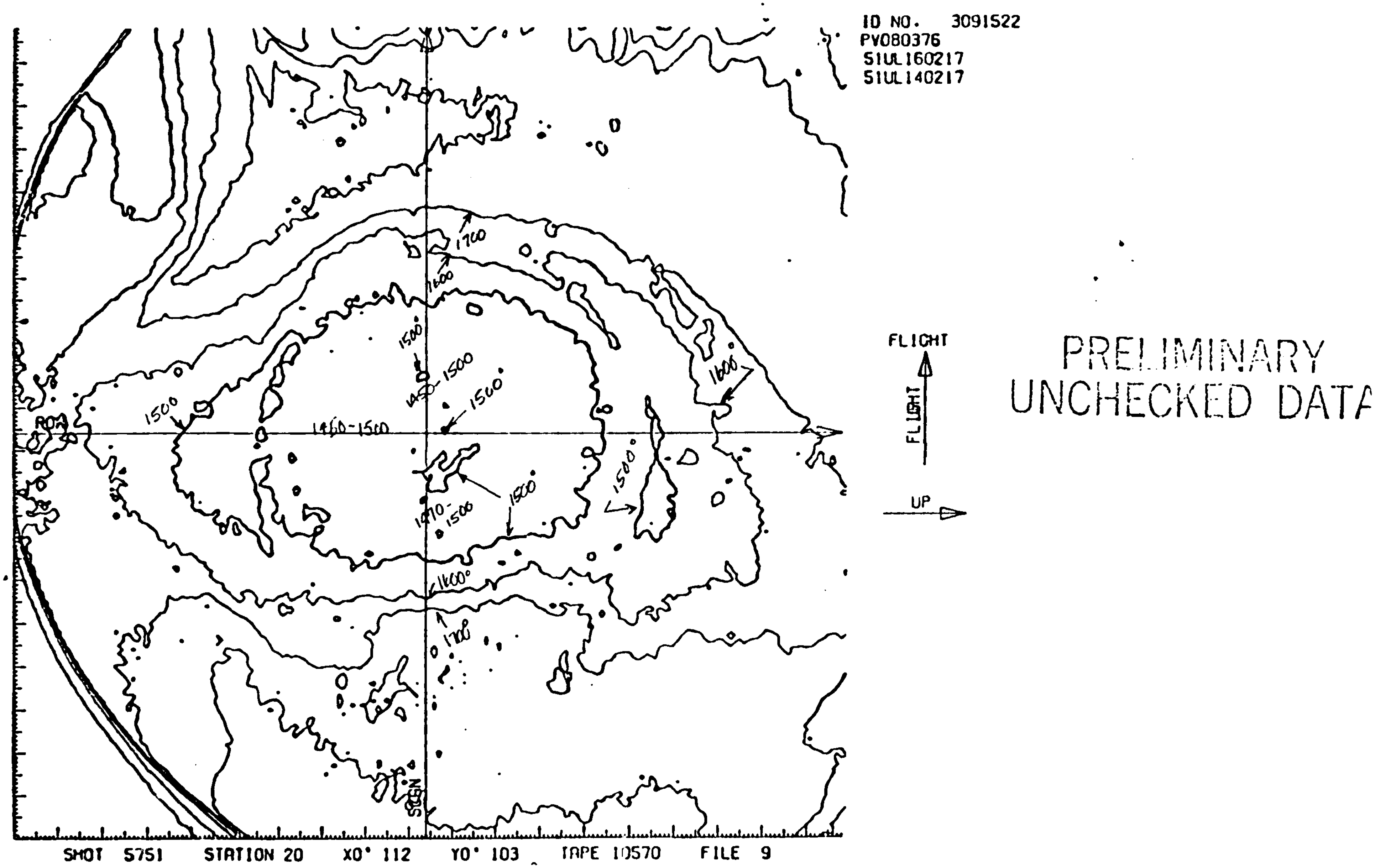

Figure A-37. Thermo Plots Test 5751 Sta. 20

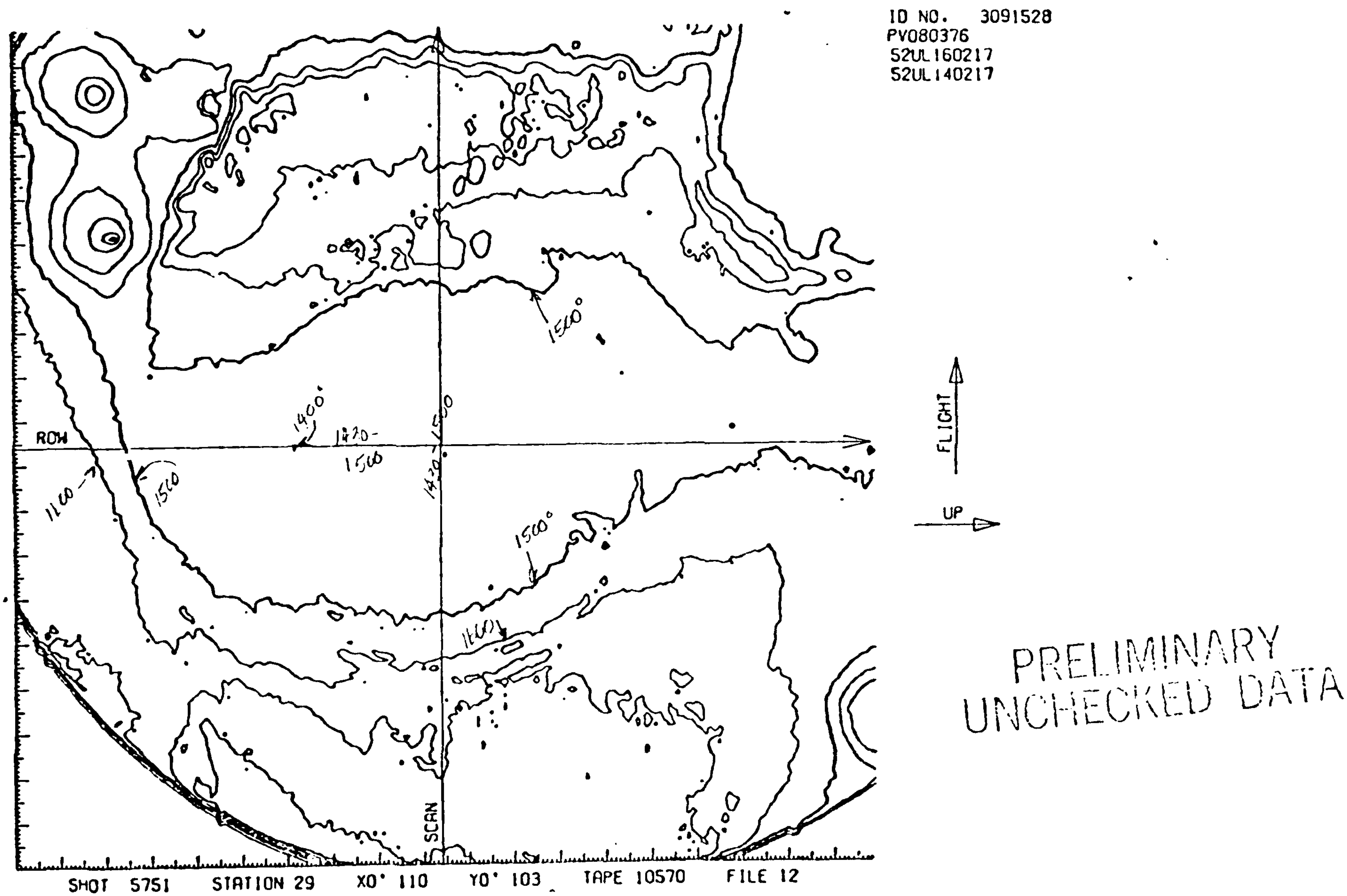

Figure A-38. Thermo Plots Test 5751 Sta. 29

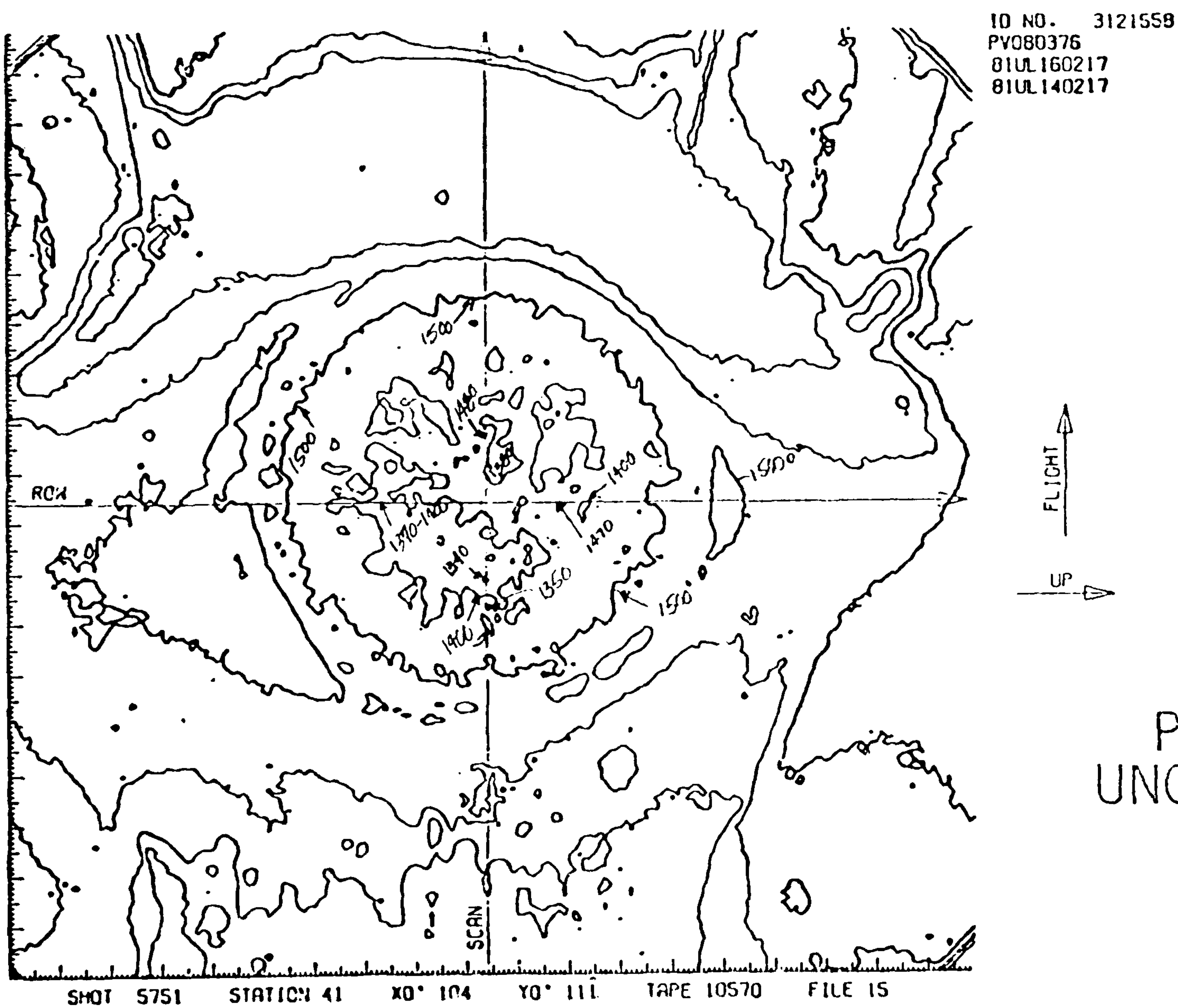

Figure A-39. Thermo Plots Test 5751 Sta. 41

PRELIMINARY
UNCHECKED DATA

APPENDIX B

TEST 5768

LASER PHOTOGRAPHS

X-RAY PHOTOGRAPHS

THERMAL PLOTS

SEE TABLE VII FOR DESCRIPTION
OF TRACK STATION NUMBERS

TEST 5768

LASER PHOTOGRAPHS

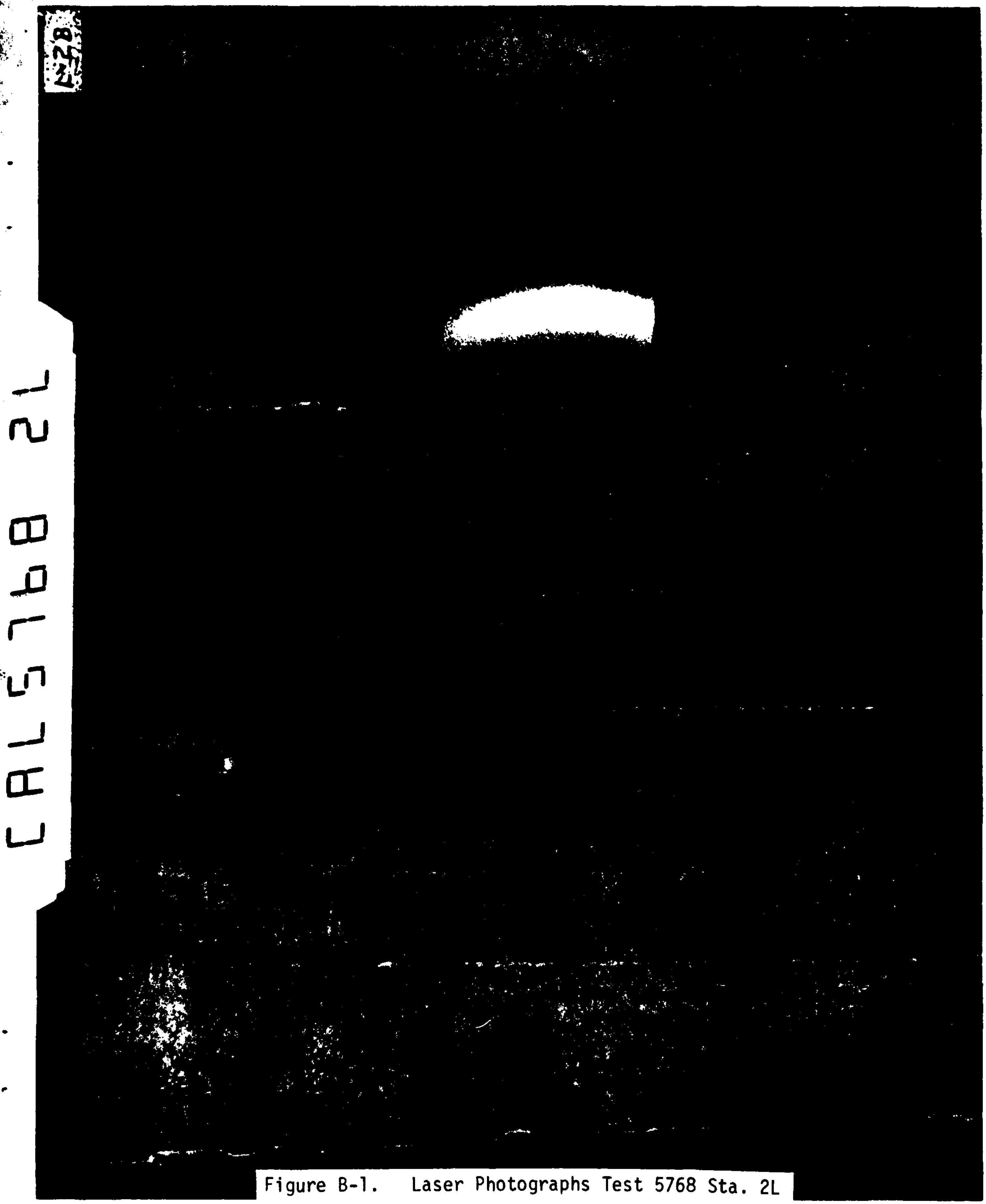

Figure B-1. Laser Photographs Test 5768 Sta. 2L

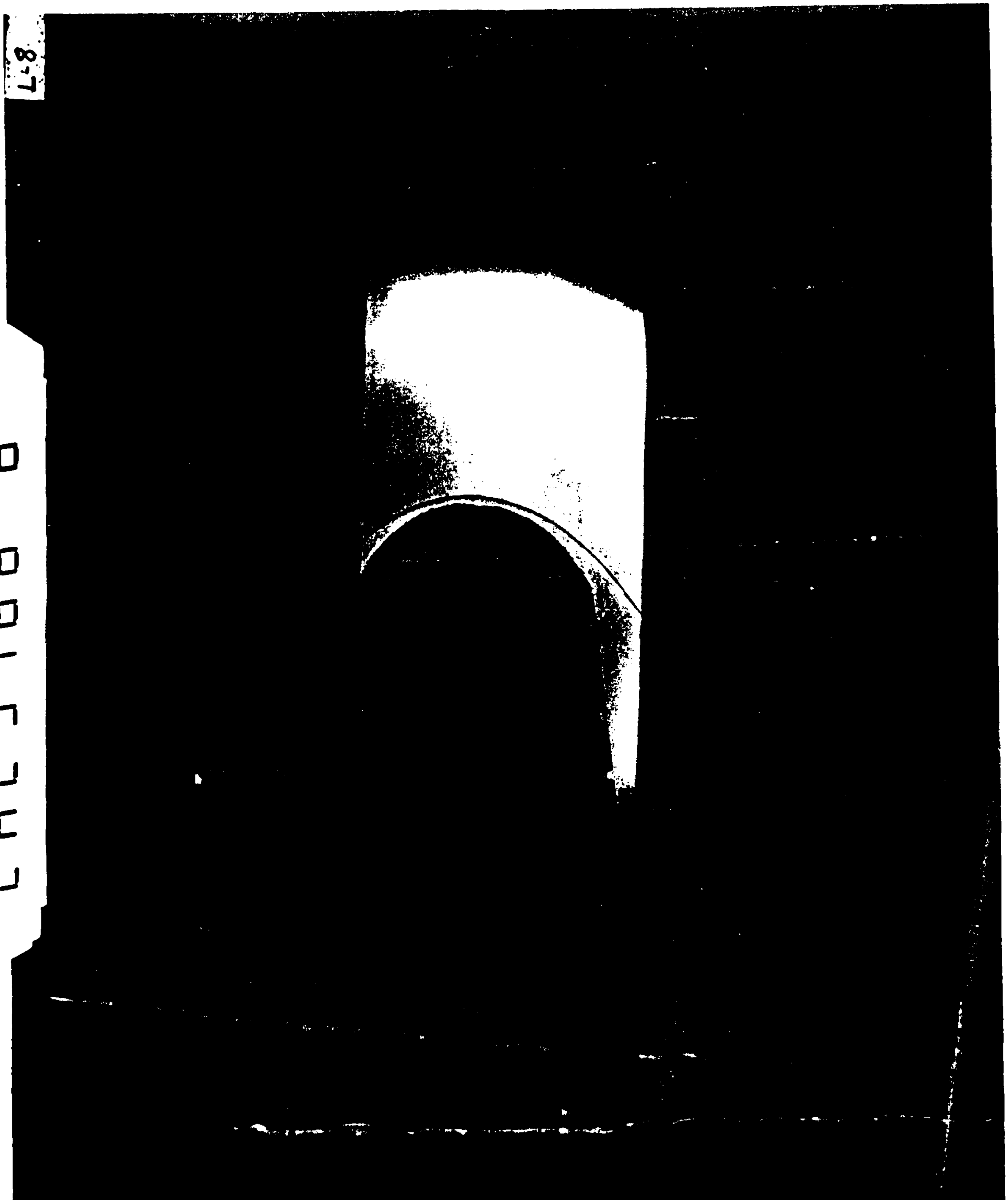

Figure B-2. Laser Photographs Test 5768 Sta. 8

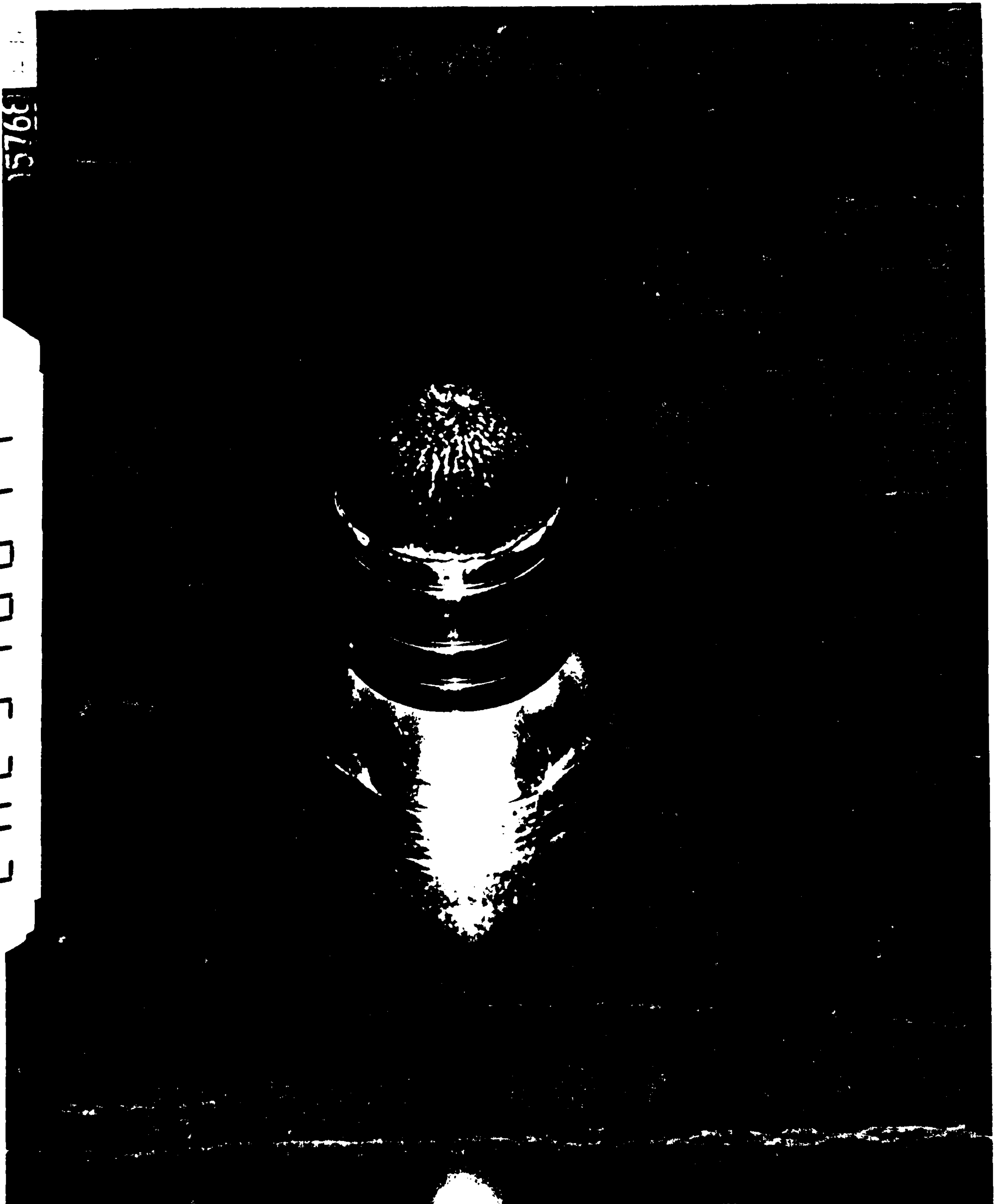

Figure B-3. Laser Photographs Test 5768 Sta. 11

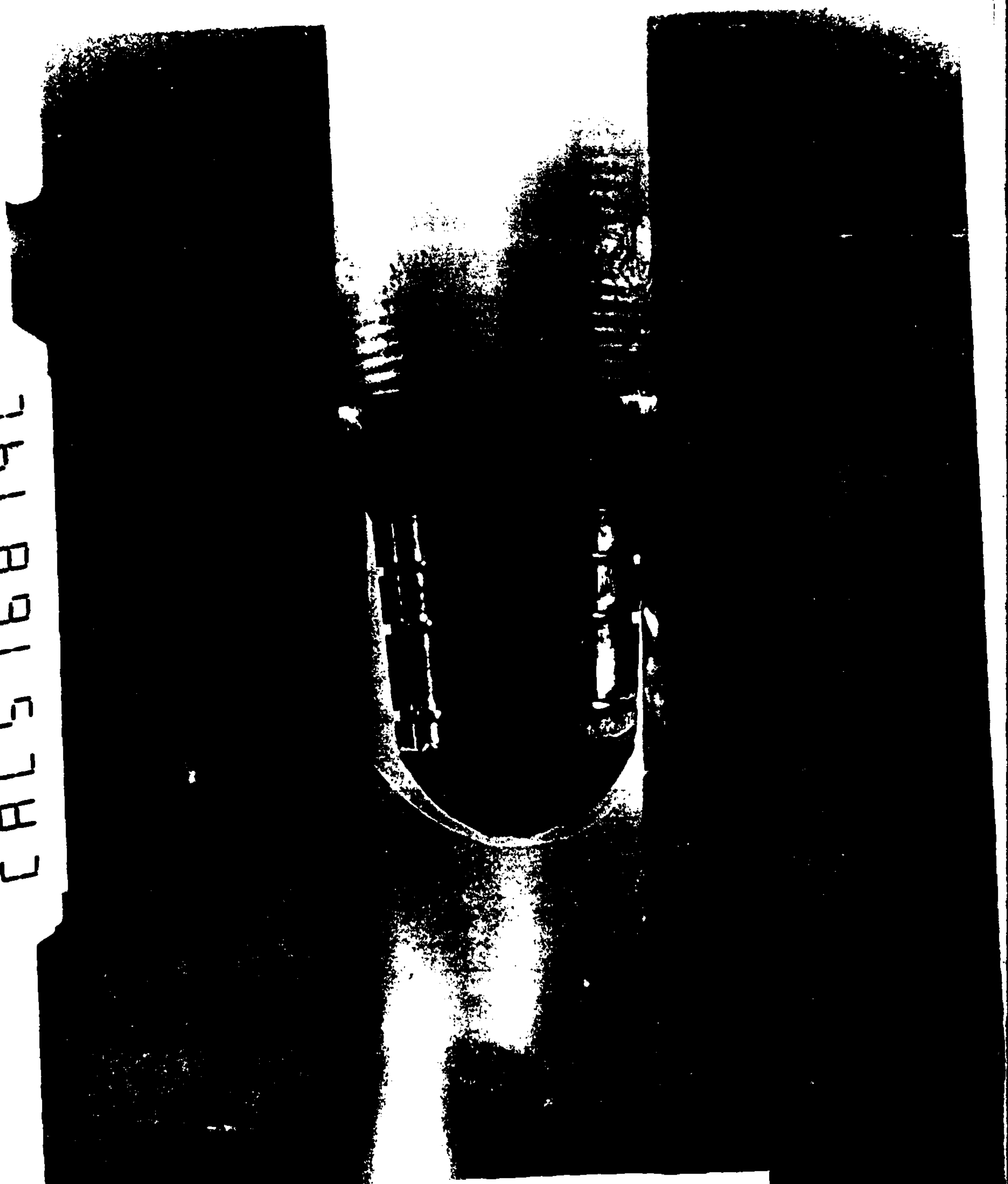

Figure B-4. Laser Photographs Test 5768 Sta. 19L

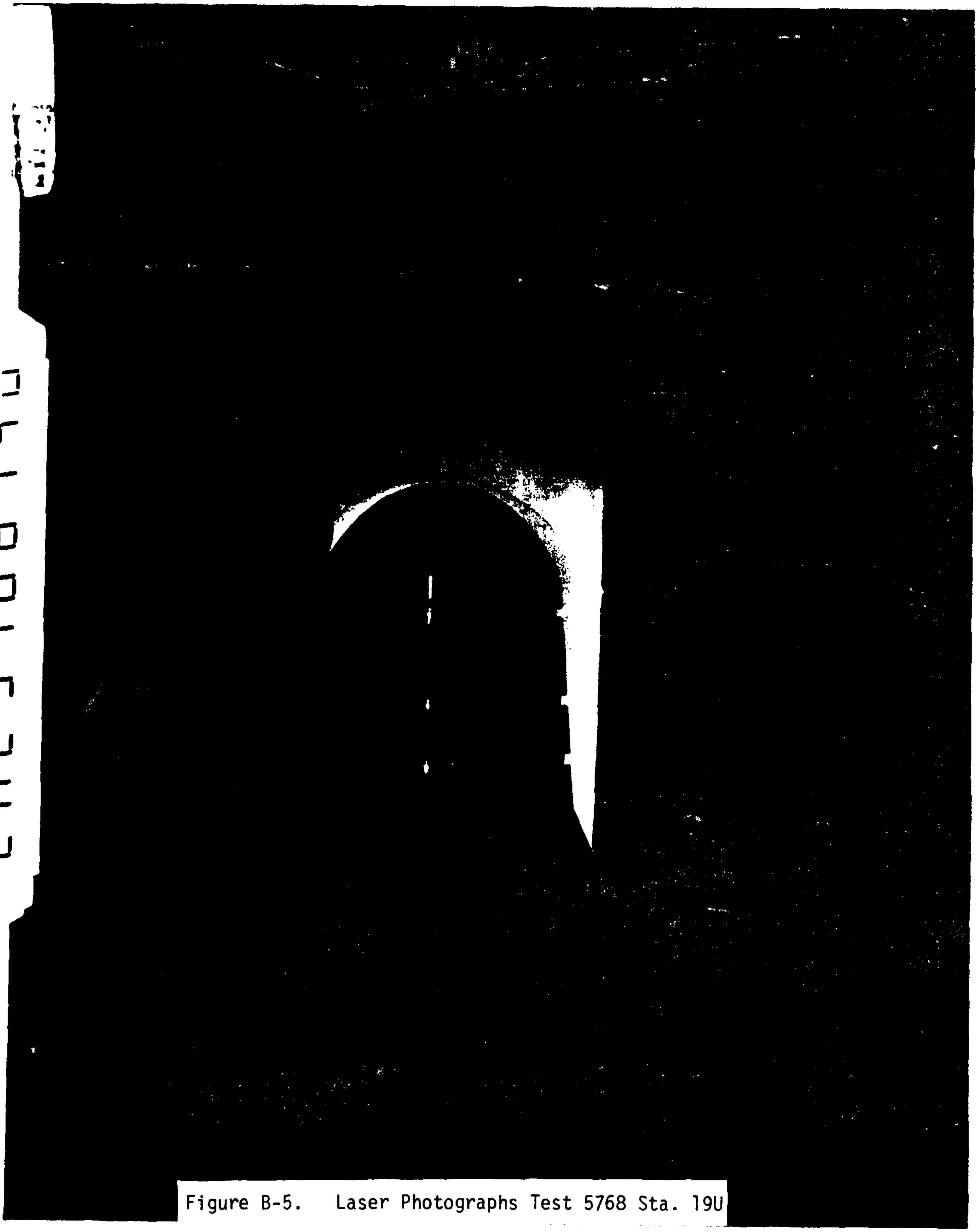

Figure B-5. Laser Photographs Test 5768 Sta. 19U

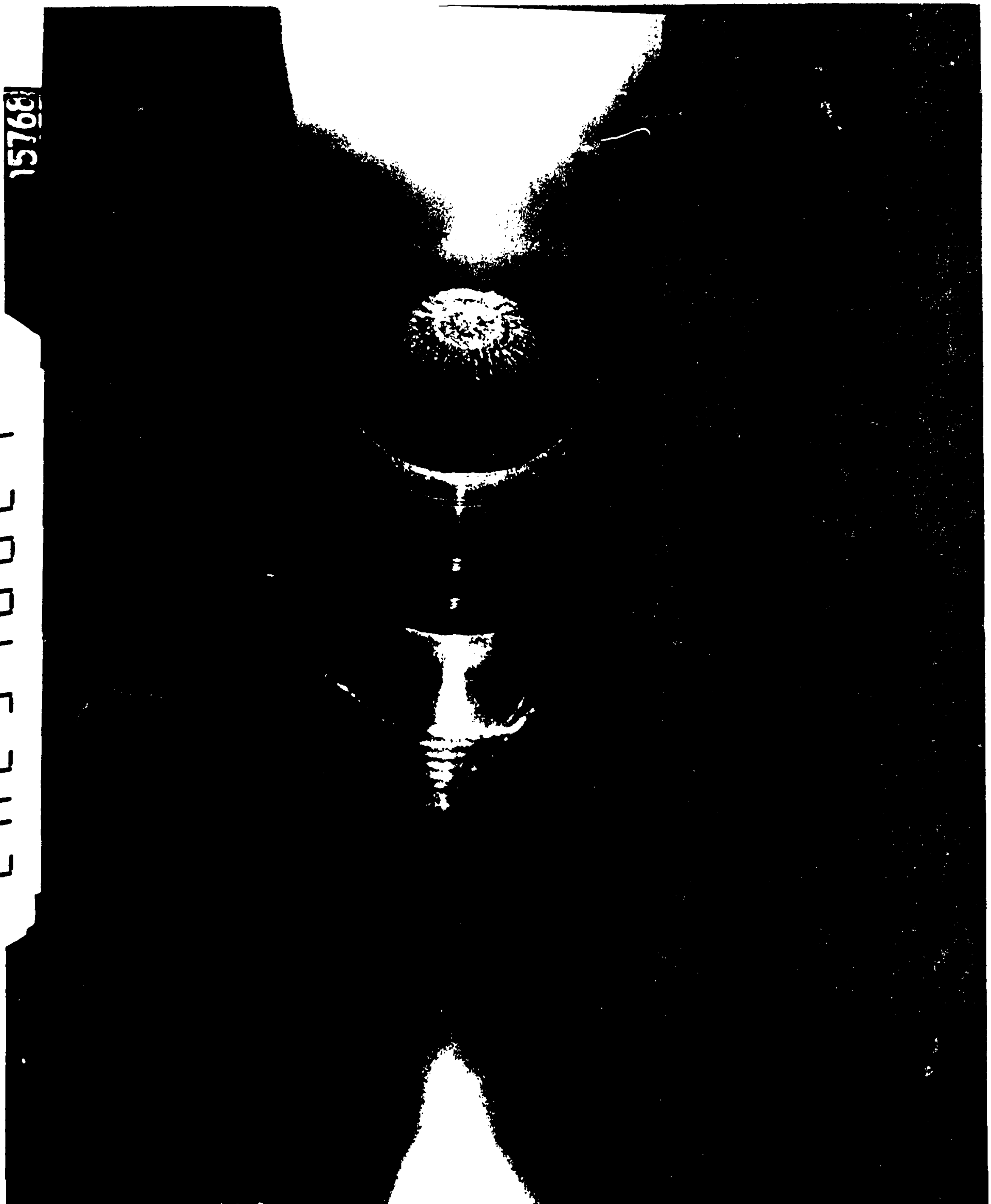

Figure B-7. Laser Photographs Test 5768 Sta. 27

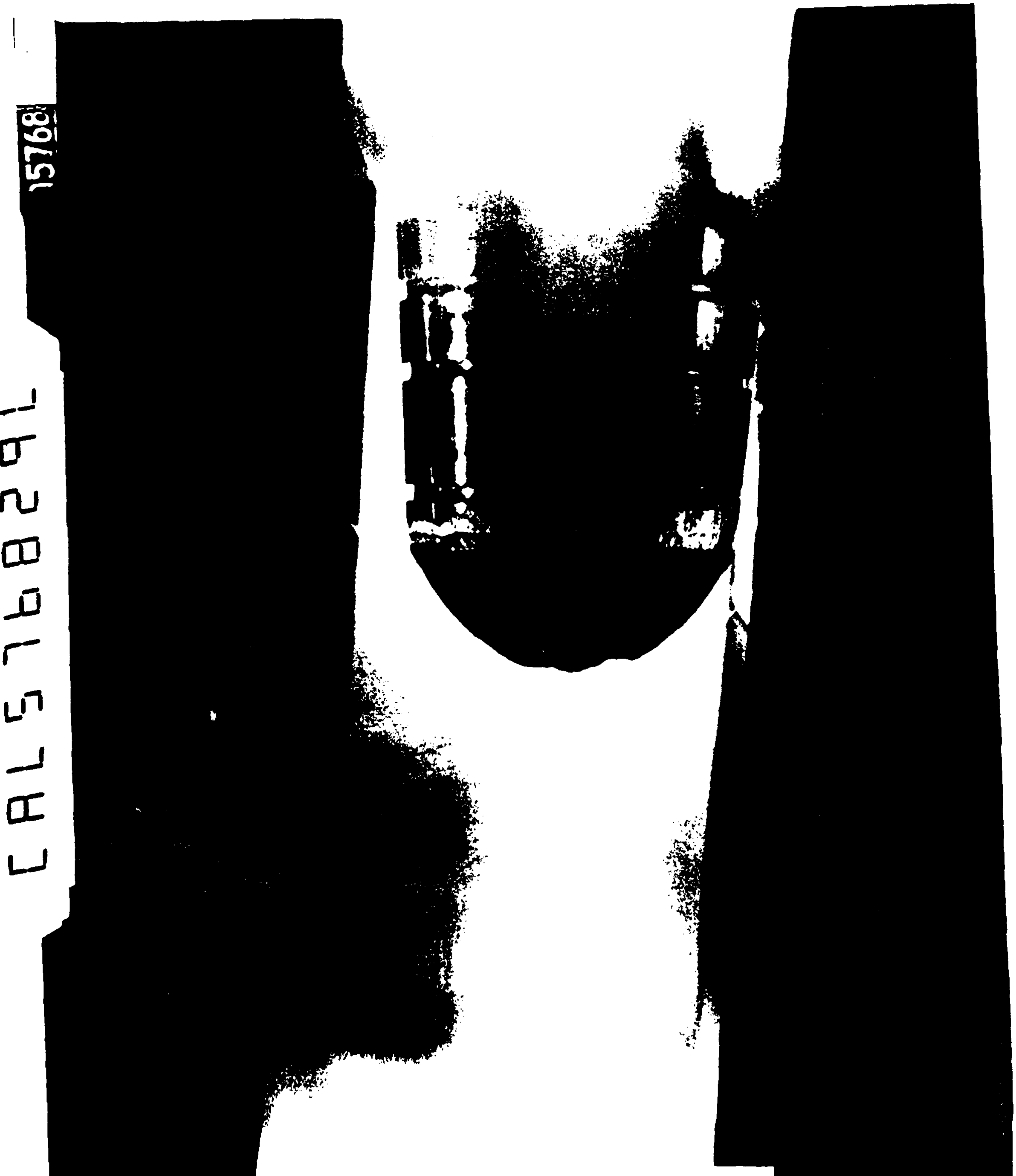

Figure B-8. Laser Photographs Test 5768 Sta. 29L

CAL576832

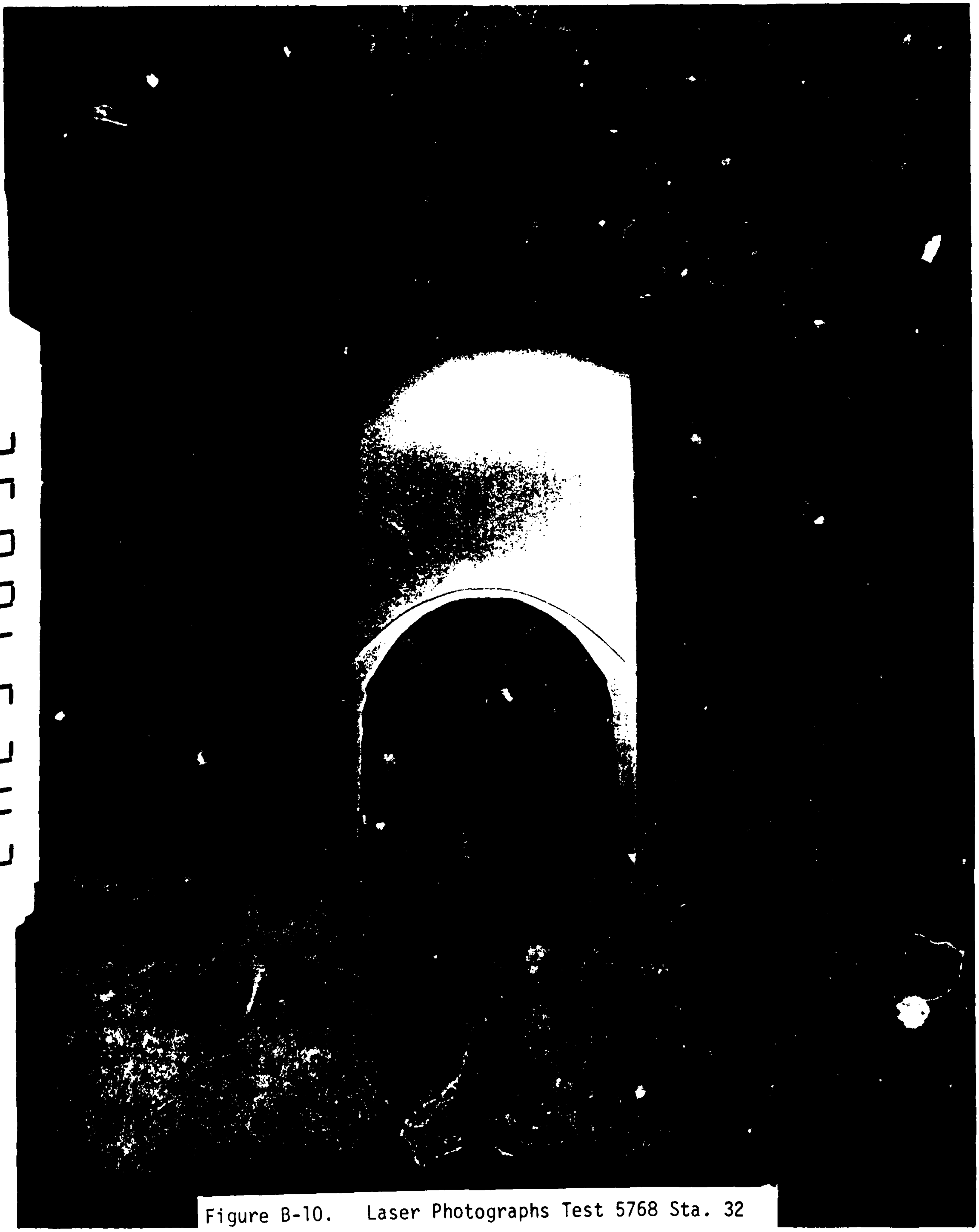

Figure B-10. Laser Photographs Test 5768 Sta. 32

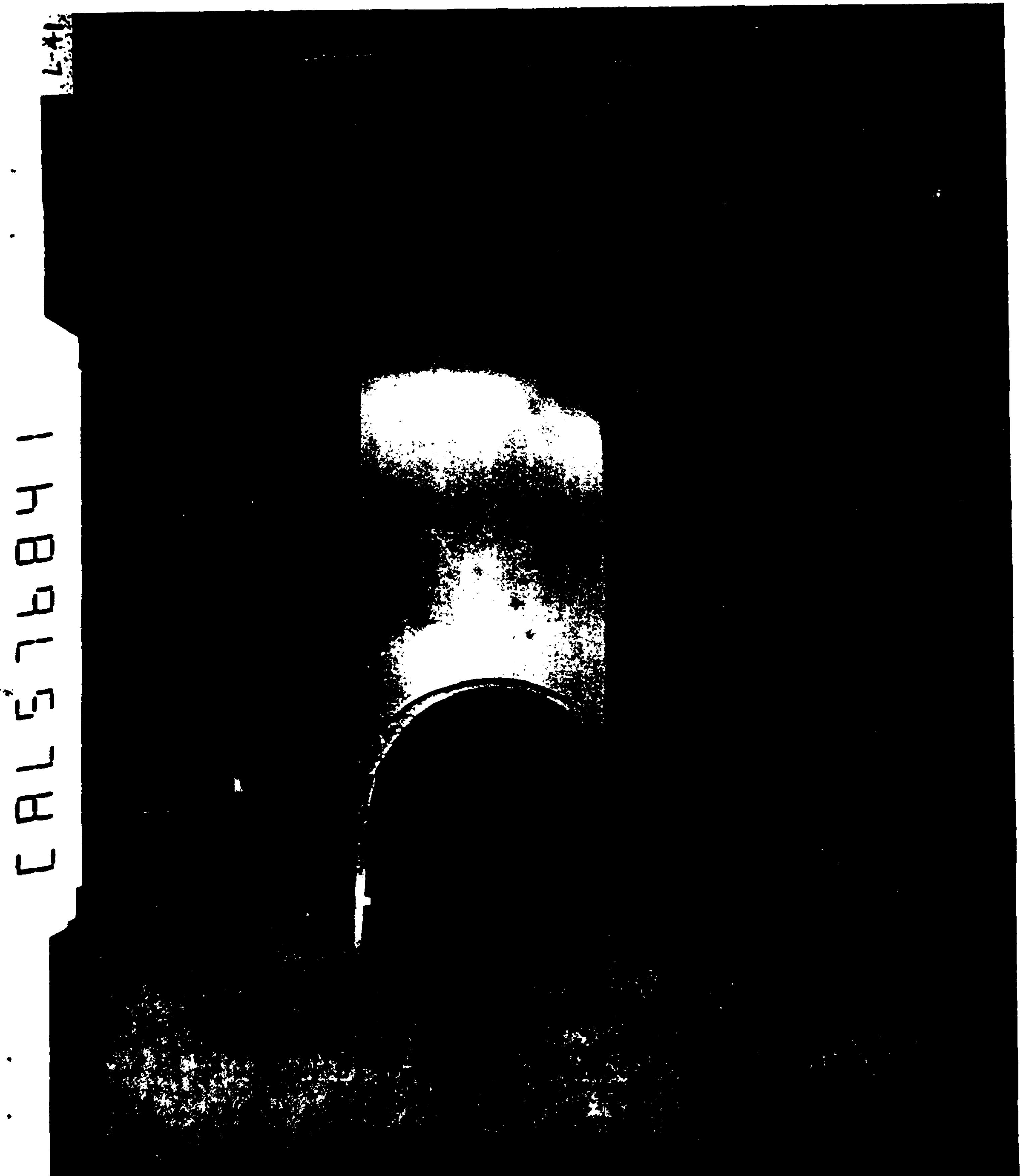

Figure B-12. Laser Photographs Test 5768 Sta. 41

TEST 5768

X-RAY PHOTOGRAPHS

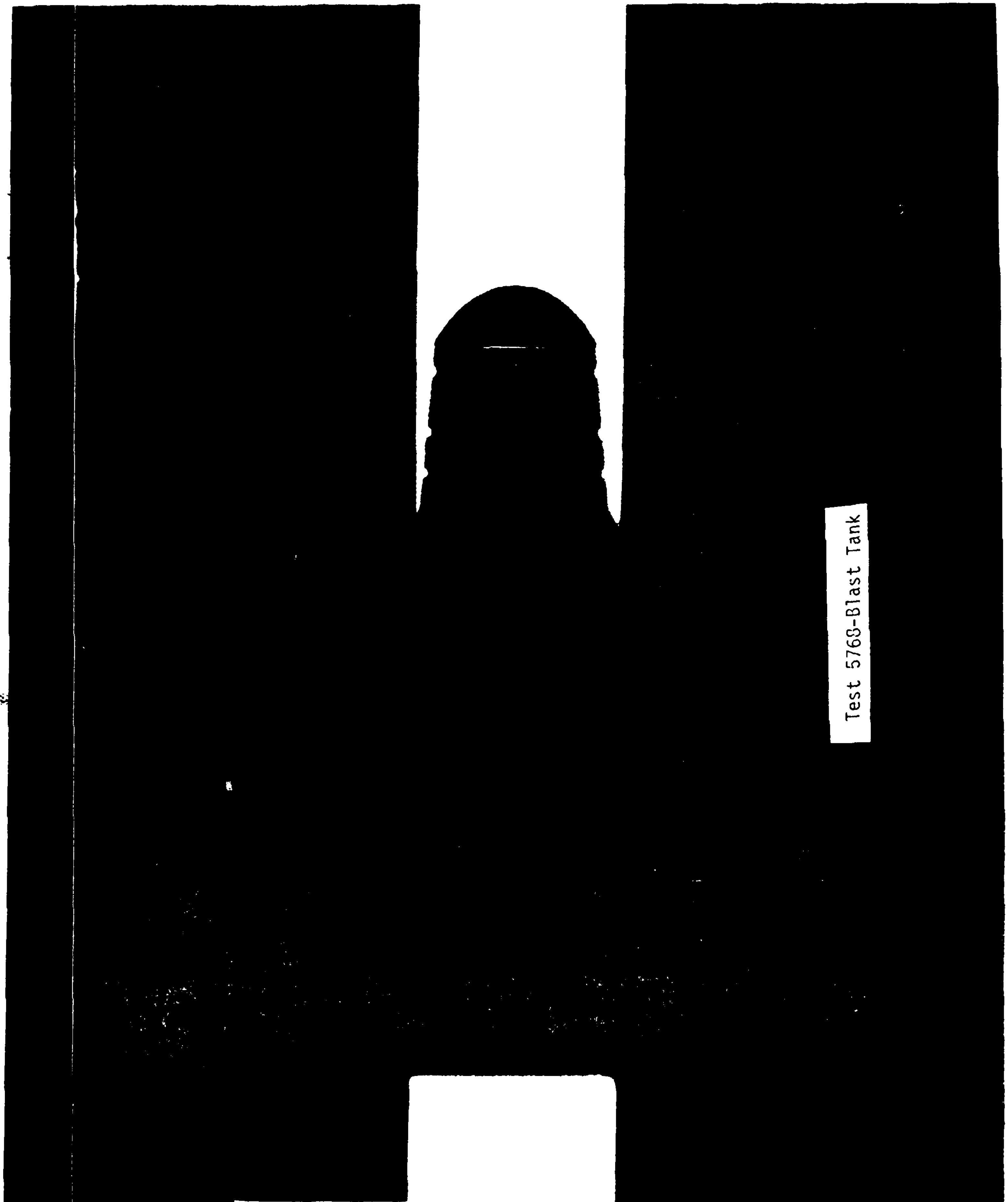

Figure B-13. X-Ray Photographs Test 5768 Blast Tank

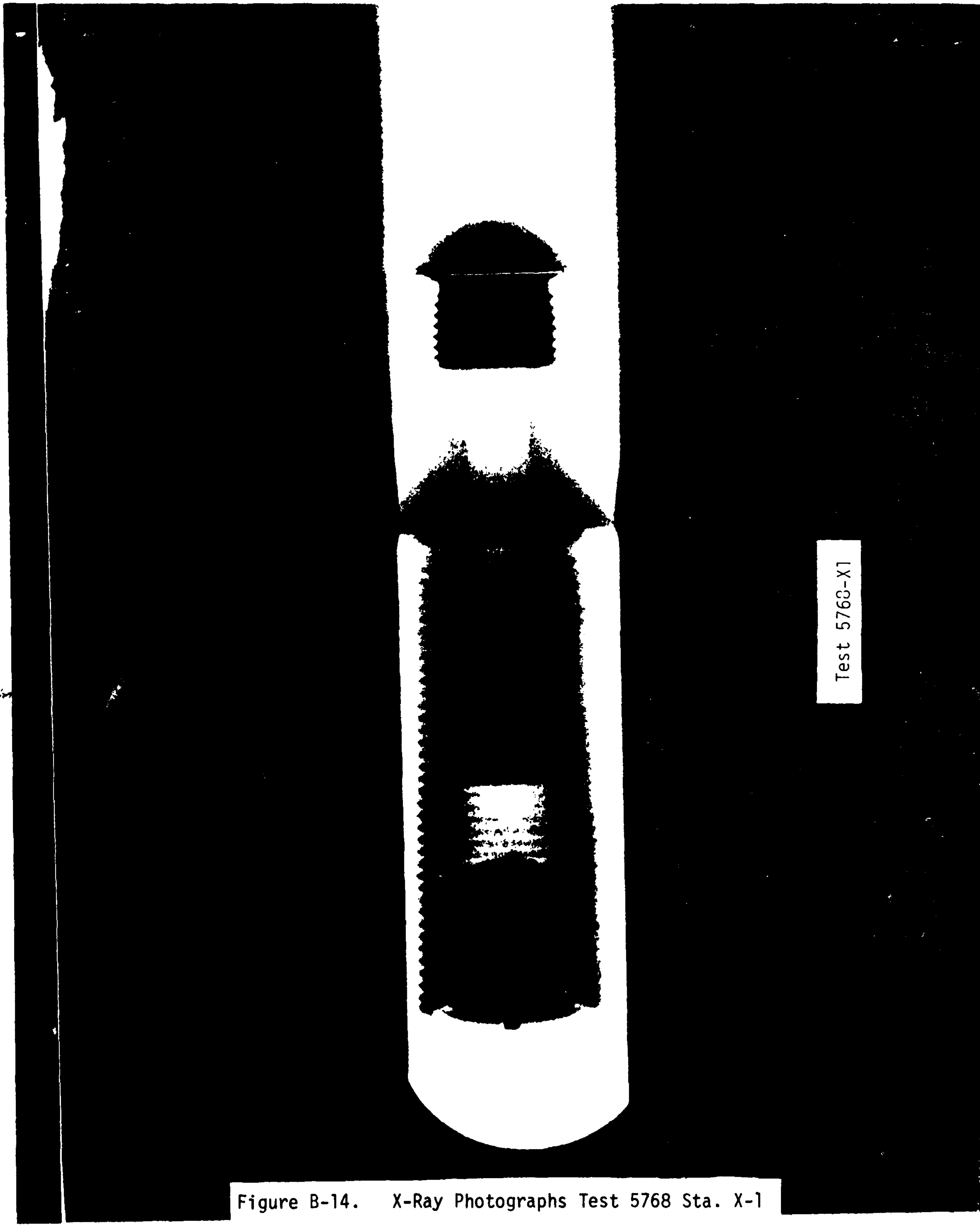

Figure B-14. X-Ray Photographs Test 5768 Sta. X-1

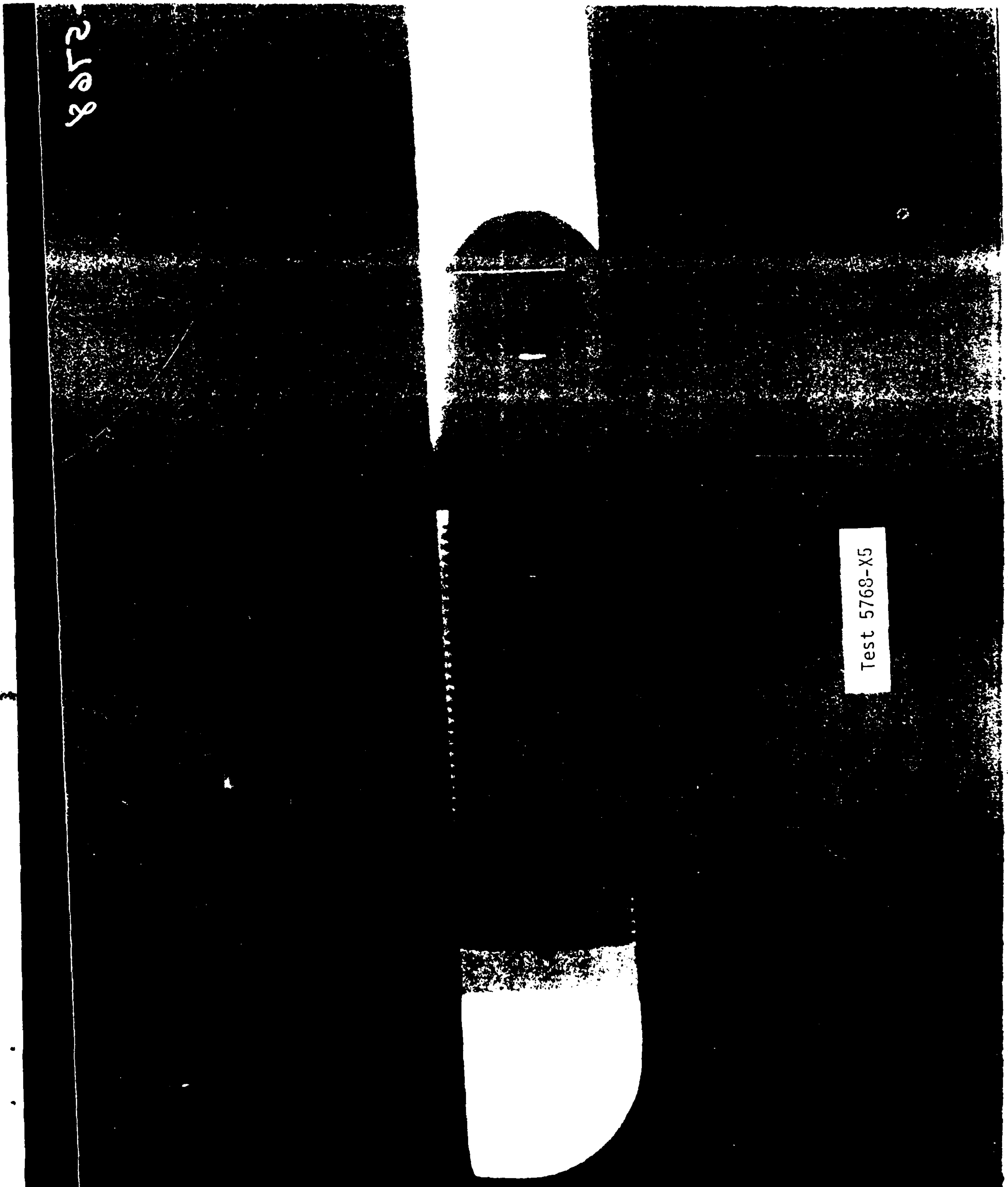

Figure B-15. X-Ray Photographs Test 5768 Sta. X-5

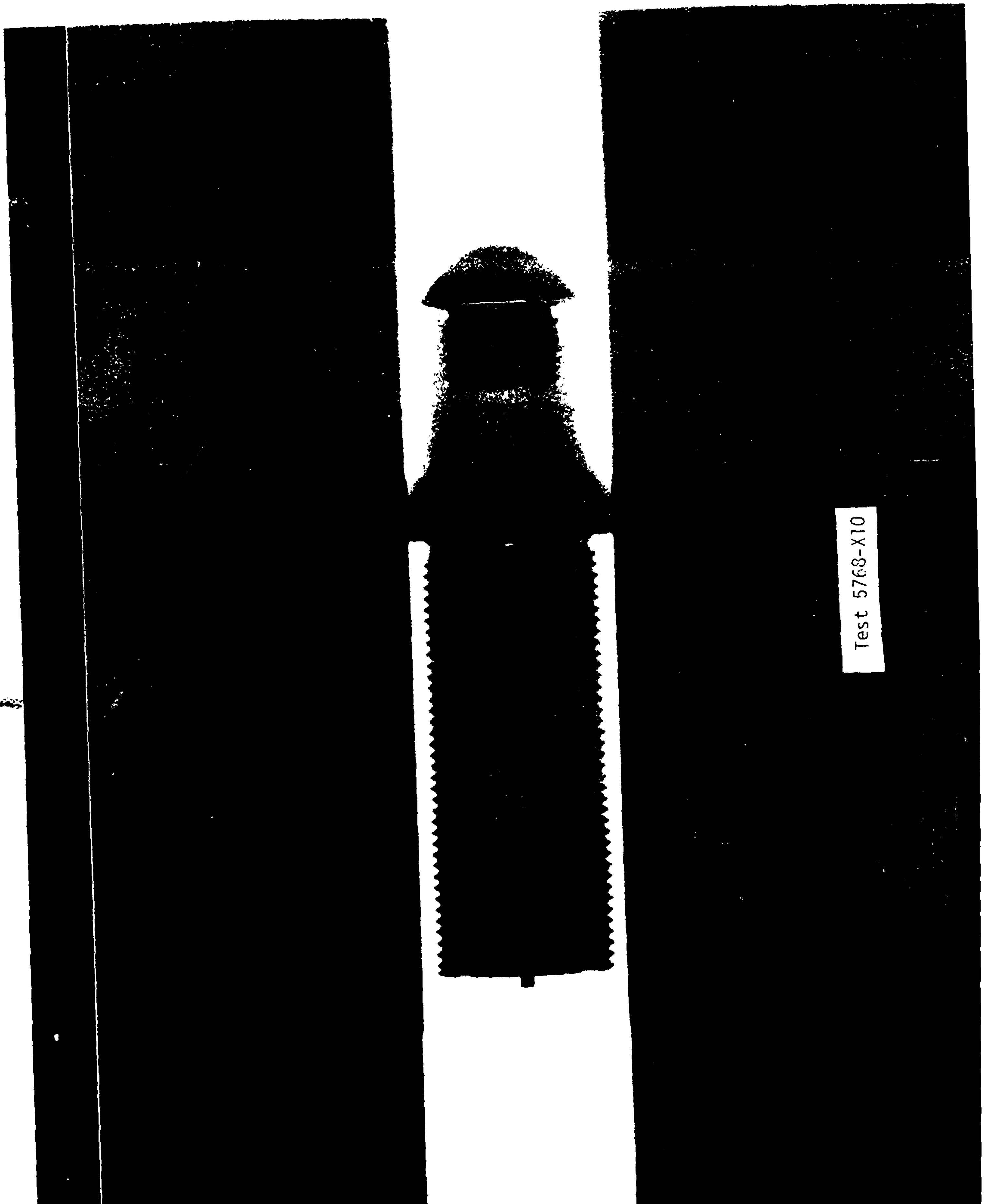

Figure B-16. X-Ray Photographs Test 5768 Sta. X-10

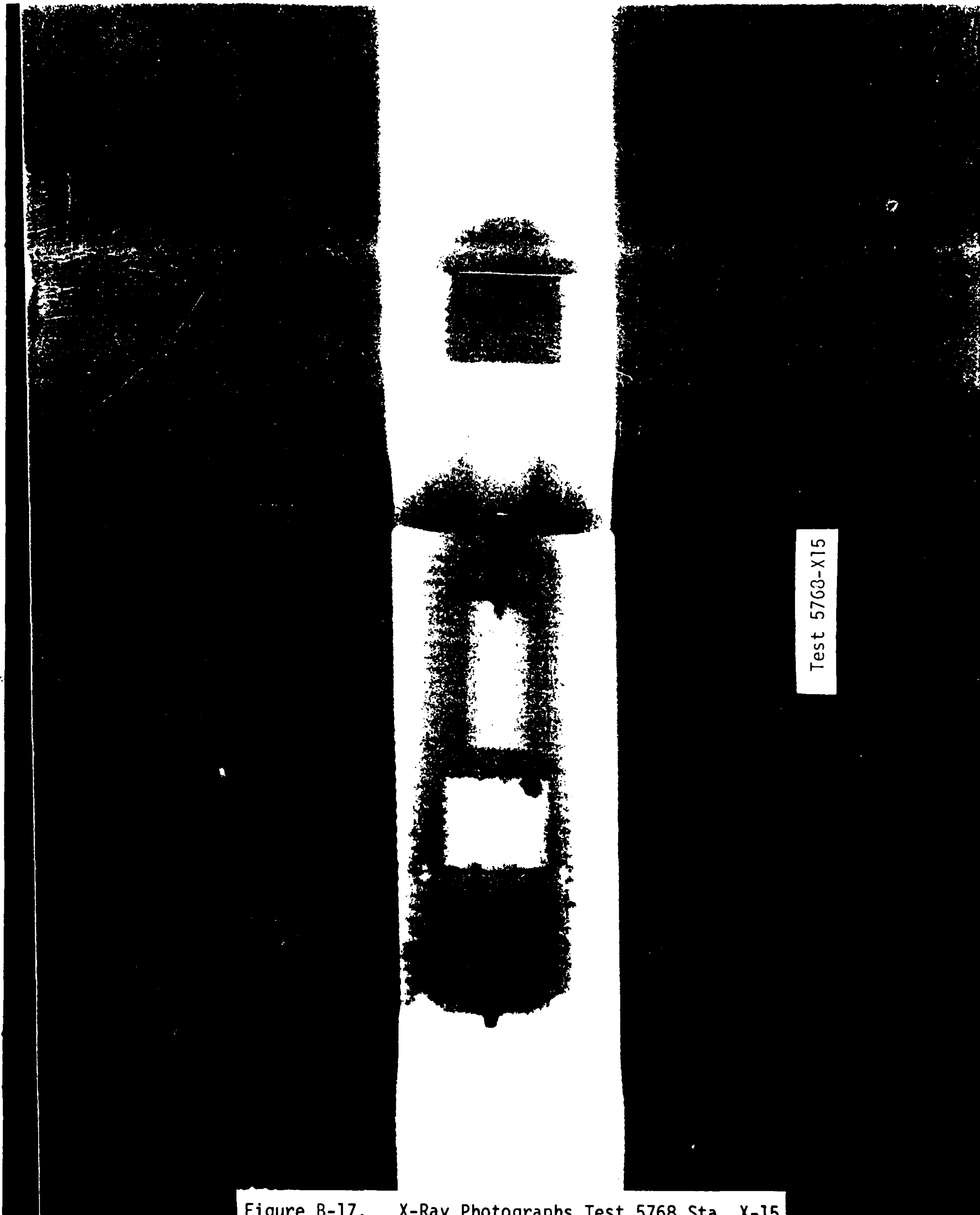

Figure B-17. X-Ray Photographs Test 5768 Sta. X-15

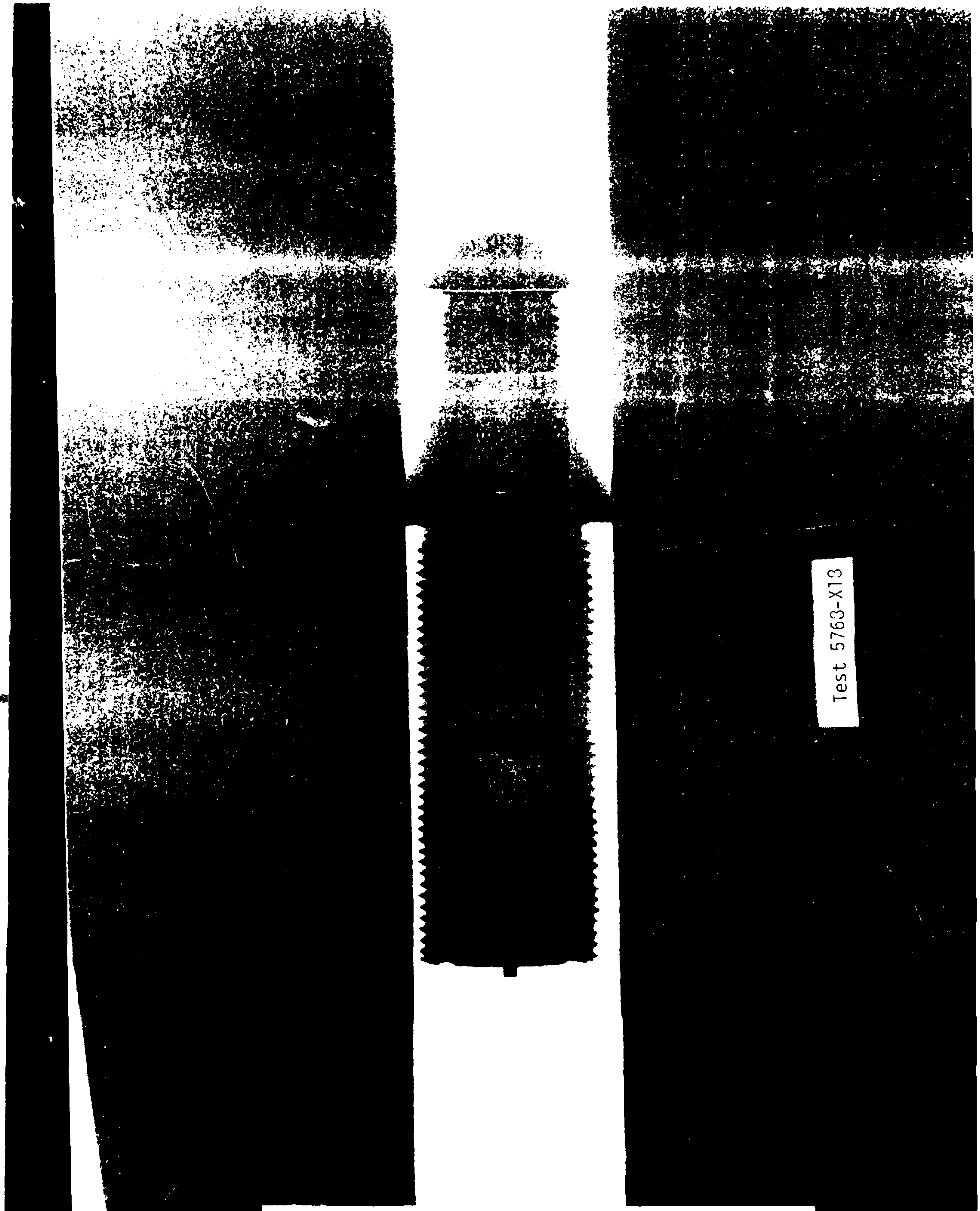

Figure B-18. X-Ray Photographs Test 5768 Sta. X-13

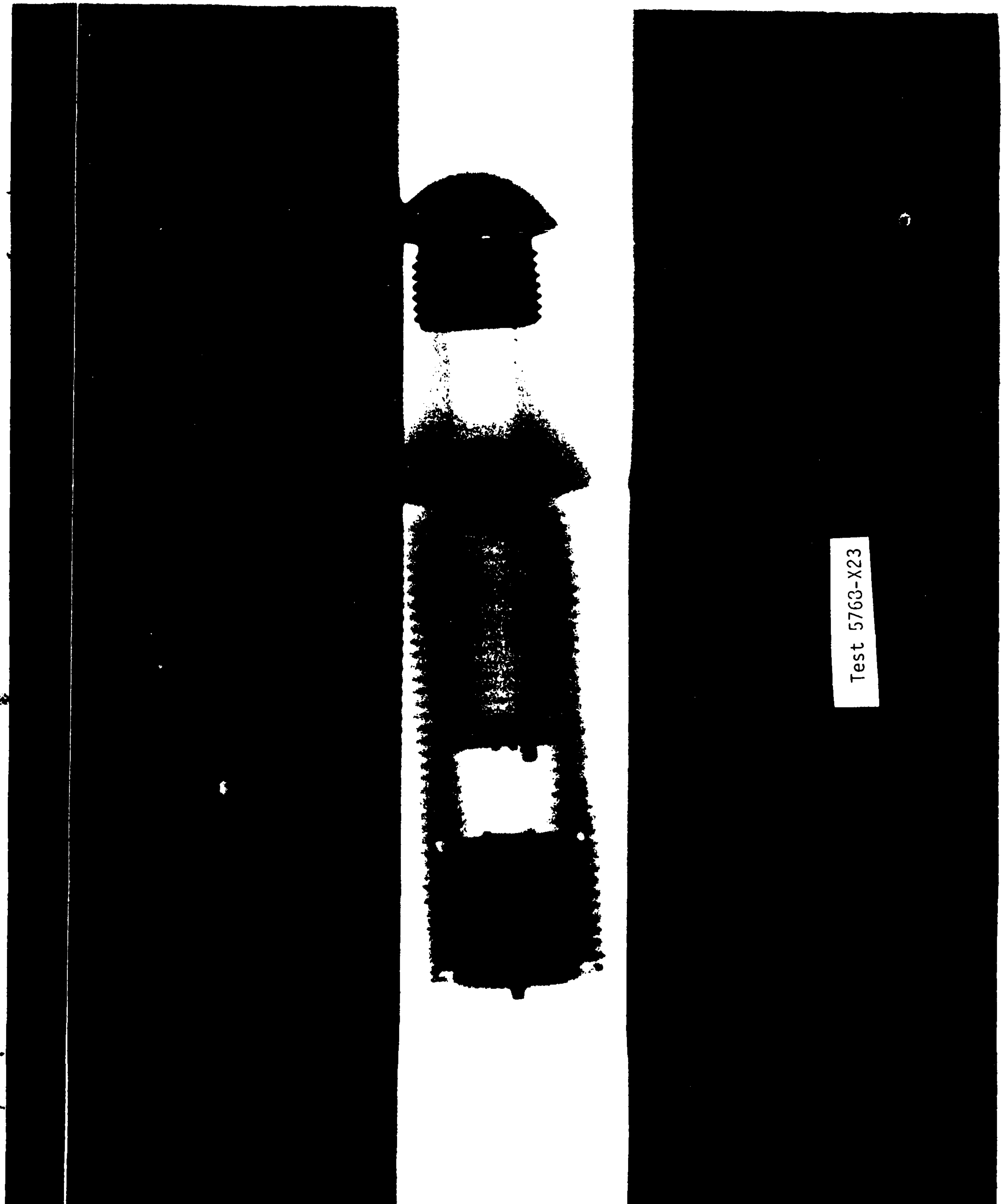

Figure B-19. X-Ray Photographs Test 5768 Sta. X-23

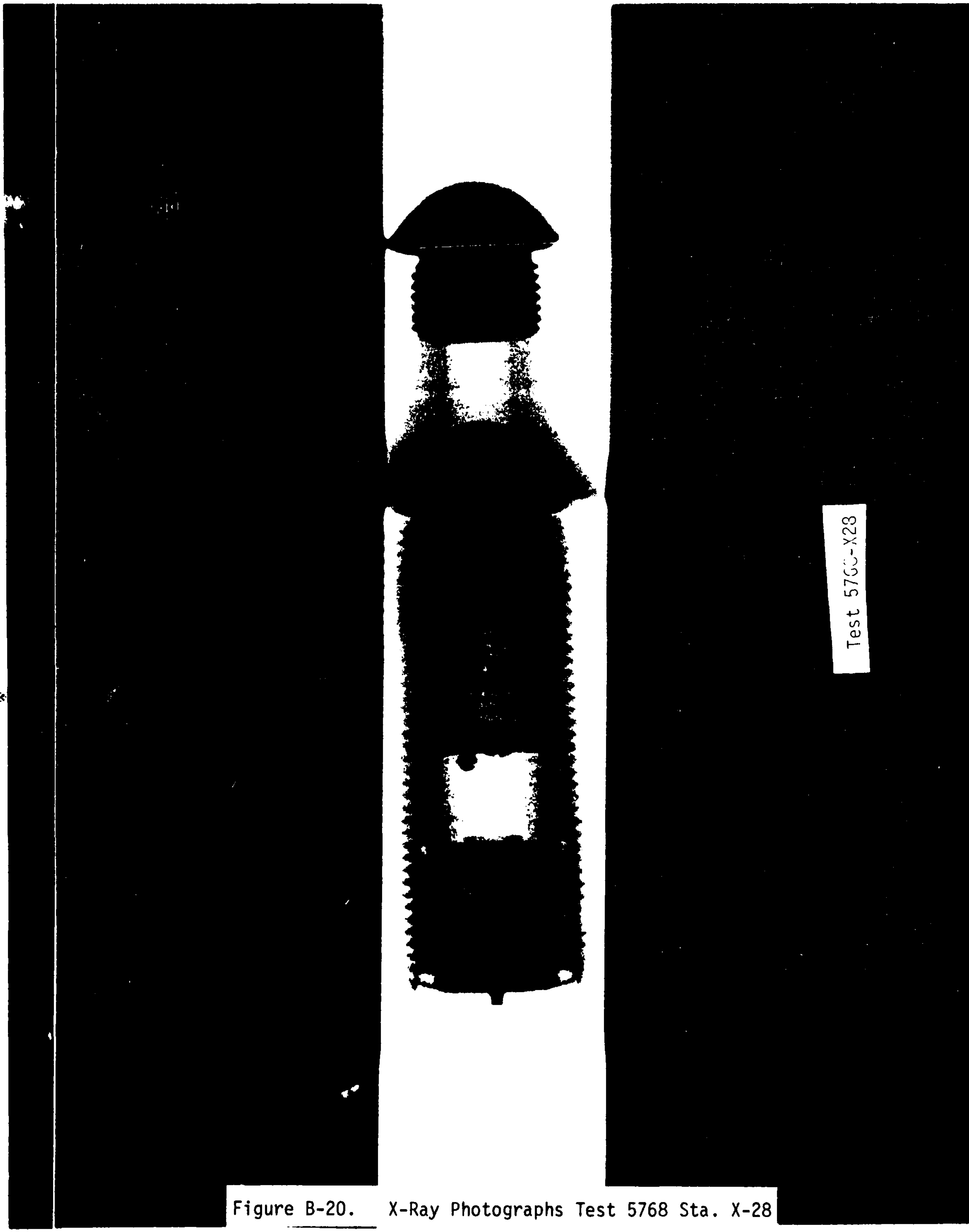

Figure B-20. X-Ray Photographs Test 5768 Sta. X-28

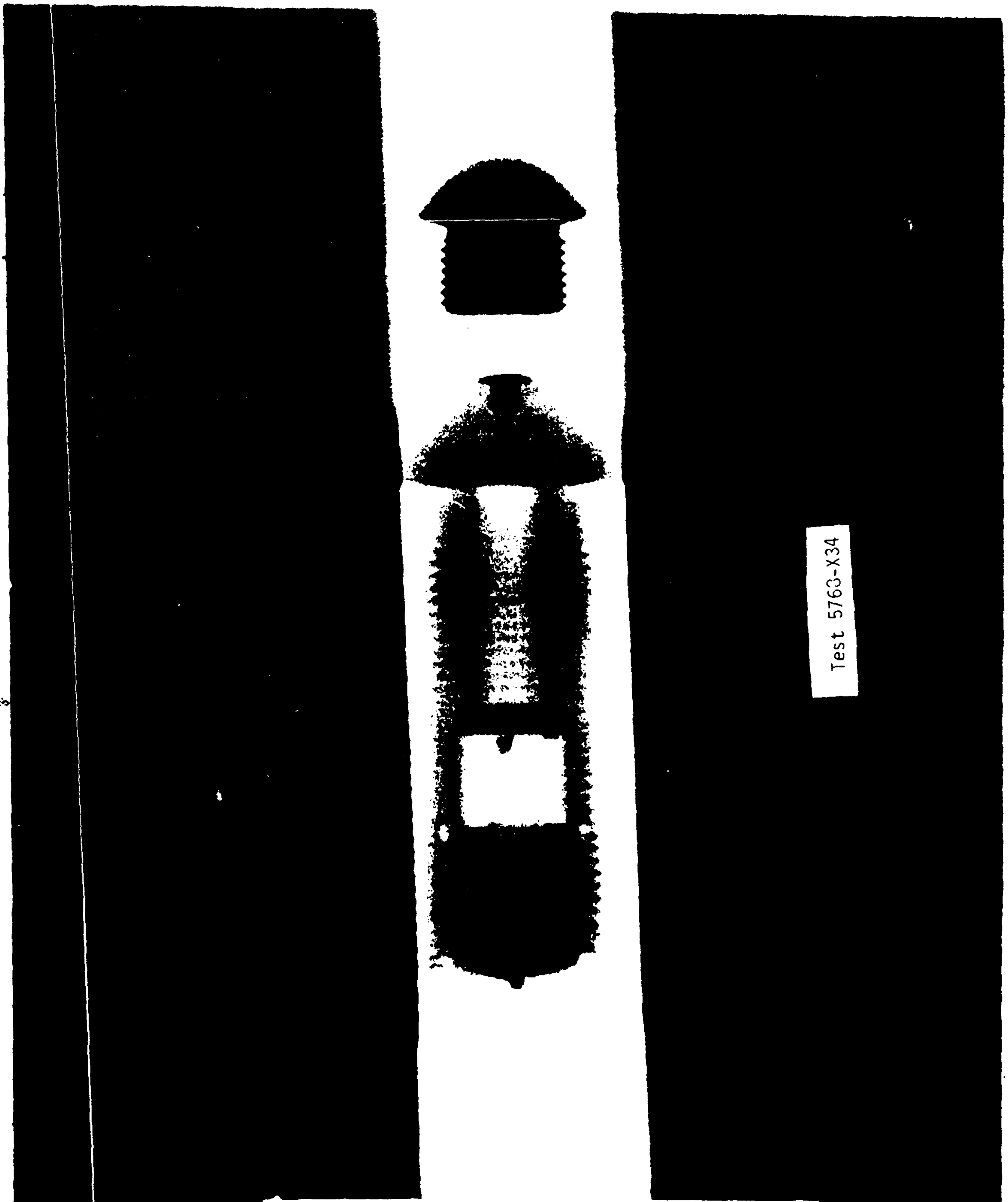

Figure B-21.   X-Ray Photographs Test 5768 Sta. X-34

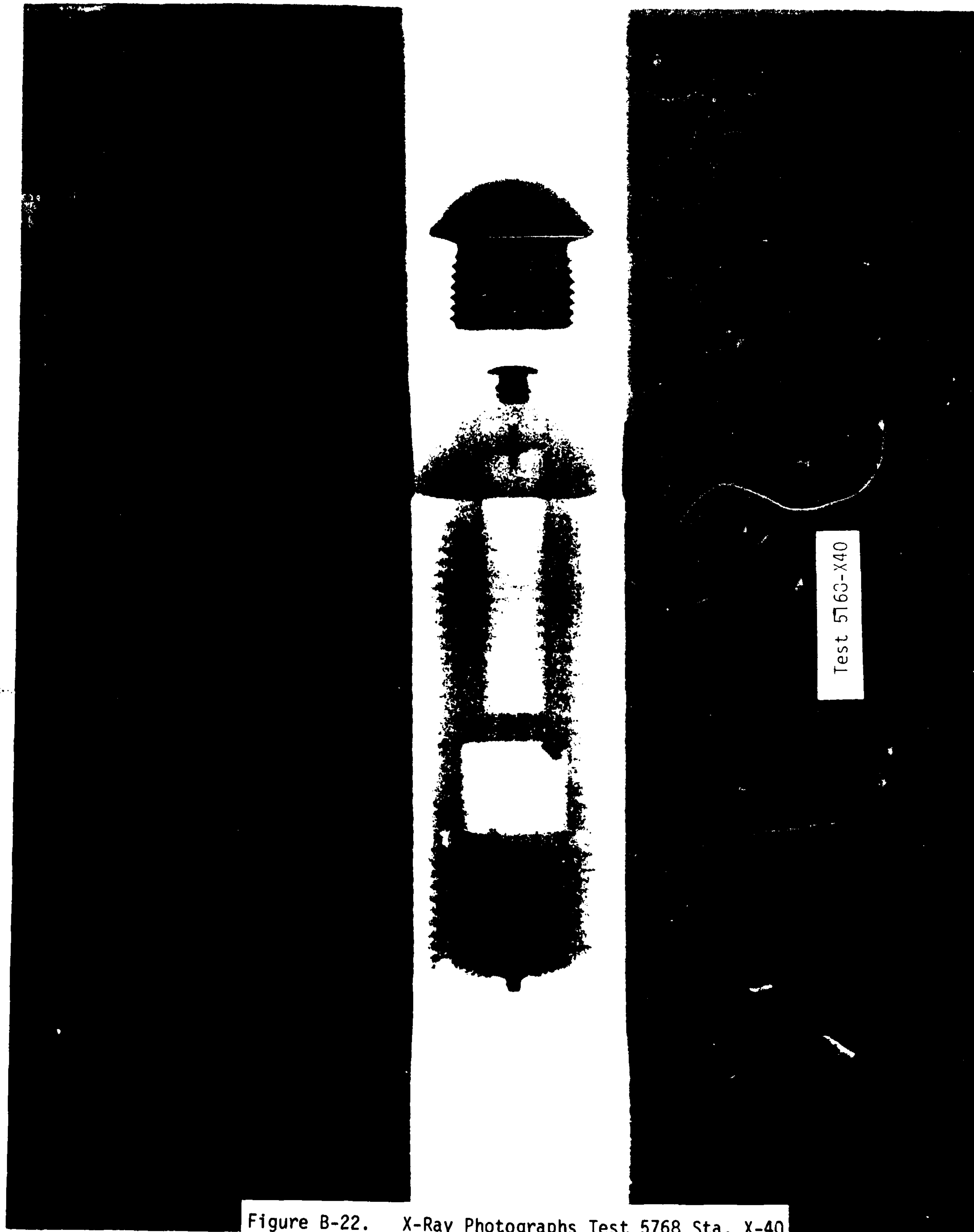

Figure B-22. X-Ray Photographs Test 5768 Sta. X-40

TEST 5768

THERMAL PLOTS

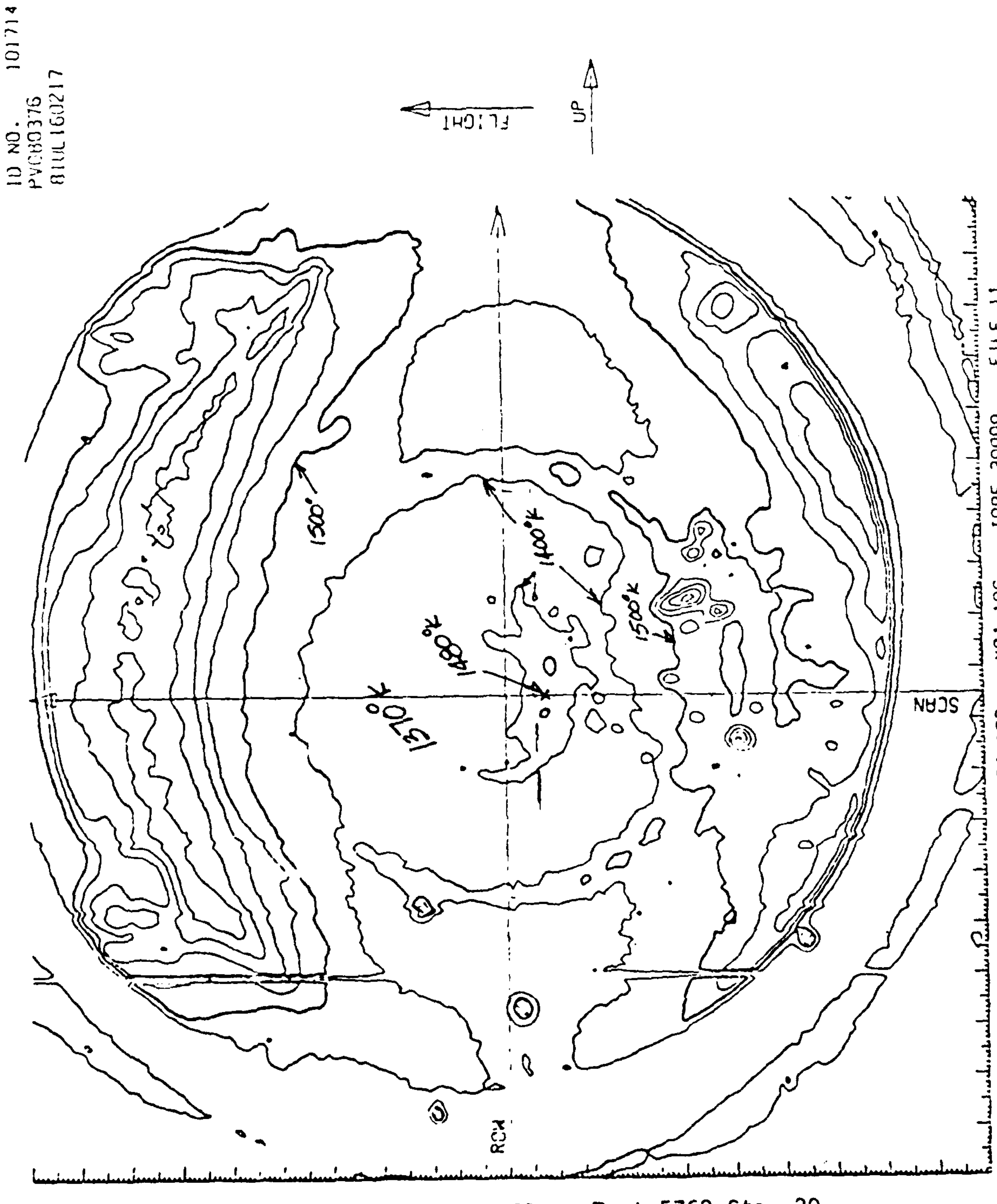

Figure B-21. Thermo Plots Test 5768 Sta. 20

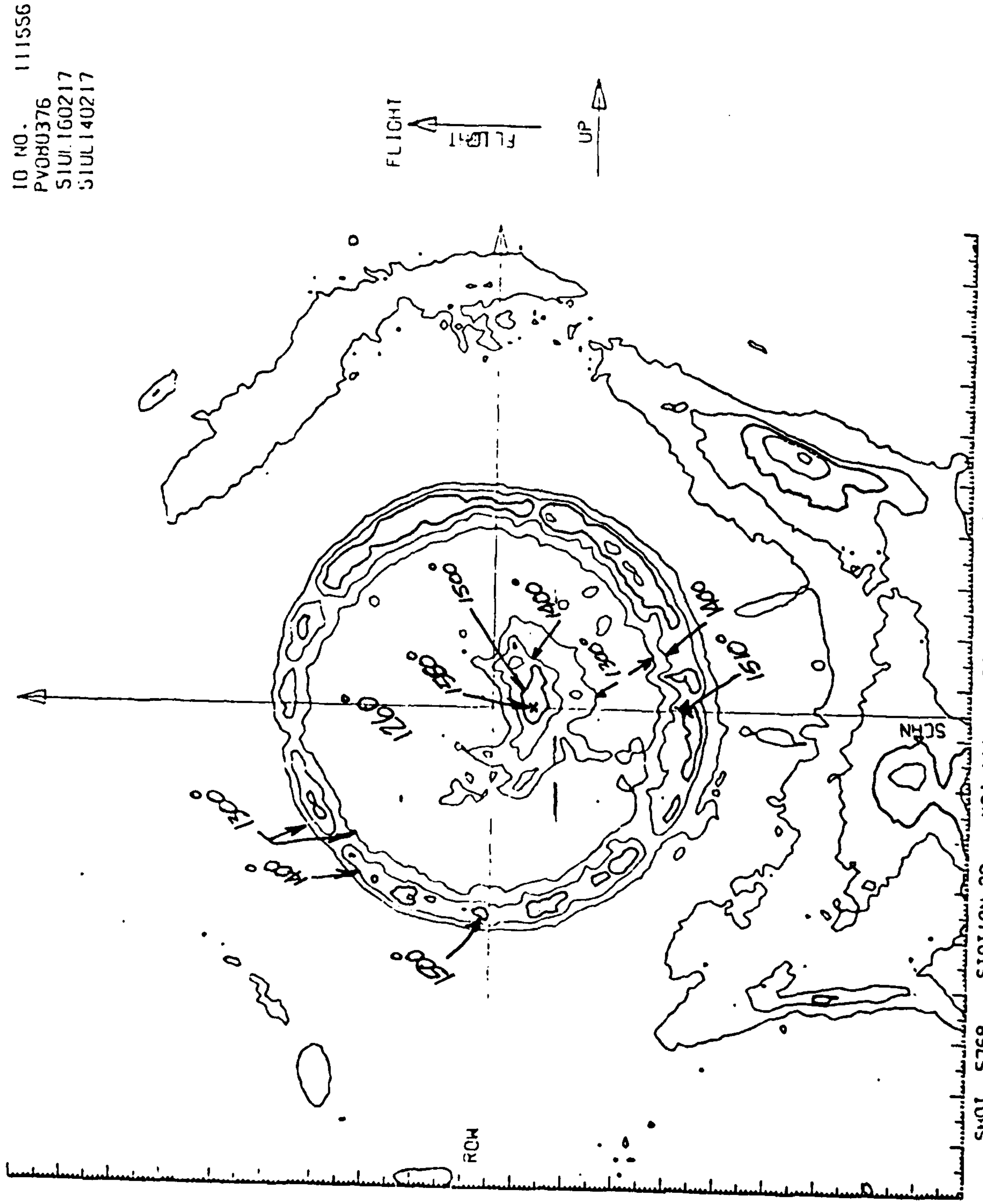

Figure B-22. Thermo Plots Test 5768 Sta. 29

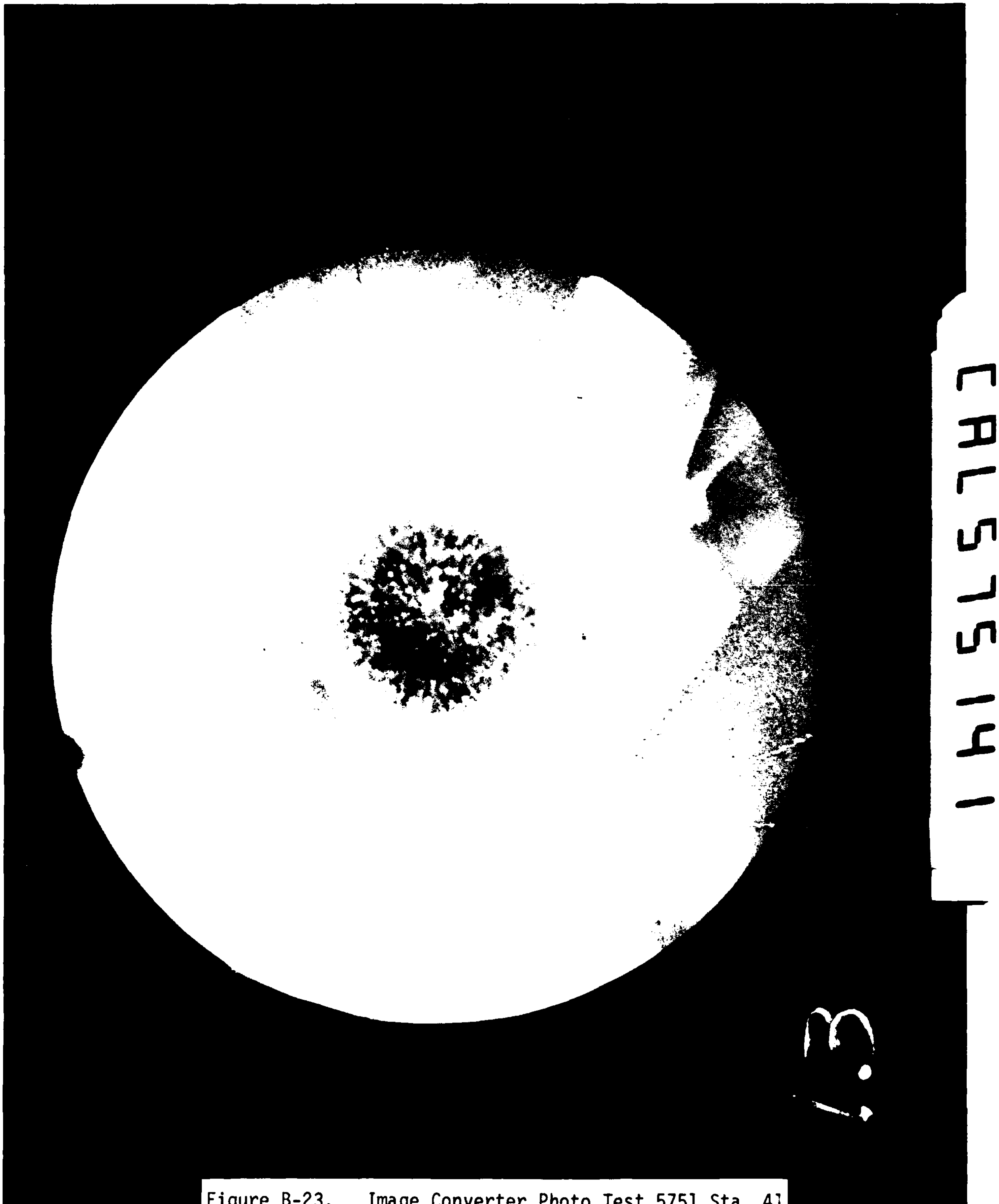

Figure B-23. Image Converter Photo Test 5751 Sta. 41

Figure B-24. Image Converter Photo Test 5768 Sta. 20

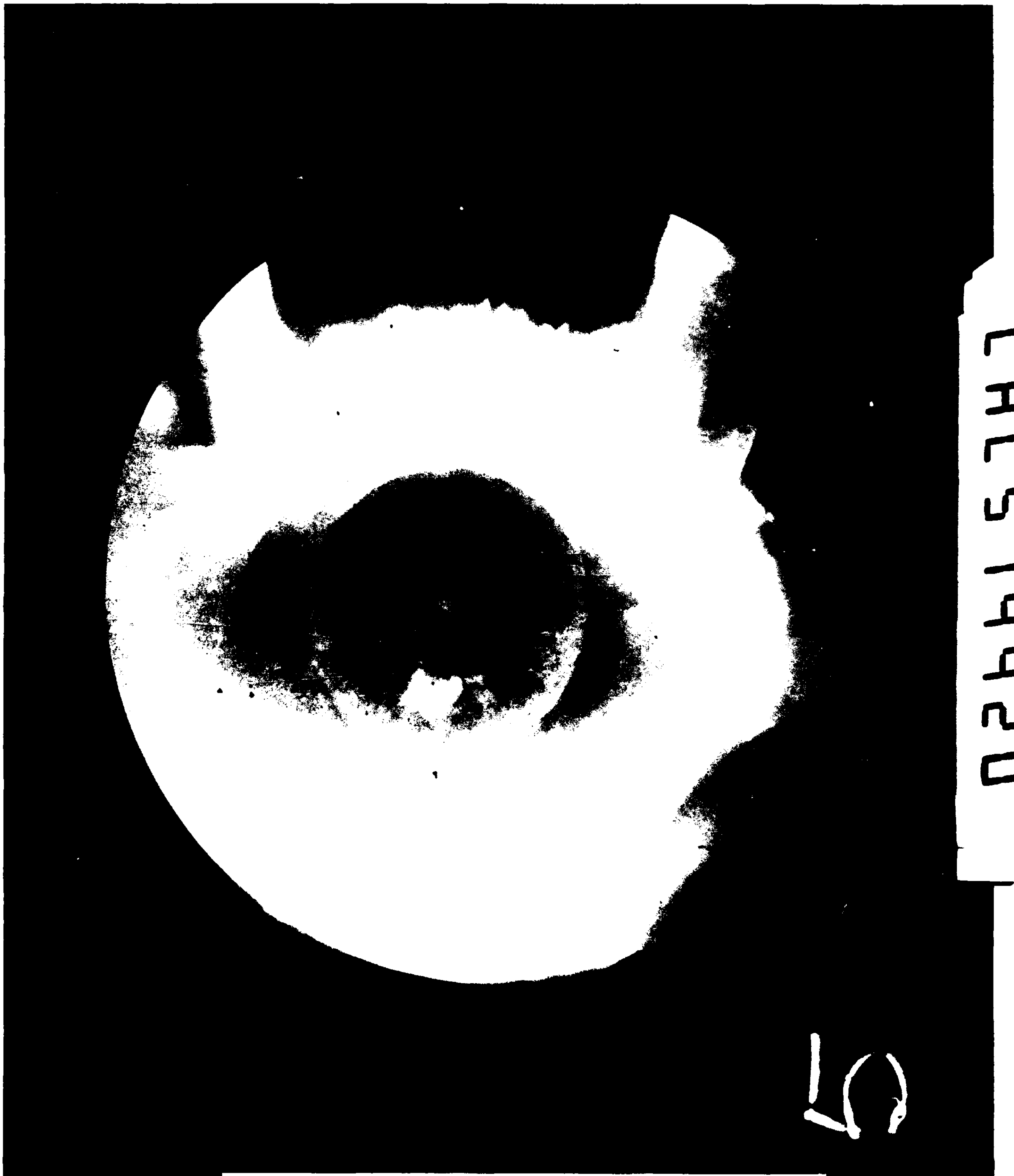

Figure B-25. Image Converter Photo Test 5749 Sta. 20

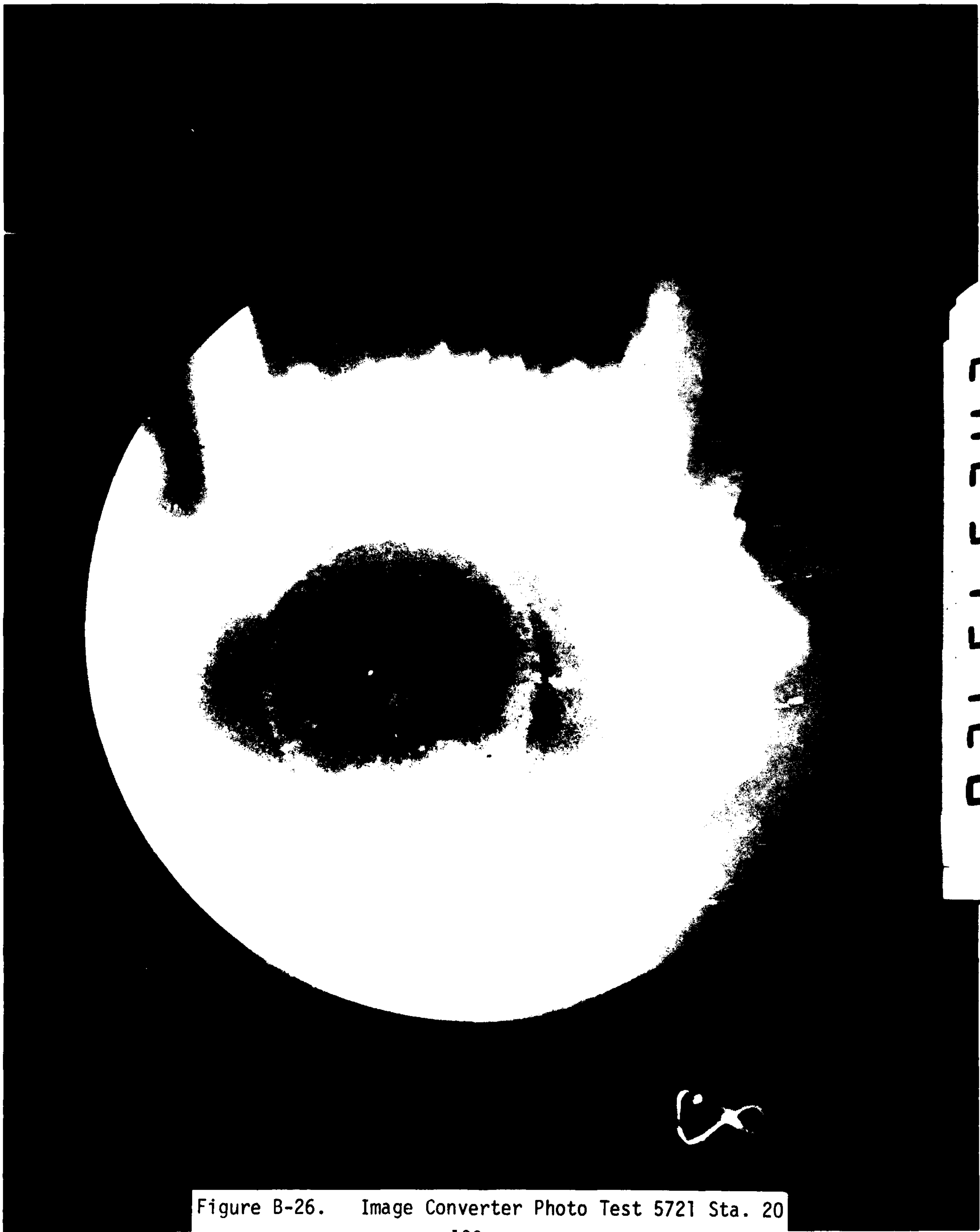

Figure B-26. Image Converter Photo Test 5721 Sta. 20

Figure B-27. Image Converter Photo Test 5768 Sta. 29

Figure B-28. Image Converter Photo Test 5751 Sta. 29

Figure B-29. Image Converter Photo Test 5749 Sta. 29